

Numerical Simulation of Two-Part Underwater Towing System

Thesis Submitted to Cochin University of Science and Technology in fulfillment of the requirements for the award of the degree of

Doctor of Philosophy

By

Lalu. P.P

Register No 3275 (2007 Admission)

Under the supervision of

Dr. K. P Narayanan

Associate Professor

Department of Ship Technology

Cochin University of Science and Technology

Kochi-682022, Kerala, India



January 2013

Dedicated to All Mighty God...

**DEPARTMENT OF SHIP TECHNOLOGY
COCHIN UNIVERSITY OF SCIENCE AND TECHNOLOGY
KOCHI-682022, KERALA, INDIA**

CERTIFICATE

This is to certify that the thesis entitled “NUMERICAL SIMULATION OF TWO-PART UNDERWATER TOWING SYSTEM” Submitted by Lalu P.P to the Cochin University of Science of Technology, Kochi for the award of Doctor of Philosophy is a bonafide record of research work carried out by him under my supervision. The contents of this thesis, in full or in parts have not been submitted to any other institute or University for the award of any degree or diploma.

Kochi-22

Date:

Dr. K.P Narayanan (Research Guide)
Associate Professor
Department of Ship Technology,
Cochin University of Science of Technology,
Kochi-22
Email: Narayanan@cusat.ac.in

Declaration

I, hereby declare that the thesis entitled “Numerical simulation of Two-part Underwater Towing system” is based on the original work done by me under the supervision of Dr. K.P Narayanan, Associate Professor, Department of Ship Technology, Cochin University of Science and Technology, Kochi. No part of this thesis has been presented for any degree from any other university or institutions.

Kochi-22

Lalu P.P

Date:

ACKNOWLEDGEMENT

I take the opportunity to express my heartfelt gratitude to my supervisor, **Dr. K.P Narayanan**, Associate Professor, Department of Ship Technology, Cochin University of Science and Technology for his unreserved guidance, constructive suggestions and inspiration in nurturing this research work.

I am thankful to **Dr. K. Sivaprasad**, HOD, Department of Ship Technology, Cochin University of Science and Technology for providing me opportunity to work in this area.

I am grateful to **Dr. C.G Nandakumar**, Associate Professor, Department of Ship Technology, Cochin University of Science and Technology for providing me invaluable suggestions during the study.

I am thankful to Prof.(Dr.) K. **Prabhakaran Nair** , Dean National Institute of Technology Calicut, Kozhikode for give us opportunity for conducting laboratory experiments at Offshore laboratory NITC, Kozhikode.

I am grateful to **Dr. B ANIL**, Head, Centre of Engineering Research and Development, (CERD) Thiruvandapuram for funding for the 32 CPU cluster computational facility, for the development and testing of parallel CFD code for this project.

The services of the Office staff of Department of Ship Technology, Cochin University of Science and Technology are acknowledged with sincere thanks.

Above all, I express my indebtedness to the “**ALMIGHTY**” for all His blessing and kindness.

(Lalu P.P)

ABSTRACT

The motion instability is an important issue that occurs during the operation of towed underwater vehicles (TUV), which considerably affects the accuracy of high precision acoustic instrumentations housed inside the same. Out of the various parameters responsible for this, the disturbances from the tow-ship are the most significant one. The present study focus on the motion dynamics of an underwater towing system with ship induced disturbances as the input. The study focus on an innovative system called two-part towing. The methodology involves numerical modeling of the tow system, which consists of modeling of the tow-cables and vehicles formulation. Previous study in this direction used a segmental approach for the modeling of the cable. Even though, the model was successful in predicting the heave response of the tow-body, instabilities were observed in the numerical solution. The present study devises a simple approach called lumped mass spring model (LMSM) for the cable formulation. In this work, the traditional LMSM has been modified in two ways. First, by implementing advanced time integration procedures and secondly, use of a modified beam model which uses only translational degrees of freedoms for solving beam equation. A number of time integration procedures, such as Euler, Houbolt, Newmark and HHT- α were implemented in the traditional LMSM and the strength and weakness of each scheme were numerically estimated.

In most of the previous studies, hydrodynamic forces acting on the tow-system such as drag and lift etc. are approximated as analytical expression of velocities. This approach restricts these models to use simple cylindrical shaped towed bodies and may not be applicable modern tow systems which are diversified in shape and complexity. Hence, this particular study, hydrodynamic parameters such as drag and lift of the tow-system are estimated using CFD techniques. To achieve this, a RANS based CFD code has been developed. Further, a new convection interpolation scheme for CFD simulation, called BNCUS, which is blend of cell based and node based formulation, was proposed in the study and numerically tested. To account for the fact that simulation takes considerable time in solving fluid dynamic equations, a dedicated parallel computing setup has been developed. Two types of

computational parallelisms are explored in the current study, viz; the model for shared memory processors and distributed memory processors. In the present study, shared memory model was used for structural dynamic analysis of towing system, distributed memory one was devised in solving fluid dynamic equations.

Finally the developed numerical model has been validated experimentally through towing tank trials. For this purpose, a detailed experimental set-up has been made including the fabrication of towed body and associated electronics, sinusoidal input motion generation mechanism, sensors for real time measurement of pitch and heave etc. Finally, heave instability of the towed body was experimentally estimated, compared with simulated values.

Keywords: Fluid structure interaction, underwater towing, CFD, Time integration, parallel computing, Finite difference method

Contents

	Page No.
Chapter 1. Introduction	
1.1 Background	1
1.2 Two-Part Towing System	2
1.3 Overall objectives	4
1.4 Scope of the present study	5
1.5 Methodology	5
1.6 Organization of the Report	6
Chapter 2. Literature Review	
2.1 Previous and Related Studies	8
2.2 Time/Space Discretisation of Equation of Motion	11
2.3 Parallel Computations	12
2.4 Verification of Numerical Model	12
Chapter 3. Mathematical Formulations	
3.1 Mathematical Modelling of Tow System	14
3.2 Lumped Mass-Spring System Model (LMSM)	15
3.3 Governing Equations	16
3.4 Estimation of Drag Forces	18
3.5 Implementation of the Boundary Condition	19
3.5.1 Boundary Condition at the Depressor	19
3.5.2 Boundary Condition at the Junction of the Three Cables	20
3.6 Initial Condition	21
3.7 Finite Difference Implementation	21
3.8 Kinematics and Dynamics of the Tow-Fish	21
3.8.1 Motion Dynamics	23
3.8.2 Kinematics of the Tow-point	24
Chapter 4. Improved Lumped-Mass-Spring Model	
4.1 Time Discretisation Procedure	26
4.2 Characteristics of Time Integration Schemes	27
4.2.1 Stability	28
4.2.2 Number of Implicit Systems to be Solved	28
4.2.3 Accuracy	28
4.2.4 Numerical Dissipation	29
4.2.5 Self-starting	29
4.2.6 Overshooting	29
4.3 Implementation of Time integration schemes	30
4.3.1 Houbolt Scheme	30
4.3.2 NewMark's method	31

4.3.3	Box Method	31
4.3.4	HHT- α method	31
4.4	Implementation of HHT-Alfa Method in LMSM	31
4.5	Improved Bending Rigidity formulation for LMSM	32

Chapter 5: Numerical Solution to Hydrodynamic

Equations

5.1	Previous and Related Studies	38
5.2	Present Contributions	39
5.3	Governing Equations	40
5.4	Turbulence Modelling	40
5.4.1	SST-K- Ω Turbulence Model	41
5.5	Finite Volume Discretisation	42
5.6	Discretisation of Convective Term	43
5.7	Diffusion Term	43
5.8	Source Term	44
5.9	Velocity -Pressure Coupling	44
5.10	Implementation of Physical Boundary Conditions	45
5.11	Latest Convection Differencing Schemes	45
5.12	NV Approach for Unstructured Meshes	46
5.13	Node based formulation	47
5.14	Development of New Convection Interpolation Scheme (BNCUS)	48
5.15	Solution Techniques for Systems of Linear Algebraic Equations	49
5.16	Test cases	51
5.17	Gradient estimation	54
5.18	Blended Node and cell based Formulation for CFD simulations	60
5.19	Hydrodynamic Analysis of the tow-fish hull	67
5.20	Conclusion	69

Chapter 6: Numerical Experiments

6.1	Overview	71
6.2	Test case1: Two-Part Towing	71
6.2.1	Results and Discussion	73
6.3	Test Case 2:Tow-Ship Manoeuvring Examples - Single Point Towing	75
6.4	Testing of Time Integration Schemes	78
6.4.1	Euler Scheme	80
6.4.2	HHT- α	81
6.4.3	Newmark's method	82
6.5	Parallel Computations	83
6.5.1	Shared-memory multiprocessors	84
6.5.2	Distributed-memory multiprocessors	84
6.6	Parallel Programming Paradigms	85
6.7	Message Passing	86
6.8	Code Parallelisation -for Shared Memory Architecture	87

List of Tables

Table 5.1	Test Cases and results
Table 5.2.	Solver setting
Table 5.3.	Test case for Blended scheme
Table 6.1.	Kinematic details of tow-point
Table 6.2.	Some OPEMP Directives
Table 6.3.	MINPACK functions
Table 6.4	Platforms tested
Table 6.5	Cluster Details
Table 8.1.	Weight and Mass Moment of Inertia of the Towed Body

List of Figures

- Figure 1.1.a Single point towing system
- Figure 1.1.b Two-part towing system
- Figure 3.1 Lumped mass-spring cable model.
- Figure 3.2. Components of Drag forces on the cable
- Figure 3.3 Boundary condition at the junction of the three cables
- Figure 3.4. Degrees of freedom of a generic towed body
- Figure 3.5 Different types of tow-point configuration
- Figure 4.1. Cable Segment
- Figure 4.2 Deformed beam
- Figure 4.3 Improved cable model
- Figure 4.4 Schematic beam model
- Figure 4.5 Equivalent nodal forces
- Figure 5.1 Generic Control Volume
- Figure 5.2 Variation of Φ around the face f
- Figure 5.3 Estimation of cell face value by node based approach
- Figure 5.3a Numerical solution procedure
- Figure 5.4. Plotted Stream lines using PARAVIEW (test case-1)
- Figure 5.5. Plotted Stream lines using PARAVIEW (test case 2)
- Figure 5.6a. Type 1 Mesh Regular - 256 cells
- Figure 5.6b, Type 2 Mesh Random 256 cells
- Figure 5.6c Type 3 Mesh Perturbed, 256 cells
- Figure 5.6d. Assumed distribution of scalar Φ
- Figure 5.7 Gradient: CDS
- Figure 5.8 Gradient: Node based
- Figure 5.9. Gradient: blended scheme
- Figure 5.10 Gradient: CDS
- Figure 5.11 Gradient: Node based
- Figure 5.12 Gradient: blended scheme
- Figure 5.13 Comparism of L2 norm of various schemes.

- Figure 5.14 Variation of L2 Norm with blending factor
- Figure 5.15 a,b,c,d,e and f :Test case1, Effect of blending factor on stability and accuracy
- Figure 5.16 Performance of BNCUS2 at different blend factors
- Figure 5.17 Performance of BNCUS1 at different blend factors
- Figure 5.18 Performance comparism of BNCUS2 and BNCUS1.
- Figure 5.19a Node based higher order scheme, Limiter Koren
- Figure 5.19b CDS as higher order scheme, Limiter Koren
- Figure 5.20a Node based higher order scheme, Limiter SUPERBEE
- Figure 5.20b CDS as Higher order scheme, Limiter SUPERBEE
- Figure 5.21a Node based higher order scheme, Limiter UMIST
- Figure 5.21b CDS as Higher order scheme, Limiter UMIST
- Figure 5.22a Node based higher order scheme, Limiter VANLEER
- Figure 5.22b CDS as Higher order scheme, Limiter VANLEER
- Figure 5.23 Relative performances of various limiters
- Figure 5.24 Comparism of CDS and Node based formulation with various limiters
- Figure 5.25 Figure 5.25 Drag v/s angle of attack of the towed body
- Figure 5.26 Pitching moment v/s angle of attack of the towed body
- Figure 5.27 Lift v/s angle of attack of the towed body
- Figure 6.1 Simulated configuration of the two-part towing system
- Figure 6.2. Sinusoidal tow point disturbance given (input motion)
- Figure 6.3 Towed body and depressor heave
- Figure 6.4. Experimental heave values from literature
- Figure 6.5. Simulated Plan View of the path of ship and towed body
- Figure 6.6 Simulated depth variations
- Figure 6.7 Depth variation of the towing system when the ship is suddenly stopped
- Figure 6.8a Heave response for Hoboult Schme $\gamma = 1.0$
- Figure 6.8b Heave response for Hoboult Schme $\gamma = 1.2$
- Figure 6.8c Heave response for Hoboult Schme $\gamma = 1.5$
- Figure 6.8d Heave response for Hoboult Schme $\gamma = 1.6$
- Figure 6.9 Heave response for Euler Scheme
- Figure 6.10 Heave response $\alpha=0.0$
- Figure 6.11 Heave response $\alpha=-0.1$
- Figure 6.12 Heave response $\alpha=-0.3$
- Figure 6.13 Heave response $\alpha=-0.25$

- Figure 6.14 Heave response $\alpha=0.4$
- Figure 6.15 Heave response $\alpha=0.5$
- Figure 6.16 Heave response $\alpha=-0.33$
- Figure 6.17. Heave response with Newmark method
- Figure 6.18 Shared memory system
- Figure 6.19 Distributed-memory multiprocessors
- Figure 6.20 Cluster systems
- Figure 6.21 Computational time for 26 degrees of freedom
- Figure 6.22 Computational time for 120 degrees of freedom
- Figure 6.23 Computational time for 170 degrees of freedom
- Figure 6.24 CPU utilization of the serial code (without OPENMP)
- Figure 6.25 CPU utilization of the Parallel code (with OPENMP no of CPU =4)
- Figure 6.26 Parallel computing setup
- Figure 6.27 Software Front End for logging into the network and application deployment
- Figure 6.28 Mesh visualiser for partitioned mesh
- Figure 6.29 Computational time v/s no of CPUs for test case -1
- Figure7.1. Variation of heave ratio with length of depressor cable
- Figure 7.2. Variation of heave ratio with length of secondary cable
- Figure 7.3. Variation of heave ratio with the length of the primary cable
- Figure 7.4. Effect of Depressor mass on the heave response of the towed body and depressor
- Figure 7.5 Effect of wave frequency on the heave response of the towed body
- Figure 7.6 Effect bending rigidity of the cable on the heave ratio
- Figure 8.1 Towed body
- Figure 8.2 Towed body structure
- Figure 8.3 Pressure sensor
- Figure 8.4 Tri-axis Accelerometer
- Figure 8.5 Electronic Diagram
- Figure 8.6 6-channel Data Acquisition System
- Figure 8.7 Depressor
- Figure 8.8 Sinusoidal wave motion mechanism
- Figure 8.9 Assembled sensor array
- Figure 8.10 Finished assembly of the towed body
- Figure 8.11 Carriage speed control
- Figure 8.12 Mass Moment of Inertia Estimation

Figure 8.13	Towing tank
Figure 8.14	deployment of towed body
Figure 8.15	Measured time based heave data
Figure 8.16	Simulated Heave data

Nomenclature

English Symbols

a ,	Acceleration
C_d	Drag coefficient
C_l	Lift coefficient
e	added mass for the cable segment
F_D	Drag force
g	Acceleration due to gravity
I	Moment of inertia
K	Stiffness Matrix
C	Damping coefficient matrix
M	Mass Matrix
m	Mass
n	Direction cosines vector
P, p	Pressure at the cell centre
Pe	Peclet Number
Re	Reynolds Number
T	Tension in the cable
t	Time
U, U(u,v,w)	Velocity Vector
V	Volume
X, X(x,y,z)	Position Vector

Greek Symbols

Γ	Diffusivity
μ	Dynamic viscosity
ν	Kinematic viscosity
ν_t	Kinematic eddy viscosity
ρ	Density
σ	Stress tensor
ψ	TVD limiter
Ω	[p, q, r] is the tow-fish angular velocity

Abbreviations

BD	Blended Differencing
Bi-CG	Bi-Conjugate Gradient
BNCUS	Blended node and cell based upwind scheme
CDS	Central Difference Scheme
CFD	Computational Fluid Dynamics
CPU	Central processing Unit
DNS	Direct Numerical Simulations
DSM	Distributed Shared Memory
FCT	Flux Corrected Transport
FEM	Finite Element Method
FVM	Finite Volume Method
HHT	Hilber, Hughes and Taylor
LES	Large eddy Simulation
LMSM	Lumped Mass Spring Model
MPI	Message Passing Interface

NVA	Normalised Variable Approach
PISO	Pressure Implicit with Splitting of Operators
PVM	Parallel Virtual Machines
QUICK	Quadratic Upstream Interpolation for Convective Kinematics
SE	Strain Energy
SIMPLE	Semi-Implicit Method for Pressure-Linked Equations
SSH	Secure Socket Shell
SST	Shear Stress Transport
TV	Total Variation
TVD	Total Variation Diminishing
UDS	Upwind Differencing Scheme
UMIST	Upstream Monotonic Interpolation for Scalar Transport
UTV	Underwater Towed Vehicles
RANS	Reynolds Averaged Navier-Stokes Equation
CERD	Centre of Engineering Research and Development

Introduction

Contents	1.1 Background
	1.2 Two-Part Towing System
	1.3 Overall objectives
	1.4 Scope of the present study
	1.5 Methodology
	1.6 Organization of the Report

1.1 Background

As an effective tool for marine applications, the underwater towed vehicles (UTV) play an important role in naval defense [Ohkusu, *et.al*, 1987], ocean exploration and ocean research [Feng, 2004]. The system mainly consists of a tow-fish, which is towed underwater by a ship through long cables. On the oceanographic point of view, UTV has various missions, such as monitoring of ocean environment, underwater survey and inspection of pipeline on seabed etc. For this purpose, these vehicles are often used to house high precision acoustic instrumentations, which require very high motion stability. However, these are subjected to several disturbances, which make them unstable, leading to the reduced accuracy of instrumentation inside. So to reduce these instabilities is a great concern for the researchers worldwide. These instabilities are attributed to the parameters like surface water waves, underwater currents, sub-surface turbulence and other external disturbances such as the motion of the supporting vessel and other subsystems [Koterayama, *et.al*, 1988]. David, [David, *et.al*, 2005] classified these disturbances into two: viz environmental and human related. Out of these, one of the environmental effects of the disturbance from the ship due to waves is a significant one, which affects the motion stability of the towed vehicle considerably [Anderson, 2002]. Since, these vehicles operate at a depth of water of 100m or more, the surface ocean waves have little direct influence on the motion stability of towed body, except by the transfer of disturbances through the tow-cable [Chapman, 1984].

A conventional towed system consists of a single cable and its towed vehicle, which is found less efficient in reducing the transfer of ship induced disturbances to the towed body [Chapman, 1984]. An alternative approach is the use of a two-part towing system, which devises multiple cables and towed bodies. Previous studies in this area have shown that two-part towing was efficient in decoupling the towed vehicle from the adverse effects of these disturbances [Wu, *et.al*, 2001].

1.2 Two-Part Towing System

Unlike conventional towing system (see figure 1.1a), which uses a single cable to tow the fish; two-part towing requires three cables (Figure 1.1b). They are primary, secondary and depressor cable. All these are joined using a sheave. A heavy depressor, which is usually a lead ball, will be attached to the end of the depressor cable. It serves two purposes. Primarily, it increases the effective depth of the tow-fish. Secondly, it reduces the transmission of periodic disturbances from the tow-ship to the cable [Wu, *et.al*, 2001]. Unlike single point towing system, more recently introduced two-part one, received a little attention from the researchers worldwide for its dynamic modeling and the subsequent study of the effect of these ship induced disturbances on its motion stability.

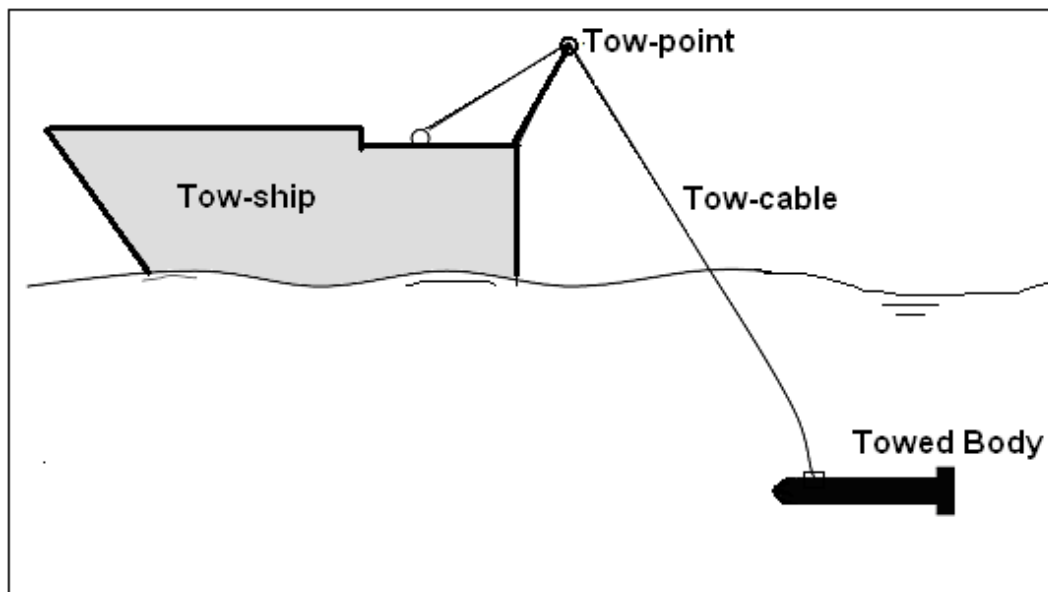


Figure 1.1.a Single point towing system

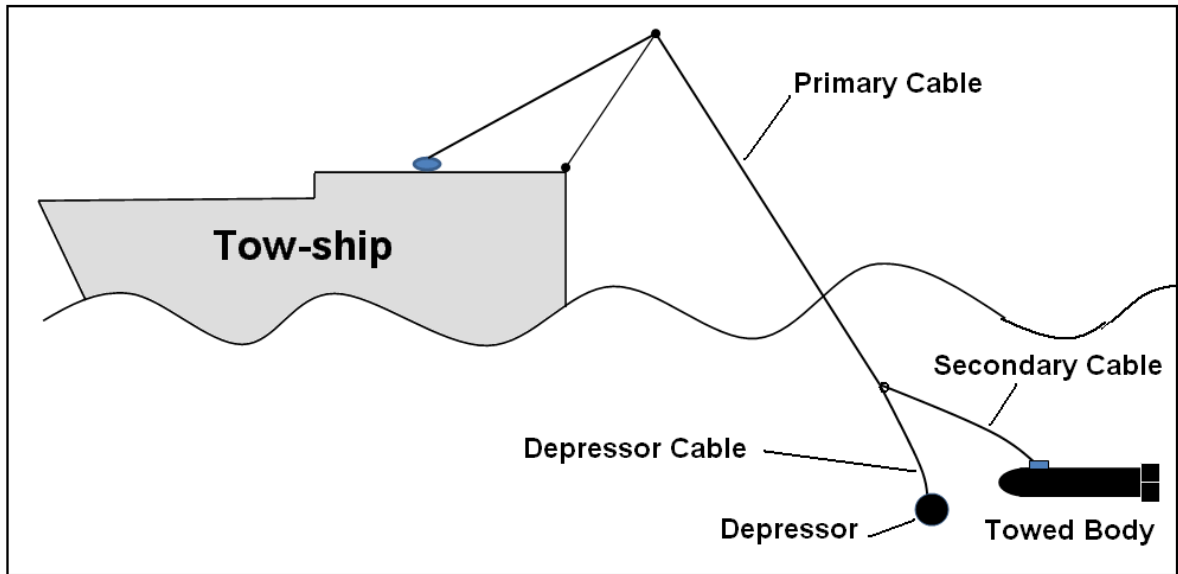


Figure 1.1.b. Two-part towing system

The dynamic analysis of a towed system is a two-step procedure, viz, cable modeling and vehicle formulation. Historically, two methodologies were evolved for modeling the cable. These are segmental approach and lumped-mass-spring model (LMSM) [Ablow *et.al*, 1984]. For the former, the cable is modeled as continuous system and resulting partial differential equations are solved by finite difference or any suitable approximation method. However, in the LMSM approach, the cable is modeled as point masses joined together by mass-less elastic elements of finite length. All the forces along the cable are assumed to be concentrated at the mass points. In spite of the simplicity offered by LMSM, most of the previous studies devised segmental formulation for simulating the motion dynamics of both single point and two-part towing [Ablow, 1984],[Eric,2004]. But, the present study utilises the lumped mass formulation for the modeling of the cable as it is simpler to implement compared to segmental one.

Very few works are reported for the case of two-part towing, to develop a numerical model and to study the dynamics of towing process. An exception to this, is the work done by Wu,[Wu *et.al*,2000]. Even though, the model has been successful in simulating the system dynamics of the two-part towing, formulation lacks sufficient numerical stability, primarily, due to the use of relatively less stable BOX type scheme [Ablow, 1984] for time integration

of the differential equation of motion. To circumvent this, advanced HHT- α time integration procedure [Hughes, 1987] has been implemented for solving the equation of motion. Also, in most of the previous studies that are related to motion dynamics of two-part towing system, hydrodynamic forces exerted on the towed body such as drag and lift are approximated as analytical expression for the formulation of equation of motion of the same. This approach severely restricts these numerical models [Wu, *et.al*, 2001] to use simple cylindrical shaped towed bodies and may not be applicable modern tow systems which are diversified in shape and complexity of the towed body. Hence, in this particular study, drag and lift of the towed body are numerically estimated using CFD techniques. The facts that, the commercial CFD codes are not open-source softwares; most of them run with patented technologies and the lack of in-depth documentation about their numerical schemes and implementation prompted us the development of a RANS based CFD code for the project. Also, the developed code can be used as a platform for testing or experimenting emerging numerical schemes in computational fluid dynamics, as a future extension of the research work. To account for the fact that simulation takes considerable time in solving fluid dynamic equations, a dedicated parallel computing setup has been developed and hydrodynamic equations are solved in it. Further, the developed model has to be validated with experimental results. Previous studies in this direction, have shown that, two-part towing was efficient for reducing the in-plane (vertical) responses like pitch and heave, while out of plane responses like sway etc, are not benefited. Hence, the present study is limited to simulation of heave response of the towed body. Detailed experimentation set-up has been made for real-time measurement of the same.

1.3 Overall objectives

The overall objectives of the study are summarized below

1. Develop a numerical model of the two-part towing system with sufficient numerical stability to handle dynamic simulation of highly flexible multi-body systems.

2. To study the effect of the wave disturbances transmitted from the tow-ship to the depressor and towed body. Subsequently conduct a parametric study on the motion stability of the towed vehicle.
3. Develop an numerical model which include the full hydrodynamics of the towed body using computational fluid dynamics techniques (CFD)
4. Development of a parallel CFD code which is required for the objective number 3
5. Develop and integrate experimental set-up which is necessary to validate the numerical model.

1.4 Scope of the present study

The scope of the present study is limited to following.

The development of numerical model for the simulation of two-part underwater towing system with cable model as LMSM and subsequent testing of the same for numerical stability and accuracy.

To study numerical stability of the developed model for the simulation of towing process, following time integration procedures are implemented and subsequently tested.

- Newmark
- Houbolt
- Euler
- HHT- α
- Further, the effect of following parameters on the heave (vertical motion) of the towed body was investigated
 - Length of depressor, primary and secondary cables.
 - Weight in water of the depressor.
 - Frequency of input disturbance.
 - Effect of bending rigidity of the tow cable

For the experimental verification of the numerical scheme, towing tank trails are selected rather than the actual sea trails. In this experiment only heave of the towed body is compared with simulated values.

1.5 Methodology

Because of the geometrical configuration and fluid drag, which holds second order relationship with velocity, the differential equation of motion of the marine cables is nonlinear, results in, analytical solution of the same is practically impossible, implying that, this type of problems can only be solved by numerical techniques. Finite difference method was chosen as the numerical discretisation scheme for the equation of motion as it offers following advantages over integral formulations

- Easier to understand the underlying physics for the case of difference equation which is obtained by discretisation of the governing equation in the differential form, compared to discretised equations obtained through integral formulation.
- The formation of difference equation and a set of simultaneous equations for further solution, from differential one are much simpler, compared to integral formulations like finite element method.

Thus a set of nonlinear algebraic equations are obtained by converting differential equations into difference equations and subsequently solved. Hence an iterative numerical methodology has been devised to simulate the dynamic performance of the two-part towing system. The program was made initially in MATLAB software and later changed to FORTRAN owing to the better speed characteristics of the language. Further, the entire program was rewritten using parallel computing techniques. Two types of parallelisms are explored in this study; viz shared memory and distributed memory models. While, shared memory programming models were used for the hydro-structural analysis of the two-part towing, distributed computing method with message passing interface (MPI) was devised for solution of hydrodynamic equations. The equations are solved in a BEOWULF cluster consist of 8 number of GNU/LINUX machines which are interconnected by high speed ETHERNET interface. The computer cluster was sponsored by CERD, Government of Kerala.

1.6 Organization of the Report

The first chapter of the report discusses the definition of the problem and the list of objectives. While, chapter 2 deals with literature survey, chapter 3 is mainly concentrated on the cable modeling and vehicle formulation. Chapter 4 discusses modified LMSM.

Chapter 5 is all about the development of theoretical framework for solving fluid mechanics equations. Chapter 6 discusses the numerical experiments. Chapter 7 is about design optimization of two-part towing system and chapter 8 discusses experimentation part. Finally chapter 9 concludes the report.

Literature Review

Contents	<i>2.1 Previous and Related Studies</i>
	<i>2.2. Time/Space Discretisation of Equation of Motion</i>
	<i>2.3 Parallel Computations</i>
	<i>2.4 Verification of Numerical Model</i>

2.1 Previous and Related Studies

Over the last forty years, a significant body of research has led to the development of numerical cable models which can assist in the accurate positioning and navigation of long (Kilometer scale), submerged towed systems [Eric, 1987]. The first such model was based on lumped mass spring system (LMSM). Paul and Soler [Paul, *et.al*, 1972] presented a two dimensional formulation in which, the inertial forces were considered insignificant. In earlier studies, the LMSM was devised to simulate the motion of towed systems during relatively steady tow-ship manoeuvres in which inertial effects are negligible. This quasi-static implementation was used to solve for the motion of a towed system during straight tows at a steady speed. Both Chapman [Chapman, 1984] and Sanders [Sanders, 1982] presented three-dimensional quasi-static lumped parameter models. Chapman calculated the steady state profile of a tow-cable during straight tows and turns of varying diameters. This work showed that a towed system undergoes large transient motions as it enters and exits the turns. This emphasised the need for cable models to include inertial effects in order to accurately capture these transient motions.

Shan Haung [Shan, 1994] presented a LMSM which considers the inertial effects. In his method, the forces as well as the masses are lumped at node points and equation of motion

is formed based on the Newton-Euler theorem. The resulting equations are solved using finite difference method.

The main advantages of LSM are the relative ease of dealing with the strong nonlinearities associated with the hydrodynamic loads, and the ability to assemble a compact numerical model from the linear elements. As reported by Shan Huang [Shan, 1994] through his research in single point towing systems, representation of cable as discrete mass and linear spring elements, results in reduced numerical oscillations in the solution space because the LSM work as a low pass filter which damp out spurious high frequency numerical oscillations. For these reasons the LSM formed the basis for a significant body of towed systems research. Such lumped mass implementations have been presented by Vaz and Patel [Vaz, *et.al*, 1995] and Driscoll *et al.* [Driscoll *et.al*, 1996]. Both Driscoll and Huang [Shan, 1994] accounted for the elasticity of the tow- cable by using linear spring elements. In both cases, the spring stiffness was calculated from the material properties of the tow-cable.

An alternative approach that has been developed in parallel was segmental one. It was developed by Ablow and Schechter [Ablow, *et.al*, 1983]. In this model, cable is treated as a long thin flexible circular cylinder in arbitrary motion. It was assumed that, the dynamic motion of the cable is determined by gravity, hydrodynamic loading and inertial forces. Then the governing equations are formulated based on a local coordinate system, which moves with the cable. The equations are discretized using finite difference method, subsequently solved using an implicit scheme, which is centered at time and space. This formulation worked well for the simulation of the conventional towing system but numerical instabilities are found when it tries to apply for the two part towing system.

Most of the approaches described above, are mainly devised to analyze the single point towing system for predicting real-time estimation of depth and trail of the towed body. Very few studies have been reported for analysing the ship induced disturbances on the dynamics of the tow-fish. An exception to this is the work done by Chapman [Chapman, 1984]. He has devised a two-dimensional numeral model to study the response of a neutrally buoyant fish, which is towed using a fared cable and is subjected to ship induced disturbances. He identified two dominant modes of transmission of disturbances down to the cable, namely longitudinal as well

as transverse oscillations. It has reported that transverse modes of the cable are considerably damped, while the longitudinal mode prevails [Chapman, 1984]. This may be due to larger normal drag exerted by the fluid (second order damping force) compared to tangential one for the case of slender bodies like marine cables. Also, it has found that overall amplitude of the motion of the tow-fish is proportional to the sine of the angle made by top of the cable with the horizontal, provided that combined natural frequencies of the ship and cable system does not coincide with that of external disturbances. However, the study was limited to single point towing. Further, the tow cable not only transmits but also generates disturbances [Samuel, *et.al* 1993]. These disturbances depend on the cable used, mass and drag of the depressor and mass and drag of the tow-fish. For example, the cable may shed vortices causing it to strum. This strumming can be removed with the use of faring. Another effect is kiting which can be either ship-induced or tow-fish-induced. Ship-induced kiting causes sway in the tow-fish whereas tow-fish-induced kiting causes sway and roll in the tow-fish.

Recently, Wu [Wu, *et.al*, 2000] developed a three dimensional numerical model to simulate dynamic performance of the two-part towing system considering the ship disturbance as the input. It was found that the degrees of freedom which lie on the central vertical plane of the towed body such as pitch and heave were reduced considerably rather than the out-of-plane responses like yaw and roll. Even though, the model was successful in simulating the dynamic performance of the two-part towing system, numerical oscillations were found in the solution space. Further, mathematical modeling of tow system and solution methodology devised in this particular study was much complicated compared to LMSM approach.

Considering all these factors it was decided to investigate the dynamic performance of the two-part towing system with ship induced motion as the input disturbance. Also, Lumped mass formulation was selected considering simplicity of the formulation and added numerical stability compared to other schemes like Ablow and Schechter model [Ablow, 1983] and Finite element model. A two dimensional model was attempted considering the fact that only in-plane (vertical) responses are benefited maximum by two-part towing system. Only longitudinal mode of cable oscillation, for the transfer of periodic disturbances from the tow-

point to the towed body, was considered for the study. The formulation of the towed vehicle was based on the Kirchoff's equation of motion for rigid bodies [Thor, 1994].

2.2. Time/Space Discretisation of Equation of Motion

For all spatial discretization methods, the resulting equations are typically written as a non-linear matrix equation known as the semi-discrete equation of motion, because the time derivatives of the vector of dependent variables are left as continuous functions. The equations of motion for LMSM are most often presented in matrix form as a system of second-order ordinary differential equations – the semi-discrete equation of motion. Most temporal integration schemes in use today have their roots in the method developed by Buckham [Buckham, *et.al*, 1999]. Newmark [Hughes, 2004]. Hughes and Belytschko [Ted Belytschko, *et.al*, 1983] provide a summary of the development of these types of methods in the context of finite element solution of structural dynamic problems. The methods typically employ temporal finite differences, with a variety of different schemes used to interpolate the solution over the time step. Thomas [Thomas, 1994] studied the three “classic” methods (Newmark, Houbolt, and Wilson- θ) and their applicability to the mooring dynamics problem. He concluded that Houbolt was the best choice.

In addition to Newmark and its variants which are popularly employed with finite element based models, researchers in the cable dynamics field have devised a variety of different schemes for the temporal integration problem. Chiou and Leonard [Chiou, 1979] used simple backward finite differences. Sun et al. [Sun Y,1998] used the generalized trapezoidal rule which is a first-order variant of the Newmark method. Sanders [Sanders V, 1988] used a computationally expensive but fourth-order accurate Runge-Kutta procedure.

In spite of all these developments, none of the previous studies related to two-part towing, considered the implementation of time integration procedures other than, the classical ‘BOX’ type scheme [Ablow, 1983]. In the BOX scheme, the governing equations are discretised on the half-grid point in both space and time. This method was first employed for the solution of tow cable dynamics by Ablow and Schechter [Ablow, 1983]. The BOX method has got

unconditional stability for the case of linear problems, but was subjected to phenomenon known as Crank-Nicolson noise [Gobat, 2000] in the solution space. Therefore, the present study considers the use of advanced time integration procedures such as HHT- α scheme and other classical variants like Newmark, Houbolt and Euler.

2.3 Parallel Computations

Due to the nonlinear characteristics of mathematical model (due to the presence of nonlinear drag forces) of underwater towing problems (see equation 3.3), the solver is heavily loaded, and it takes very large computational time even, with very few numbers of discretised nodes of the cables. As the serial programming has limitations in terms of computational speed, parallel computational approaches are adopted in this particular study. While, application of parallel computing is a common sight in numerical codes for the solution of fluid dynamic equations, most of the codes for the towing simulation are serially programmed. The present study employs shared memory based parallel computing techniques to solve the model equations of towing problems.

2.4 Verification of Numerical Model

Finally the developed numerical model needs to be verified by experimental methods. Early efforts of cable model validation involved experiments with very short cables (less than 5 m) with one end fixed, and either an anchor or a buoy attached to the other end. Chiou and Leonard [Chiou, 1979] used data from a submerged buoy given an initial disturbance to validate their cable model. Huston and Kamman [Kamman, 1999] validated their finite segment cable model using experimental data from a hanging chain and a submerged buoy. Delmer and Stephens [Delmer, 1983] and Palo et al. [Palo, 1995] used experimental ‘anchor last’ data to verify their respective lumped-mass cable models. Yamamoto et al. [Yamamoto,1996] validated their lumped-mass cable model using experimental data in the open ocean to depths of over 5000 m. Chapman [Chapman,1984] take the validation of the cable model one step further by validating a complete towed system. This system includes a tow point with prescribed motion and a passive towed body attached to the lower end of the cable. The dynamics model of the system showed good agreement with experimental tow tank data. Seto

et al. [Seto, 1999] went beyond this by including an actively controlled tow-fish, as well as the dynamics of the towing vehicle into their simulation. The simulation was then validated against experimental data.

While, a lot of previous studies, put efforts on the experimental verification of single point towing process, very few such initiatives are reported in the case of two-part towing. For the verification of the numerical model for the two-part towing system, Wu [Wu, 2001] devised an experiment which simulates the motion of the tow ship in a sinusoidal wave field and the corresponding heave and pitch responses of the towed vehicle were measured. The same experimental approach has been used in this particular study to validate the developed numerical model. The experiments were performed at offshore laboratory NIT, Kozhikode which is equipped with a model ship towing tank facility.

Mathematical Formulations: Cable and Towed Body

Contents	3.1	<i>Mathematical Modeling of Tow System</i>
	3.2	<i>Lumped Mass-Spring System Model (LMSM)</i>
	3.3	<i>Governing Equations</i>
	3.4	<i>Estimation of Drag Forces</i>
	3.5	<i>Implementation of the Boundary Condition</i>
	3.5.1	<i>Boundary condition at the depressor</i>
	3.5.2	<i>Boundary Condition at the junction of the three cables</i>
	3.6	<i>Initial Condition</i>
	3.7	<i>Finite Difference Implementation</i>
	3.8	<i>Kinematics and Dynamics of the Tow-Fish</i>
	3.8.1	<i>Motion Dynamics</i>
	3.8.2	<i>Kinematics of the Tow-point</i>

3.1 Mathematical Modeling of Tow System

Mathematical models for towed underwater systems can be categorised in several different ways. The most often cited distinguishing characteristic of such a model is the method used to discretise the physical system in space. As per that, the prevailing approaches fall into the categories of finite elements, finite differences, and lumped mass spring system (LMSM). The earliest numerical attempt to model this kind of systems was attributed to the work by Walton and Polachek [Walton, 1960]. They formulate the equations of motion for discrete elements and use centered finite differences to discretize the time derivative

terms and step the solution forward in time. With the addition of cable extensibility by Polachek *et al.* [Polachek, 1963], a remarkably complete treatment of the nonlinear time domain problem using LMSM existed as early as 1963. The terminology, lumped-mass-spring system arises from the lumping of the mass and externally applied forces at adjacent nodes which are joined by mass-less springs.

In contrast to the summation of forces approach used by lumped parameter methods, finite element methods derive their governing equations through principles of virtual work. One advantage of this approach is the possibility of a more sophisticated treatment of mass. Examples of such derivations include, McNamara [McNamara, 1988], Paulling and Webster [Webster, 1995]. The majority of state-of-the-art programs currently being used for riser modeling are based on finite elements.

A third approach is to write the continuous partial differential equations for force and moment balance and then apply a spatial discretisation scheme based on finite differences. Finally, the equations are solved in a nonlinear solver. This is the approach taken by Ablow and Schechter [Ablow and S. Schechter, 1983]. The present study employs LMSM as the spatial discretisation method to model the tow cable mathematically and is discussed in the next section in detail.

3.2 Lumped Mass-Spring System Model (LMSM)

In lumped-mass-spring-system approach, the cable is discretised as point masses joined together by mass-less elastic elements of finite length. The model has the following advantages over the other methods [Shan, 1994].

- Versatility: The LMSM has the advantage that it can be easily extended to other underwater towing problems that involve material nonlinearity for the cable; unsteady state, non-uniform cable and oscillatory current.
- Easy implementation of a variety of boundary condition.

Figure 3.1 shows the cable model discretised through LMSM. The governing equations of the same are described in the literature in detail [Shan, 1994]. The discretised cable model consists of many point masses and mass-less linearly elastic springs. All the forces along the cable are assumed to be concentrated at the mass points, which are numbered by i , which ranges from 1 to N . The lumped mass consists of mass of the cable as well as the

added mass, which will arise because, some mass of fluid is also accelerated by the cable due motion of the same in fluid.

The effect of added mass is assumed to be independent of the component of motion parallel to the cable segment due to small diameter of the cable. Thus, only when an element of the cable has transverse acceleration, does it possess additional inertia, whilst, if it is accelerated longitudinally, hydrodynamic force due to inertia was assumed negligibly small.

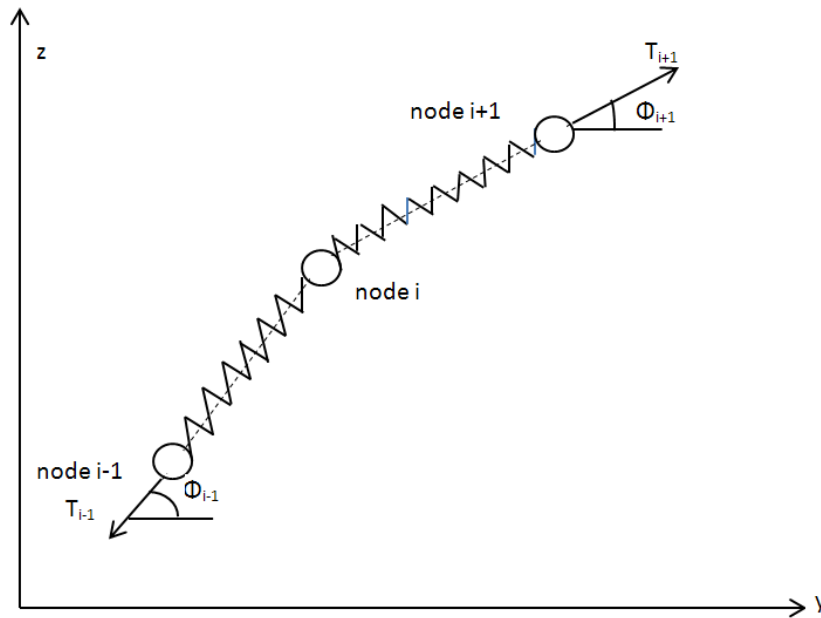


Figure 3.1 Lumped mass-spring cable model.

3.3 Governing Equations

The lumped mass at the i^{th} node is

$$m_i = \frac{1}{2}(m_{i+1} + m_{i-1}) \quad (3.1)$$

Where, m_{i+1} is the mass of the $i+1^{\text{th}}$ cable segment

m_{i-1} is the mass of the $i-1^{\text{th}}$ cable segment

By invoking Newton's laws of motion for the i^{th} node as shown in figure 3.1

$$m_i a_i = F_i \quad (3.2)$$

Where, m_i is the average mass of the two cable segments which lie on either side of the

node i , which includes the contribution of added mass also.

The matrix form of the equation 3.2 can be written as

$$\begin{bmatrix} A_{11} & A_{12} \\ A_{21} & A_{22} \end{bmatrix} \begin{bmatrix} \ddot{y}_i \\ \ddot{z}_i \end{bmatrix} = \begin{bmatrix} F_{yi} \\ F_{zi} \end{bmatrix} \quad (3.3)$$

Where

$$A_{11} = A_{22} = m_i + \frac{1}{2} \left[e_{i+1} (1 - \cos^2 \Phi_{i+1}) + e_{i-1} (1 - \cos^2 \Phi_{i-1}) \right] \quad (3.4)$$

e_{i+1} is the added mass for the $i+1^{\text{th}}$ cable segment.

e_{i-1} is the added mass for the $i-1^{\text{th}}$ cable segment.

Φ_{i+1} is the inclination of the cable segment above the node i with respect to the y axis as shown in figure 3.1.

$$A_{12} = A_{21} = -\frac{1}{2} (e_{i+1} \cos \Phi_{i+1} \sin \Phi_{i+1} + e_{i-1} \cos \Phi_{i-1} \sin \Phi_{i-1}) \quad (3.5)$$

The external forces acting on the node i along y and z direction (F_{yi} and F_{zi}) are given by

$$F_{yi} = T_{i+1} \cos \Phi_{i+1} - T_{i-1} \cos \Phi_{i-1} + F_{Dy} \quad (3.6)$$

$$F_{zi} = T_{i+1} \sin \Phi_{i+1} - T_{i-1} \sin \Phi_{i-1} + F_{Dz} - m_i g \quad (3.7)$$

T_{i+1} and T_{i-1} are the tension forces on the cable segments, which lie on the either side of the i^{th} node. Similarly F_{Dy} and F_{Dz} are the components of drag forces along y and z directions (see Appendix-I).

- k – Added mass coefficient,
- l - Length of the cable segment,
- σ cross-sectional area of the cable
- μ density of the cable
- ρ is the density of the fluid
- g the acceleration due to gravity.

The tension is determined from the elastic properties of the cable and deformation. Assuming the cable to be linearly elastic and by utilizing the hooks law, the cable tensions at either side of the node i namely T_{i+1} and T_{i-1} can be estimated (see Appendix -I)

3.4 Estimation of Drag Forces

The hydrodynamic drag on the i^{th} node is expressed as one half of each drag acting on the two segments lying on either side of that node. The drag on each segment was resolved into two components, namely the normal component and tangential component each as a function of relative velocity in that direction.

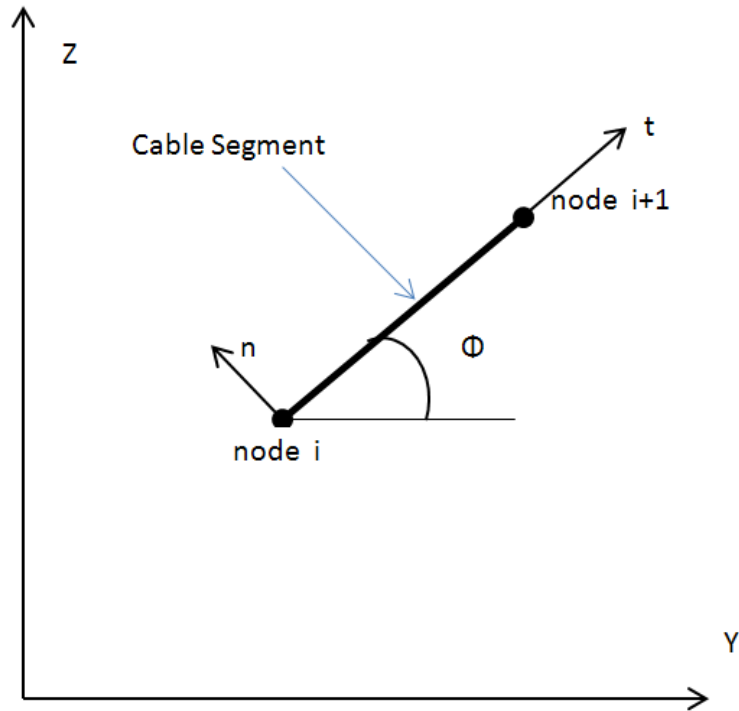


Figure 3.2. Components of Drag forces on the cable

Figure 3.2 shows two orthogonal co-ordinate systems [Y-Z] which is earth fixed and [t-n] which moves with the cable segment. The relation between these two co-ordinates systems are defined by the Euler angle Φ .

$$(t, n) = (j, k)[D] \quad (3.8)$$

Where the transformation matrix $D = \begin{bmatrix} cp & sp \\ -sp & cp \end{bmatrix}$ and $sp = \sin(\Phi)$ $cp = \cos(\Phi)$

The average drag acting on node i is given by

$$F_D^i = 1/2 (F_D^{i+1} + F_D^{i-1})$$

Where F_D^{i+1} and F_D^{i-1} are the drag forces acting on cable segments which lie on either side of the node i (For drag expression see Appendix-I).

3.5 Implementation of the Boundary Condition

Boundary condition must be given at the top end of the primary cable, at the depressor and at the tow-fish. Additional boundary condition must be enforced at the junction of the three cables. Assuming the dynamic load on the vessel because of the tow-system is negligible compared with the other loads acting on the vessel; it may be possible to decouple the dynamic motion of the vessel from the motion of the cable system. Thus the boundary condition at the top end was determined by the dynamic motion at the tow-point.

3.5.1 Boundary Condition at the Depressor

The depressor was assumed to be weighted ball. S_y and S_z are the projected area of the depressor along the plane perpendicular to Y and Z-axis respectively. C_{dy} and C_{dz} are the corresponding drag coefficients. The equation of motion for the depressor is formed based on the Newton-Euler formulation

$$\begin{bmatrix} a_{11} & a_{12} \\ a_{21} & a_{22} \end{bmatrix} \begin{bmatrix} \ddot{y}_o \\ \ddot{z}_o \end{bmatrix} = \begin{bmatrix} F_{y0} \\ F_{z0} \end{bmatrix} \quad (3.9)$$

Where the vector $[y_0, z_0]$ describes the position of the depressor with respect to the earth fixed co-ordinate system. $[F_{y0}, F_{z0}]$ is the vector of external forces acting on the depressor.

Also $a_{11} = M_0 + m_0 + M_{ay}$

$a_{22} = M_0 + m_0 + M_{az}$

$a_{12} = a_{21} = 0$

Where m_0 = mass of the cable segment connected to the depressor.

M_0 = mass of the Depressor.

M_{ay} and M_{az} are the contribution of added mass of the depressor along Y and Z direction respectively.

$$F_{y0} = T_0 \cos \Phi_0 + F_{dy} + D_y \quad (3.10)$$

$$F_{z0} = T_0 \sin \Phi_0 + F_{dz} + D_z - (M_0 + m_0)g + F_{\text{Depressor buoyancy}} \quad (3.11)$$

D_y and D_z are the Y and Z Component of drag on the depressor. The symbol ϕ_0 is the inclination of cable segment connected to the depressor with the horizontal. F_{dy} and F_{dz} are the y and z components of the drag on the connecting cable segment to the depressor. The boundary condition imposed at the tow-fish side is discussed in section 3.7.

3.5.2 Boundary Condition at the Junction of the Three Cables

The application of boundary condition at the junction of the three cables (primary, secondary and depressor cables, see figure 1.1b) is described in this section. Invoking Newton's law at the junction of the three cables as shown in figure 3.3

$$\begin{bmatrix} m_i & 0 \\ 0 & m_i \end{bmatrix} \begin{bmatrix} \ddot{y}_i \\ \ddot{z}_i \end{bmatrix} = \begin{bmatrix} F_{y_i} \\ F_{z_i} \end{bmatrix} \quad (3.12)$$

The right hand side of the equation is obtained by taking

$$\sum F_{y_i} = T_{i+1} \cos \Phi_{i+1} - T_{i-1} \cos \Phi_{i-1} - T_{n+1} \cos \Phi_{n+1} \quad (3.13)$$

$$\sum F_{z_i} = T_{i+1} \sin \Phi_{i+1} - T_{i-1} \sin \Phi_{i-1} - T_{n+1} \sin \Phi_{n+1} \quad (3.14)$$

Where, m_i = average of mass of primary, secondary and depressor cable segments connected to node i.

T = tension in the cable.

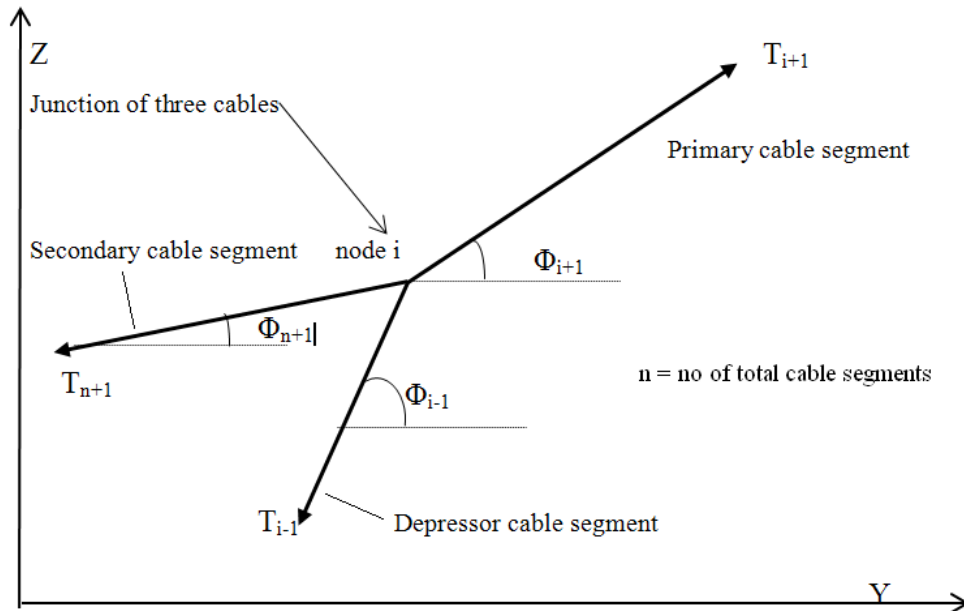


Figure 3.3 Boundary condition at the junction of the three cables

3.6 Initial Condition

To complete the formulation, a set of initial condition must be specified for each node in the line. This includes both initial position and initial velocities, as required second order ordinary differential equations.

$$y_i = a, \quad \dot{y}_i = b, \quad z_i = c, \quad \dot{z}_i = d \quad \text{For all } i = 0, 1, 2, \dots, n; \quad (3.15)$$

Where the vector $[a, c]$ denotes initial position and $[b, d]$ is the initial velocity of the cable segment.

3.7 Finite Difference Implementation

The time domain is divided into a set of discrete steps $t = j\delta t$, ($j = 1, 2, 3, \dots$). Assuming nodal position, velocity and acceleration are known at previous time step $t = j\delta t$, the question is how to find out the unknowns at the next time step $t = (j+1)\delta t$ through the governing equations complemented by boundary condition.

$$\ddot{y} = \frac{1}{\Delta t^2} (y_i^{j+1} + y_i^{j-1} - 2y_i^j) \quad \ddot{z} = \frac{1}{\Delta t^2} (z_i^{j+1} + z_i^{j-1} - 2z_i^j) \quad (3.16)$$

$$\dot{y} = \frac{1}{\Delta t} (y_i^j - y_i^{j-1}) \quad \dot{z} = \frac{1}{\Delta t} (z_i^j - z_i^{j-1}) \quad (3.17)$$

Substituting above equations in equation 3.4b we will get the final equation of motion and by solving the same it is possible to get the real-time nodal positions of the cable segments. The tension is calculated by equation 3.8a and equation 3.8b. The assembled equations are solved using a nonlinear solver which uses Newton-Krylov method.

3.8 Kinematics and Dynamics of the Tow-Fish

The kinetic and kinematic equations of motion are derived based on a right-handed orthogonal coordinate system, which is fixed, at the center of buoyancy of the body. This is assumed to be approximately, at the geometric center of the body. Also, rigid body dynamics is assumed throughout. The equations of motion of the same are discussed in literature [Thor I Fossen, 1994].

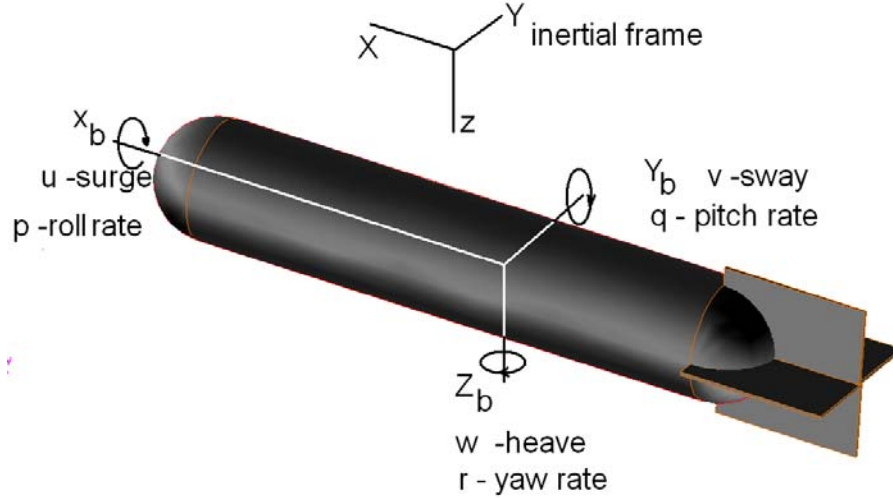


Figure 3.4. Degrees of freedom of a generic towed body

Figure 3.4 shows the possible motions of a towed body. This includes three rotary motions namely pitch, heave and roll and three translator motions namely surge, heave and sway. As shown in the figure axes x_b and z_b lie in the plane of symmetry containing the rudder. The x_b axis points out of the nose; y_b axis completes the right-handed reference frame. Thus two coordinate frames are used: one body fixed and the other global inertial reference frame.

The variable $X_I = [x, y, z]^T$ is the tow-fish position relative to an inertial frame,

$\Phi_I = [\phi, \theta, \psi]^T$ are the Euler angles representing the tow-fish attitude with respect to the inertial frame.

$V = [u, v, w]^T$ is the tow-fish velocity represented in the body fixed frame

$\Omega = [p, q, r]^T$ is the tow-fish angular velocity with respect to the axes represented in the body fixed frame.

The state of the towed body can be written as follows

$$X = [X_I, \Phi_I, V, \Omega]^T \quad (3.18)$$

The transnational kinematic equation is

$$\dot{X}_I = RV \quad (3.19)$$

Where

$$R = \begin{bmatrix} c\psi c\theta & -s\psi c\theta + c\psi s\theta s\phi & s\psi s\theta + c\psi c\theta s\phi \\ s\psi c\theta & c\psi c\theta + s\psi s\theta s\phi & -c\psi s\theta + s\psi c\theta s\phi \\ -s\theta & c\theta s\phi & c\theta c\phi \end{bmatrix} \quad (3.20)$$

Where symbol s, c and t means sine, cosine and tangent respectively. The rotational kinematic equation is

$$\begin{bmatrix} \dot{\phi} \\ \dot{\theta} \\ \dot{\psi} \end{bmatrix} = \begin{bmatrix} 1 & s\phi t\theta & c\phi t\theta \\ 0 & c\phi & -s\phi \\ 0 & s\phi/c\theta & c\phi/c\theta \end{bmatrix} \begin{bmatrix} p \\ q \\ r \end{bmatrix} \quad (3.21)$$

3.8.1 Motion Dynamics

The dynamic equation of motion of the towed body was formulated using Kirchoff's equation of motion. Kirchoff's equation for motion of a rigid body in an ideal fluid, generalized to include exogenous forces and torques, are given by [Eric M, 2004]

$$\begin{bmatrix} M & D^T \\ D & J \end{bmatrix} \begin{bmatrix} \dot{V} \\ \dot{\Omega} \end{bmatrix} = \begin{bmatrix} MV + D^T \Omega + F_{\text{ext}} \\ (J\Omega + DV) \times (MV + D^T \Omega) \times V + M_{\text{ext}} \end{bmatrix} \quad (3.22)$$

F_{ext} and M_{ext} are the external force and moment vector acting on the towed body and are explained in Appendix-I. Equation 3.22 represents the final equation of motion of the tow-fish. The matrix D represents the inertial coupling between the translational and rotational motion [Eric M, 2004]. The matrix M and J represent mass and the rotational inertia matrix and is discussed in Appendix-I.

3.8.2 Kinematics of the Tow-point

To couple the dynamics of the tow fish to that of the cable system, kinematic relations has to be derived. These relations are obtained by transforming the velocity components of the cable end to the local coordinate system fixed to the body. This velocity is subsequently equated with the velocity of the tow point. Figure shows the different type of towing configuration. It can be seen that type 1 is the most general and is considered in the present study.

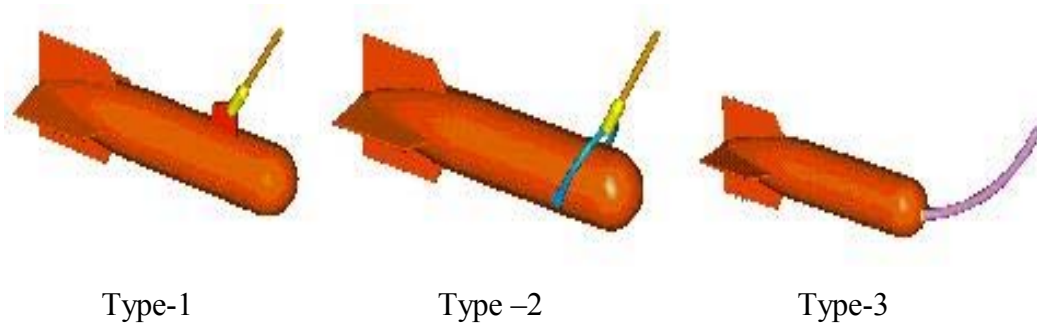


Figure 3.5 Different types of tow-point configuration

The connecting equation for the cable termination and tow point of the body was given by

$$\mathbf{V} + \boldsymbol{\Omega} \otimes \mathbf{r} = \mathbf{R}\mathbf{V}_{\text{cabletowpoint}} \quad (3.23)$$

Where, \mathbf{R} is the matrix to transform kinematic parameters from cable tow-point to local co-ordinate fixed on the towed body and \mathbf{r} is the position vector of the tow point with respect to local co-ordinate system. The symbol \otimes denotes cross product and \mathbf{V} is the linear velocity vector of the towed body with respect to body fixed frame.

Improved Lumped-Mass-Spring Model

Contents	4.1	<i>Time Discretisation Procedure</i>
	4.2	<i>Characteristics of Time Integration Schemes</i>
	4.2.1	<i>Stability</i>
	4.2.2	<i>Number of implicit systems to be solved</i>
	4.2.3	<i>Accuracy</i>
	4.2.4	<i>Numerical dissipation</i>
	4.2.5	<i>Self-starting</i>
	4.2.6	<i>Overshooting</i>
	4.3	<i>Time integration schemes</i>
	4.3.1	<i>Houbolt's Scheme</i>
	4.3.2	<i>NewMark's method</i>
	4.3.3	<i>Box Method</i>
	4.3.4	<i>HHT-α method</i>
	4.4	<i>Implementation of HHT-Alfa Method in LMSM</i>
	4.5	<i>Improved Bending Rigidity formulation for LMSM</i>

The chapter discusses about the two improvements that are made for traditional LMSM viz, the implementation of advanced time integration schemes for overall enhancement of the stability of the numerical scheme and second is the inclusion of bending rigidity in the cable formulation. A modified beam model which uses only translational degrees of freedoms for solving beam equation has been implemented in this particular study. This would avoid the assemblage of rotational degrees of freedom for the solution of equation of motion. The time discretization procedure is discussed first.

4.1 Time Discretisation Procedure

Numerical models for towing systems require the discretisation of the physical system in time and space. The resulting equations are typically written as a non-linear matrix equation known as the semi-discrete equation of motion, because the time derivatives of the vector of dependent variables are left as continuous functions.

$$M\ddot{x} + C\dot{x} + Kx = F(t) \tag{4.1a}$$

Where x denotes three dimensional space and F is the external force vector. The equations of motion for LMSM are most often presented in matrix form as a system of second-order ordinary differential equations with time as one of the independent variable. Therefore, the solution needs to progress over time with the help of a suitable time integration scheme. Most temporal integration schemes in use today have their roots in the method developed by Buckham and Nahon [Buckham, *et.al*, 1999]. These methods are broadly classified into single step and multi-step methods. Single step methods are attractive because of their computational simplicity and are selected throughout of this study. The main objective of these schemes is to provide an optimum blend of numerical diffusion to damp out high frequency oscillations in the solution and preserve low frequency modes without loss of accuracy. Hughes and Belytschko [Ted Belytschko, *et.al*, 1983] provide a summary of the development of these types of methods in the context of linear finite element structural dynamics. Most classical methods can now be cast into unified multi-parameter integration schemes where an adjustment in the parameters leads to one of several different methods with different numerical properties. Thomas [Thomas, 1994] studied the three “classic” methods (Newmark, Houbolt, and Wilson) and their applicability to the mooring dynamics problem.

In addition to Newmark and its variants which are widely employed with finite element based models, researchers in the cable dynamics field have employed a variety of different schemes for the temporal integration problem. Chiou and Leonard [Chiou, 1979] use simple backward finite difference method. Sun et al. [Sun Y, 1998] use the generalized trapezoidal rule which is a first-order variant of the Newmark method. Paulling and

Webster [Pauling, 1996] use the Adams-Moulton method, which in first-order form reduces to the trapezoidal rule. Sanders [Sanders V, 1988] used a computationally expensive but fourth-order accurate Runge-Kutta procedure.

The most popular time/space discretisation scheme used in the solution of underwater towing problems is the ‘Box’ method, in which the governing equations are discretised on the half-grid point in both space and time. This method was first employed for the solution of tow- cable dynamics by Ablow and Schechter [Ablow,1983]. Since then it has been widely employed in both towing and mooring applications [Howell ,1992]. Single step family of time integration methods were widely used in the solution of towing/mooring dynamics problems [Gobat,2000], though, most of them are less accurate than LMS (linear multi-step) methods such as Adam-Badsforth one. The reason may be the requirement of more computational storage of the historical time step data.

4.2 Characteristics of Time Integration Schemes

While, there is not yet a universally accepted “perfect” time integration method, Hilber and Hughes (1978) gave a list of characteristics that a marching scheme should possess in order to be competitive and efficient:

1. Unconditional stability when applied to linear problems: Unconditional stability allows the time step to be chosen based on accuracy and resolution concerns, without regard for purely numerical issues.
2. No more than one set of implicit equations to be solved at each time step: This minimizes computational expense compared to schemes which may achieve a high order of accuracy at a significant computational cost.
3. At least second-order accuracy: This is a reflection of the constraints imposed by Dahlquist’s theorem which states that a third-order accurate method with the most appropriate stability conditions does not exist. Again, without a significant increase in computational effort, second-order accuracy is the best we can do.
4. Controllable algorithmic dissipation in the higher modes: In some cases with sufficiently small temporal and spatial discretisation, it may be desirable to have less high frequency numerical dissipation.
5. Self-starting, no information is needed prior to time step zero: Accuracy at time step zero (and thus accurate algorithm starting information) is critical in transient analysis

applications. It is less important in cases where we can slowly ramp up a forcing scenario and are not concerned with start-up transients.

4.2.1 Stability

An integration scheme is said to be stable if the numerical solution, under any initial conditions, does not grow without bound [Bathe, 1998]. An algorithm is unconditionally stable for linear problems if the convergence of the solution is independent of the size of the time step Δt . Otherwise the algorithm is conditionally stable for values of Δt less than a critical value Δt_{cr} . The value of the critical time step is equal to a constant multiplying the smallest natural period of the system and it depends also on the material damping of the system. Therefore, unconditionally stable schemes are generally preferred, as in that case the size of the time step is determined only by the accuracy of the solution. Furthermore, all integration schemes can be classified as either explicit or implicit methods. The great advantage of explicit schemes is that the solution does not involve the inversion of the stiffness matrix. However, Dahlquist [Dahlquist,1973] demonstrated that all explicit methods are conditionally stable with respect to the size of the time step. On the other hand most implicit integration methods are unconditionally stable, but the inversion of the stiffness matrix at each time step makes them computationally expensive.

4.2.2 Number of Implicit Systems to be Solved

Hilber and Hughes [Hughes, 1987] suggest that the algorithm should not require the solution of more than one implicit system, of the size of the mass and stiffness matrices, at each time step. Although, algorithms that require two or more implicit systems of the size of the mass and stiffness matrices to be solved at each time step possess improved properties (e.g. [Argyris et al,2000]), they require at least twice the storage and computational effort of simpler methods.

4.2.3 Accuracy

Another parameter that comes next to stability in terms of importance is the accuracy of the numerical scheme. In general, the accuracy depends on the size of the time step. The smaller the time step, the more accurate is the solution. An integration scheme is convergent if the numerical solution approaches the exact solution as Δt tends to zero. According to Hilber and Hughes [Hughes, 1987] the second order accurate methods are immensely

superior to the first order accurate methods. Furthermore, Dahlquist theorem suggests that a third order accurate unconditionally stable linear multistep method does not exist [Hughes, 1987].

4.2.4 Numerical dissipation

The necessity for time integration algorithms to possess numerical damping is widely recognized. Due to poor spatial discretization, the most of the approximate methods like finite difference one, cannot represent accurately at high-frequency modes. Strang and Fix [Strang, 1986], and others, showed that modes corresponding to higher frequencies become more and more inaccurate. Thus, the role of the numerical damping is to eliminate spurious high frequency oscillations. Specifically in underwater towing problems, the highest modes of the system do not have to be represented in an accurate way, since the excitation from external disturbances such as waves etc, are operating at low frequency modes. Therefore, a desirable property of an algorithm is the preferential numerical damping (“filtering”) of the inaccurate high frequency modes and the preservation of the important low frequency modes.

Another way to filter the higher modes could be the use of viscous damping. However, Hughes [Hughes, 1987] argues that the use of viscous damping affects a middle band of frequencies, not the inaccurate higher frequency modes. Therefore, the only adequate way to damp out the spurious modes is the use of controllable algorithmic damping.

4.2.5 Self-starting

Integration schemes which are not self-starting require data from more than two time steps to proceed the solution. In this case, the standard practice is to assume the initial conditions. Thus, apart from the algorithm, a starting procedure should be implemented and analysed. Obviously, this requires additional computational effort and storage. Thus self-starting algorithms are generally preferred.

4.2.6 Overshooting

The term overshooting describes the tendency of an algorithm (for large time steps) to exceed heavily the exact solution in the first few time steps, but eventually to converge to the exact solution. This peculiar phenomenon was first discovered by Goudreau and Taylor [Goudreau, 1992] as a property of the Wilson θ -method and is not related to the stability

and accuracy characteristics of the algorithms discussed so far. The overshoot in displacement and velocity is a common phenomenon. Low overshoot is preferred particularly when accurate transient dynamic analysis is to be carried out.

4.3 Implementation of Time integration schemes

While numerous time marching schemes are available, only some of the most popular are presented and implemented in this thesis. These are implicit form of Houbolt, Newmark, HHT- α and Euler [Hughes, 1987]. All these schemes are implemented in LMSM formulation and studied their performance in terms of accuracy and compared with experimental values from literature [Wu, 2002]. (See Chapter 6 section 6.3)

4.3.1 Houbolt Scheme

Houbolt method was one of the earliest algorithms to include numerical dissipation in the equation of motion for the benefit of asymptotic annihilation in which the high-frequency response is nearly annihilated in one time step [Hughes, 1987]. The Houbolt method has been available in numerous commercial finite element codes because of its asymptotic annihilation property which has been found to very useful to stabilize computations involving highly nonlinear phenomena. While the original scheme is a two-step procedure, the present study focused of single step Houbolt (SSH) method discussed in literature [Hughes, 1987]. The method is outlined by equations A2.1-A2.5 (Appendix –II).

The recommended value for controlling parameter of the scheme, γ is 3/2 to minimize velocity error and 1/2 to avoid velocity overshoot [Hughes, 1999]. From a stability and accuracy point of view, it is unconditionally stable, second order accurate and is not suitable for high frequency dynamic problems [Zhou, 2004].

4.3.2 NewMark's method

Newmark [Hughes, 1987] proposed what has become one of the most popular family of algorithms for the solution of problems in structural dynamics. The method is outlined by equations A2.6-A2.8 (Appendix –II). β and γ are the controlling parameters in the scheme. The method is implicit, and unconditional stability is guaranteed for $\beta=1/4$ and $\gamma=1/2$ [Hughes, 1987]. The trapezoidal rule is a particular case of this family, for which $\beta=1/4$ and $\gamma=1/2$. This case also corresponds to the assumption that the acceleration is constant over

the time interval $[t_n, t_{n+1}]$ and equal to $(a_n + a_{n+1})/2$. This method is also known as the average acceleration method. The method is discussed in appendix-II.

4.3.3 Box Method

Box method is the most widely used scheme for the solution of underwater towing and mooring dynamics which uses finite difference discretisation for the equation of motion. In the box method, the governing equations are discretised on the half-grid point in both space and time. This method was first employed for the solution of tow cable dynamics by Ablow and Schechter [Ablow, 1983]. The box method has got unconditional stability for the case of linear problems, but has subjected to phenomenon known as Crank-Nicolson noise [Gobat, 2000], whereby the high frequency components of the solution oscillate with every time step. In a linear problem, this noise can be removed by computing step-to-step averages after the solution is completed. For a nonlinear problem, however, the noise can be a source of instability and hence should be eliminated as the solution progresses. Given the stability problems associated with the box method, a new solution method is sought for the dynamic analysis using lumped mass spring formulation.

4.3.4 HHT- α method

Hilber, Hughes and Taylor (1977) introduced generalization of Newmark method in order to achieve controllable algorithmic dissipation of the high frequency modes. A slightly modified version of the HHT scheme, which was suggested by Hughes, is examined in the present study. The method employs Newmark equations for displacement and velocity variations. The scheme is discussed in appendix-II (eq A2.10-2.12). The main parameter which controls the scheme is α . If $\alpha=0$ the equations reduces to that of Newmark's method. It has been found that if the parameters are selected such that $\alpha = [-1/3, 0]$ and $\gamma = (1-2\alpha)/2$ and $\beta = (1-\alpha^2)/4$ an unconditional stable, second order accurate scheme results. Decreasing α may result in the increase of the numerical dissipation.

4.4 Implementation of HHT- α Method in LMSM

By neglecting fluid damping and considering force balance equations for the i^{th} node in a cable segment in two dimensional spaces as an example, lumped mass formulation gives

$$m_i \ddot{y}_i - (T_{i+1} \cos \phi_{i+1} - T_{i-1} \cos \phi_{i-1}) = F_{yi} \quad (4.13)$$

$$m_i \ddot{z}_i - (T_{i+1} \sin \phi_{i+1} - T_{i-1} \sin \phi_{i-1}) = F_{z_i} \quad (4.14)$$

This can be reduced into more general form

$$M a^{n+1} + (1 + \alpha) K d^{n+1} - \alpha K d^n = F(t_{n+\alpha}) \quad (4.15)$$

Where M, K and F are mass, stiffness matrix and external force vector respectively (See Appendix-II).

Assuming fluid damping not present the stiffness matrix becomes

$$K^n = \begin{bmatrix} \frac{T_{i+1} \cos \alpha_{i+1}}{y_i} & \frac{T_{i-1} \cos \alpha_{i-1}}{z_i} \\ \frac{T_{i+1} \sin \alpha_{i+1}}{y_i} & \frac{T_{i-1} \sin \alpha_{i-1}}{z_i} \end{bmatrix}^n \begin{bmatrix} y_i \\ z_i \end{bmatrix}^n \quad K^{n-1} = \begin{bmatrix} \frac{T_{i+1} \cos \alpha_{i+1}}{y_i} & \frac{T_{i-1} \cos \alpha_{i-1}}{z_i} \\ \frac{T_{i+1} \sin \alpha_{i+1}}{y_i} & \frac{T_{i-1} \sin \alpha_{i-1}}{z_i} \end{bmatrix}^{n-1} \begin{bmatrix} y_i \\ z_i \end{bmatrix}^{n-1} \quad (4.16)$$

$$T_{i+1} = \left(\frac{[(y_{i+1} - y_i)^2 + (z_{i+1} - z_i)^2]^{1/2} - l_{i+1}}{l_{i+1}} \right) EA \quad (4.17a)$$

$$T_{i-1} = \left(\frac{[(y_i - y_{i-1})^2 + (z_i - z_{i-1})^2]^{1/2} - l_{i-1}}{l_{i-1}} \right) EA \quad (4.17b)$$

$$\text{Where} \quad M = \begin{bmatrix} m_i & 0 \\ 0 & m_i \end{bmatrix} \quad (4.18)$$

The right hand side of equation 4.15 consists of forces like gravitational, drag, buoyancy forces etc. Out of these gravitational and buoyancy force are constant over time. But drag forces depend on the instantaneous velocity.

The time domain is divided into a set of discrete steps $t = j\delta t$ ($j = 1, 2, 3, \dots$). Assuming solution parameters are known at the previous time step $t = j\delta t$, the question is how to find out the unknowns at the next time step $t = (j+1)\delta t$. The equation 4.15 is solved for instantaneous acceleration first by assembling the stiffness and mass matrices. Subsequently the displacement and velocity vectors are corrected using equation 4.11 and 4.12. This procedure was repeated till the last time step.

4.5 Improved Bending Rigidity formulation for LMSM

Out of the various LMSM formulations for the cable, the method proposed by Shan Huang [Shan, 1994] is the most promising. But the limitation is that it does not have bending

rigidity in the cable formulation. Therefore the model is best suited for long cables having small diameter (i.e. negligible bending rigidity). But in the case of two-part towing, this cannot be ignored as secondary and depressor cables are considered to be very short compared to primary cable. Hence the present study attempts to include the bending rigidity in the cable formulation using LMSM.

Figure 4.1 shows a small segment of the cable. In segmental formulation the independent variables to be considered are rotational (moment M and slope at the two ends θ_1 and θ_2) and translational (space, tension T) ones. Subsequently, it is necessary to assemble translational and rotational equilibrium equations to get real-time position and slope of the cable segments. In the modified beam model all the degrees of freedom are of translational type. Thus, the equations to be assembled remain to be that of translational degrees of freedom rather than rotational and translational mix. The formulation has been discussed in detail in the literature [Wasfy, 2000] where it was mainly used to simulate the flexible dynamics of spatial mechanisms.

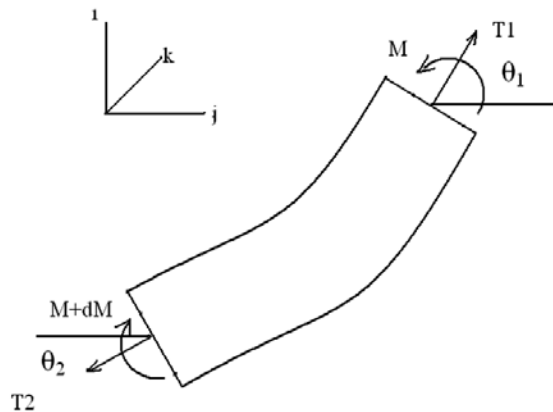


Figure 4.1. Cable Segment

Suppose we have an originally undeformed straight beam of length l (figure 4.2). Let x be the co-ordinate along the neutral axis of the undeformed beam and y be the co-ordinate of the transverse distance between the original undeflected shape of the beam and the deformed shape. The total strain energy neglecting the shear deformation of the beam according to the Euler beam theory is given by

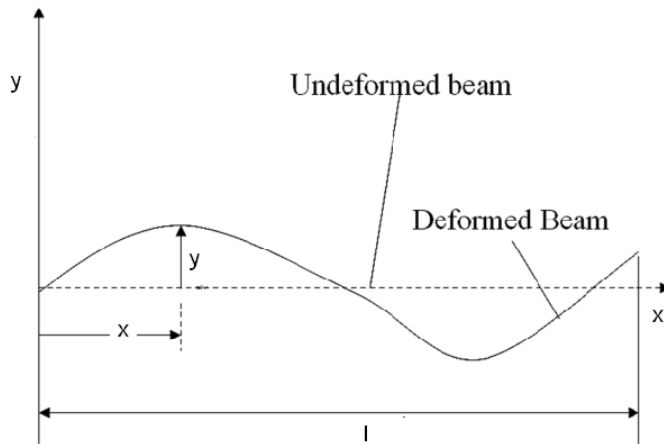


Figure 4.2 Deformed beam

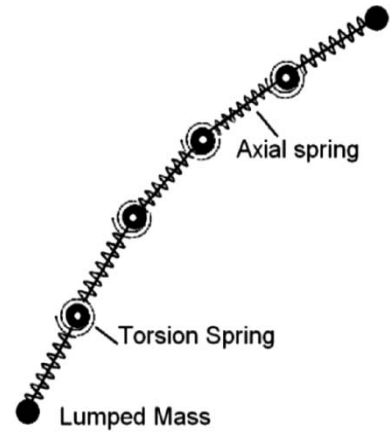


Figure 4.3 Improved cable mod

$$\text{Strain energy, } SE = \int_0^l \frac{M^2}{2EI} dx \quad (4.19)$$

Where E is the Young's modulus, I is the moment inertia of the cross-section in the transverse direction and M is the bending moment. To obtain the axial response of the modified element, two truss elements are inserted between nodes 1 and 2 and nodes 2 and 3 (Figure 4.4). Subsequently, a torsion spring was inserted at node 2 to provide bending rigidity. Hence the improved cable model is shown in the figure 4.3.

Wasfy [Wasfy, 2000] has shown that

$$\text{Strain energy} \quad SE = \frac{EI}{6} (3la^2 + 3abl^2 + b^2l^3) \quad (4.20)$$

$$\text{The coefficients a and b are} \quad a = \frac{2}{l^2} (\alpha_1 + \alpha_2)(l_1 - 2l_2) \quad (4.21)$$

$$b = \frac{6}{l^3} (\alpha_1 + \alpha_2)(l_2 - l_1) \quad (4.22)$$

The symbols α_1 and α_2 represents the inclination of cable segment 1-2 and 2-3 with respect to horizontal as shown in figure 4.4.

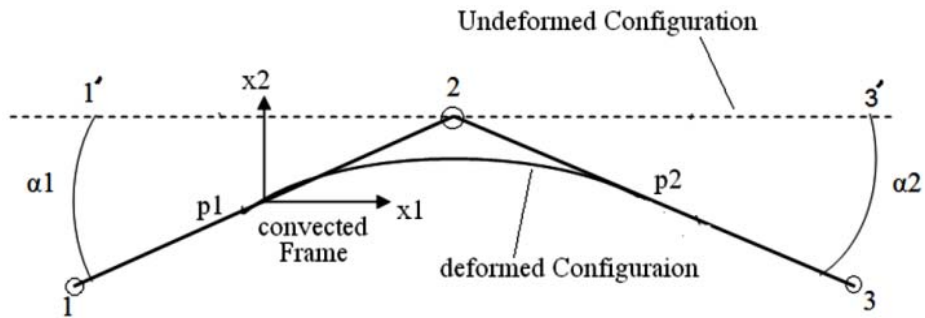


Figure 4.4 Schematic beam model

Where l_1 is the distance between nodes 1 and 2. Similarly $l_2 =$ distance 2-3

Assuming $l_1 = l_2 = l/2$ and $\alpha_1 = \alpha_2 = \alpha/2$;

$$SE = \frac{1}{2} \left(\frac{EI}{l} \right) (\alpha^2) \quad (4.23)$$

This equation represents strain energy stored in a torsion spring with stiffness k_b given by

$$k_b = EI/l \quad (4.24)$$

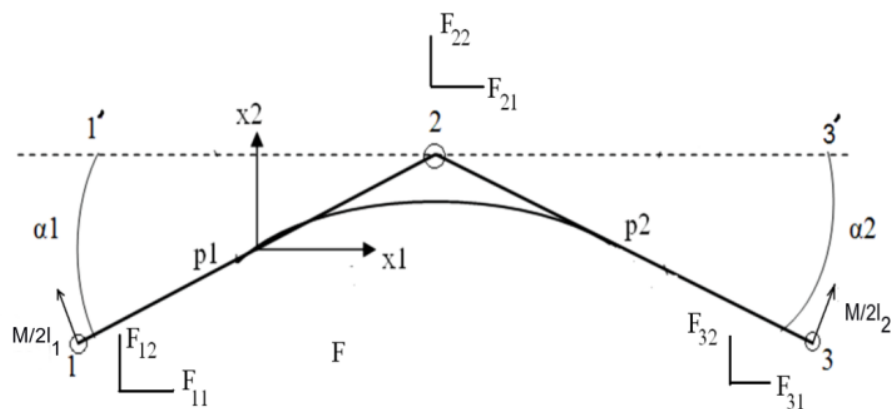


Figure 4.5 Equivalent nodal forces

The equivalent lumped nodal forces due to moment produced at the nodes are given by

$$\mathbf{F}_i^e = \begin{Bmatrix} F_{1,1} \\ F_{1,2} \\ F_{2,1} \\ F_{2,2} \\ F_{3,1} \\ F_{3,2} \end{Bmatrix} = M/2 \begin{Bmatrix} \sin(\alpha_1)/l_1 \\ \cos(\alpha_1)/l_1 \\ -\sin(\alpha_1)/l_1 + \cos(\alpha_2)/l_2 \\ -\cos(\alpha_1)/l_1 + \cos(\alpha_2)/l_2 \\ -\sin(\alpha_2)/l_2 \\ \cos(\alpha_2)/l_2 \end{Bmatrix} \quad (4.25)$$

The free body diagram with equivalent nodal forces is shown in figure 4.5. These nodal forces are attributed to rotational moments and are assembled on the right hand side of the translational equations of motion for the cable.

Numerical Solution to Hydrodynamic Equations

Contents	5.1	<i>Previous and Related Studies</i>
	5.2	<i>Present Contributions</i>
	5.3	<i>Governing Equations</i>
	5.4	<i>Turbulence Modeling</i>
	5.4.1	<i>SST-K-Ω Turbulence Model</i>
	5.5	<i>Finite Volume Discretisation</i>
	5.6	<i>Discretisation of Convective Term</i>
	5.7	<i>Diffusion Term</i>
	5.8	<i>Source Term</i>
	5.9	<i>Velocity-Pressure Coupling</i>
	5.10	<i>Implementation of Physical Boundary Conditions</i>
	5.11	<i>Latest Convection Differencing Schemes</i>
	5.12	<i>NV Approach for Unstructured Meshes</i>
	5.13	<i>Node based formulation</i>
	5.14	<i>Development of New Convection Interpolation Scheme (BNCUS)</i>
	5.15	<i>Solution Techniques for Systems of Linear Algebraic Equations</i>
	5.16	<i>Test cases</i>
	5.17	<i>Gradient estimation</i>
	5.18	<i>Blended Node and cell based Formulations</i>
	5.19	<i>Hydrodynamic Analysis of the tow-fish hull</i>
5.20	<i>Conclusion</i>	

In this chapter, the theoretical framework, which are necessary for solving fluid dynamics equations, for the estimation hydrodynamic parameters like drag, lift etc, of the towed body is detailed. Accurate estimation of these parameters was essential, for the subsequent full-hydro-structural analysis of the two-part towing system. The hydrodynamic equations are discretised and solved using finite volume techniques (FVM) as the methodology is gaining importance in this area, compared to finite element (FEM) methods [Peric M,1995]. A dedicated CFD solver has been developed for this purpose and subsequently tested. Finally the drag, lift and pitching moments of the tow body are estimated by using the developed computer code.

5.1 Previous and Related Studies

The computer simulation of a fluid flow process is a two-step procedure, viz modeling of convective flow process and diffusive one. While, convective flow process has got the direction of mean flow, diffusive one is directionless. The majority of fluid flows encountered in nature and industry are characterised by high Reynolds numbers, implying the dominance of convective effects [Vidwans, 1994]. Despite a great deal of work on the development and application of the discretisation schemes for the convective flow processes over the last few decades, no ideal scheme has yet emerged. Such ideal scheme would be one that minimizes numerical diffusion, eliminates spurious oscillations, capable of capturing peaks/troughs, robust, easy to implement, and resolves shock waves [Hrvoje Jasak, 1996]. So, research in this field continues to be relevant.

The principal problem in the discretisation of the convective terms is the calculation of the value of transported property at control volume faces and its convective flux across these boundaries. Earliest attempts in this direction lead to the development of central difference scheme (CDS), upwind difference scheme (UDS) etc. In the framework of the second-order accurate FVM, CDS work quite well in smooth regions but witness the undesirable severe oscillations around discontinuity. In order to achieve stability a lot of research has been done which are falling into one of the following categories.

- Locally analytical schemes: Although, bounded and somewhat less diffusive than UDS,

their accuracy in 2-D and 3-D is still inadequate [Hrvoje Jasak,1996].

- Upwind-biased differencing schemes, including first-order Upstream-weighted differencing [Patankar, 1981], and Leonard's QUICK differencing scheme [Leonard, 1988]. The amount of numerical diffusion is somewhat smaller than for UD, but boundness is not preserved.
- Switching schemes. In his Hybrid Differencing scheme, Spalding [Spalding, 1972], recognises that the sufficient boundedness criterion holds even for Central Differencing if the cell Peclet number(Pe) is smaller than two. Under such conditions, Hybrid Differencing prescribes the use of CD, while UD is used for higher Pe-numbers in order to guarantee boundedness. However, in typical flow situations, the Pe-number is considerably higher than two and the scheme reduces to UD in the bulk of the domain.

The quest for bounded and accurate differencing schemes continues with the concept of flux limiting eventually resulted in the evolution of Total Variation Diminishing (TVD) differencing schemes. TVD schemes have been developed by Harten [Harten, 1984], Roe [Roe, 1985], Chakravarthy and Osher [Chakravarthy, et.al, 1983] and others in which a blending factor (limiter) has been devised. The flux was constructed as the sum of lower order and a blend of difference between higher and lower order model. It offers reasonably good accuracy and at the same time guarantees boundedness. Various limiters like MINMOD, SUPERBEE, etc are available [Roe, 1985].

In order to develop a differencing scheme that is able to give good resolution of sharp profiles and at the same time follow smooth profiles as well, the Normalised Variable Approach (NVA) has been introduced by Leonard [Leonard, 1991]. The key idea in NV formulation is the estimation of slope of the solution called r-factor. This factor decides the size of the blending function.

5.2 Present Contributions

- Applied finite volume technique to solve convection-diffusion equation in fluid dynamics to estimate the drag lift characteristics of underwater bodies. The unsteady

governing equations are formed and solved in a serial solver.

- Tested various convection schemes used in CFD.
- Developed a new convection differencing scheme called BNCUS.
- Studied the performance of various flux limiters like SUPERBEE, VANLEER, KOREN, and UMIST on the performance of BNCUS scheme.
- Developed a parallel computing framework for solving incompressible hydrodynamics.
- Implement necessary code for the above objective.

5.3 Governing Equations

The governing equations of fluid mechanics in three dimensional space can be written as

- Continuity equation

$$\frac{\partial \rho}{\partial t} + \nabla \cdot (\rho \mathbf{U}) = 0 \quad (5.1)$$

- Conservation of momentum

$$\frac{\partial \rho \mathbf{U}}{\partial t} + \nabla \cdot (\mathbf{U} \mathbf{U} \rho) = \rho \mathbf{g} + \nabla \cdot \sigma \quad (5.2)$$

In order to close the system of equations, it is necessary to introduce additional, so-called constitutive relations .Eg. Generalised equation for the Newton's law of viscosity.

$$\sigma = -\left(P + \frac{2}{3}\mu \nabla \cdot \mathbf{U}\right) \mathbf{I} + \mu [\nabla \mathbf{U} + (\nabla \mathbf{U})^T] \quad (5.3)$$

Where, I -Identity Matrix

5.4 Turbulence Modeling

The most of the fluid flows, occurring in nature/industries are turbulent. This can be described as a state of continuous instability in the flow, with random fluctuations in the flow field. Several approaches are available for the simulation of turbulent flows. The most general but less popular methodologies are, computationally intensive Direct Numerical Simulation (DNS), LES (Large Eddy Simulation) etc.

An alternative approach to the simulation of turbulent flows is statistical. Separating the local value of the variable into the mean and the fluctuation around the mean, it is possible to derive the equations for the mean properties themselves. Hence the force balance equation becomes

$$\frac{\partial \bar{\mathbf{U}}}{\partial t} + \nabla \cdot (\rho \bar{\mathbf{U}} \bar{\mathbf{U}}) = \mathbf{g} - \nabla \bar{p} + \nabla \cdot (\nu \nabla \bar{\mathbf{U}}) + \overline{\mathbf{U}' \mathbf{U}'} \quad (5.4)$$

Where \mathbf{U}' is the fluctuating component and $\bar{\mathbf{U}}$ is the mean component.

The term $\overline{\mathbf{U}' \mathbf{U}'}$ is called the Reynolds stress tensor. In order to close the system, it is necessary to model the Reynolds stress tensor in terms of the mean flow quantities. The most popular approach is to use Boussinesq approximation which prescribes a relationship between the Reynolds stress and mean velocity gradient.

$$\overline{\mathbf{U}' \mathbf{U}'} = \nu_t (\nabla \mathbf{U} + \nabla \mathbf{U}^T) + \frac{2}{3} k \mathbf{I} \quad , \quad k = \frac{1}{2} \overline{\mathbf{U}' \cdot \mathbf{U}'} \quad (5.5)$$

The kinematic eddy viscosity ν_t can be evaluated in many different ways, ranging from algebraic relations and local equilibrium assumptions to the solution of transport equations. The most popular approach is to express ν_t as a function of the turbulent kinetic energy k and its dissipation rate, leading to a “two-equation” turbulent model. Out of the various two-equation turbulent models, SST-K- Ω model is a promising one [Menter, 2003] and is implemented in the CFD code.

5.4.1 SST-k- Ω Turbulence Model

The starting point for the development of the SST model was the need for the accurate prediction of aeronautics flows, with strong adverse pressure gradients and separation. Over decades, the available turbulence models had consistently failed to compute these flows. In particular, the otherwise popular k- ϵ [Jones, 1972] model was not able to capture the proper behaviour of turbulent boundary layers up to separation. Another important scheme, k- ω model [Menter, 1992] is substantially more accurate than k- ϵ in the near wall layers, and has therefore been successful for flows with moderate adverse pressure gradients, but fails for flows with pressure induced separation. In addition the k- ω model shows a strong sensitivity to the values of ω in the free stream outside the boundary layer. Thus a turbulence scheme was inevitable to resolve core turbulent flow and to capture near wall effects. Considering all these aspects Mentor [Menter, 2003] developed SST model which is blend of k- ϵ and k- ω models. The model equations are discussed in literature [Menter, 2003].

5.5 Finite Volume Discretisation

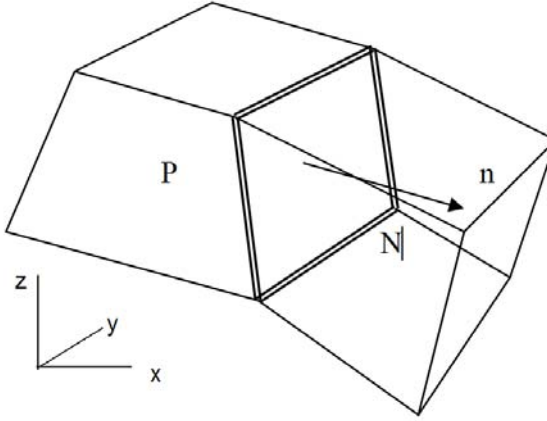


Figure 5.1 Generic Control Volume

The purpose of any discretisation practice is to transform one or more partial differential equations into a corresponding system of algebraic equations in time and space. For this, the computational domain is divided into a finite number of discrete regions, called control volumes or cells. For transient simulations, the time interval is also split into a finite number of time-steps. The finite volume method is based on the discretising the integral form of governing equation over each control volume. The basic quantities, such as mass and momentum are conserved in each cell.

General transport equation for a scalar property ϕ is:

$$\frac{\partial \rho \phi}{\partial t} + \nabla \cdot [\mathbf{U} \rho \phi] - \nabla \cdot (\Gamma_{\phi} \rho \nabla \phi) = S_{\phi}(\phi) \quad (5.6)$$

The first term in the above equation is called temporal term, second term is convective, third is diffusive term and the right hand side of the same is the source term. Applying the finite volume method, it is possible to integrate Equation 5.6 over a three dimensional control volume presented in Figure 5.1. In this figure P denotes parent cell and N neighboring cell.

$$\int \frac{\partial \rho \phi}{\partial t} dV + \int \nabla \cdot [\mathbf{U} \rho \phi] dV - \int \nabla \cdot (\Gamma_{\phi} \rho \nabla \phi) dV = \int S_{\phi}(\phi) dV \quad (5.7)$$

5.6 Discretisation of Convective Term

Using the generalised form of Gauss' theorem, the volume integrals in the convective term are transformed into surface integrals

$$\int_V \nabla \cdot [\mathbf{U}\phi] dV = \frac{1}{V_p} \sum_{f=1}^n \rho_f U_f \phi_f A_f \quad (5.8)$$

Where, A_f is the cell face area of the parent cell.

Φ_f reconstructed face value of scalar Φ .

U_f , face velocity.

V_p volume of parent cell.

n , Number of faces.

The role of the convection differencing scheme is to determine the value of Φ on the face from the values in the cell centres. In the framework of arbitrarily unstructured meshes, it would be impractical to use any values other than Φ_P and Φ_N , because of the storage overhead associated with the additional addressing information. Thus in cell centred approach most of the differencing schemes are limited to use only the nearest neighbours of the control volume in the unstructured mesh strategy.

Assuming the linear variation of Φ between P and N, the face value is calculated according to Central differencing scheme (CDS):

$$\Phi_f = f_x \Phi_P + (1 - f_x) \Phi_N. \quad (5.9)$$

Here, the interpolation factor f_x is a fraction. The scheme is supposed to be second order accurate. It has been noted, however, that CDS causes unphysical oscillations in the solution for convection-dominated problems, violating boundedness. An alternative scheme that guarantees boundedness at the expense of accuracy is Upwind Differencing (UDS). The face value of ϕ is determined according to the direction of the flow. Blended Differencing (BDS) is a combination of UDS and CDS.

5.7 Diffusion Term

The diffusion term will be discretised in a similar way. Using the assumption of linear variation of ϕ

$$\int \nabla \cdot (\rho \Gamma_\phi \nabla \phi) dV = \sum_f S_f (\rho \Gamma_\phi \nabla \phi)_f \quad (5.10)$$

$$\text{For orthogonal mesh} \quad S_f \nabla \phi_f = |S_f| \frac{\phi_N - \phi_P}{|d|} \quad (5.11)$$

For non orthogonal meshes additional correction term is needed to treat the non-orthogonality of the mesh.

5.8 Source Term

All terms of the original equation that cannot be written as convection, diffusion or temporal terms are treated as sources S . The source term was linearised by

$$S(\phi) = S_u + S_p \phi, \quad (5.12)$$

Where, S_u denote constant part and S_p is the coefficient of ϕ . Temporal terms can be discretised into two ways; either by using backward Euler or Crank-Nicholson scheme. Former is supposed to be 1st order accurate and the latter is second order accurate with respect to time.

5.9 Velocity-Pressure Coupling

Considering segregated methods, several algorithms have been developed to couple velocity and pressure. However, algorithms such as SIMPLE, SIMPLER, SIMPLEC and PISO have a similar behaviour. These are predictor-corrector procedures. The momentum equations are solved for a guessed pressure field normally, using the value of the previous time step. Solving the set of algebraic equations, a new velocity field is determined which does not satisfy the continuity. During the calculation of the momentum, a velocity field without the pressure contribution is determined and considered during the calculation of pressure. Considering the continuity equation for incompressible flow, sum of the fluxes in and out of the control volume should be zero. These fluxes are related with a face pressure gradient using the interpolation purposed by Rhie and Chow [Rhie,1982]. The continuity equation is transformed into a Poisson's equation for pressure. The solution of the resultant elliptic equation yields a new pressure field, which is then used as the initial guess of the subsequent iteration in time. The present study mainly used PISO algorithm.

5.10 Implementation of Physical Boundary Conditions

Physical boundary conditions are symmetry planes, walls, inlet and outlet etc. These are described below.

- Inlet boundary. The velocity field at the inlet is prescribed and, for consistency, the boundary condition on pressure is zero gradient.
- Outlet boundary. The outlet boundary condition should be specified in such a way that the overall mass balance for the computational domain is satisfied.
- Impermeable no-slip walls. The velocity of the fluid on the wall is equal to that of the wall itself, so the fixed value boundary conditions prevail. As the flux through the solid wall is known to be zero, the pressure gradient condition is zero gradient.

5.11 Latest Convection Differencing Schemes

Apart from regular UDS and CDS, which are 1st and 2nd order accurate in space, there are schemes of recent origin that are classed as flux limited schemes. Harten [Harten, 1984] introduced the notion of Total Variation Diminishing (TVD) to characterise oscillation-free flux-limited schemes. In TVD the schemes satisfy the following condition for every time-step:

$$TV(\varphi_{n+1}) \leq TV(\varphi_n). \text{ Where TV denotes the total variation and } n \text{ --no. of time step.}$$

The above condition is now applied to the higher-order flux-limited schemes the way suggested by Sweby [Sweby,1984]: a selected higher-order differencing scheme is written as a sum of the first-order bounded differencing scheme (UD) and a “limited” higher order correction:

$$\Phi_f = (\varphi)_{UD} + \Psi [(\varphi)_{HO} - (\varphi)_{UD}] \quad (5.13)$$

Where $(\varphi)_{HO}$ represents the face value of φ for the selected higher-order scheme and Ψ is the flux limiter. Following Van Leer [Van Leer,1983] and Chakravarthy and Osher [Chakravarthy, et.al,1983], Sweby assumes that the limiter is a function of consecutive gradients of φ . Apart from regular TVD schemes, another widely used methodology is the Normalised Variable Approach, introduced by Leonard [Leonard, 1988]. NVA has also been used in the present study. The basis of this approach is that, in order to avoid unphysical oscillations in the solution, it is require that φ_C (and consequently φ_f) is locally bounded between φ_U (value of φ in the upwind cell) and φ_D (value of φ in the neighbour cell) ,

meaning either

$$\varphi_U \leq \varphi_C \leq \varphi_D, \text{ or } \varphi_U \geq \varphi_C \geq \varphi_D \quad (5.14)$$

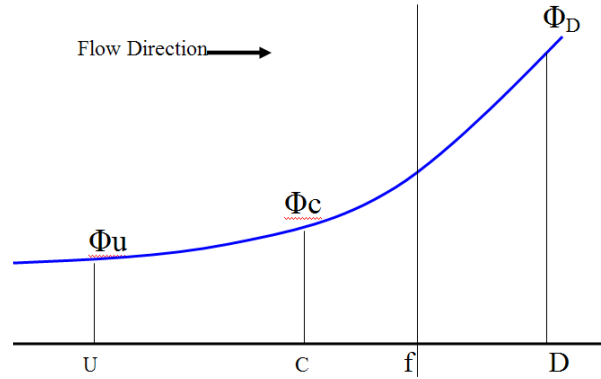


Figure 5.2 Variation of Φ around the face f

If this criterion is satisfied for every point in the domain, the entire solution will be free of any unphysical oscillations.

5.12 NV Approach for Unstructured Meshes

Jasak [Jasak,1996] modified the NV scheme for unstructured mesh. This approach has been used in the present study and are discussed

The limiting function $\psi = \psi(r)$ where $r = \frac{\varphi_C - \varphi_U}{\varphi_D - \varphi_U} = 1 - \frac{(\nabla\varphi)_f \cdot d}{2(\nabla\varphi)_c \cdot d}$ (5.15)

Where, r is called r -factor is the slope of the solution. The switching of the schemes is outlined below.

- If $r \leq 0$ or $r \geq 1$ use UDS
- $\beta_m \leq r < 1$ use CDS
- $0 < r < \beta_m$ use blended differencing scheme.

$$\varphi_f = \left(1 - \frac{r(1-f_x)}{\beta_m}\right)\varphi_C + \frac{r(1-f_x)}{\beta_m}\varphi_D \quad (5.16)$$

For good resolution, the value of β_m should ideally be kept as low as possible ($< 1/2$).

One of the drawbacks of the NV approach lies in the estimation of r -factor. As suggested in the equation 5.15 the estimation of the same in unstructured meshes does not require knowledge of the cell centred value in the upwind cell. The fact that only parent and

immediate neighbour cell will take part in the computation, leads to the reduced order of accuracy of reconstructed value at the cell face. The situation is further worsened by skewness and mesh grading effects in unstructured mesh strategy. To overcome this, Darwish and Moukalled [Darwish, 2005] suggested an improved r-factor algorithm. In this approach he devised curve fitted upwind information (exponential or parabolic) rather than that of the actual upwind cell. The alternative way that can improve order of accuracy of the numerical scheme is the use of node based approach instead of the traditional cell based one. The later approach has been selected throughout this particular study.

5.13 Node based formulation

The primary requirement of any convection interpolation scheme is the accurate estimation of flow variable on the cell face. Node based flux reconstruction is an important methodology devised in this direction. In node centred formulation nodal values of flow variable (say Φ) is interpolated from the cell centred values from cells surrounding that particular node. Then the average of distance weighted node values is taken as the cell face value (see figure 5.3).

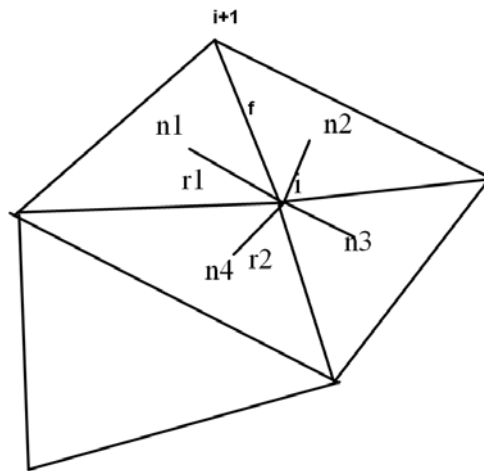


Figure 5.3 Estimation of cell face value by node based approach

$$\phi_{\text{vertex}} = \frac{\sum_{n=1}^{\text{no_of_cells}} \phi_n \frac{1}{r}}{\sum_{n=1}^{\text{noofcells}} \frac{1}{r}} \quad (5.17)$$

$$\phi_f = \frac{\phi_i + \phi_{i+1}}{2} \quad (5.18)$$

This may produce better spatial accuracy of the solution due to the presence of large number of cells surrounding a typical interior node in unstructured mesh (sometimes 64 numbers). But node based formulation fails in areas where the mesh becomes coarse, leads to numerical dissipation. A workaround to this situation is the use of a blended node based and cell based approaches. The present study proposes a new convection interpolation scheme called BNCUS which harness the good characteristics of node and cell based formulations.

5.14 Development of New Convection Interpolation Scheme (BNCUS)

This section describes the development of new convection interpolation scheme. Blended node and cell based upwind scheme (BNCUS). As discussed earlier, the sole purpose of the convection differencing scheme is to determine the value of ϕ on the face (ϕ_f) from the values in the cell centres which is necessary to evaluate the integral equation 5.10

For the case of flux limited schemes

$$\Phi_f = (\phi)_{UD} + \Psi [(\phi)_{HO} - (\phi)_{UD}] \quad (5.19)$$

Where $(\phi)_{HO}$ represents the face value of ϕ for the selected higher-order scheme and Ψ is the flux limiter which is used to blend higher and lower order scheme. In most of the cases the higher order scheme was selected as central difference scheme (CDS) which is supposed to be second order accurate in space. But this order of accuracy has been a subject of intense debate when it comes to unstructured meshing strategy. On the other hand, distance weighted node based reconstruction gives minimum second order accuracy even on an unstructured grid [Boris D, 2009]. But one of the problems of node based flux reconstruction is the numerical dissipation near to a discontinuity in the flow field. This may be attributed to the averaging effect due to large number of nearby cells. Thus, this particular study devises a blend of upwind scheme and node based scheme for the estimation of face flux.

The following flux limiters (Ψ) are included in the study

1. VANLEER- [Vanleer,1974]

$$\text{The limiting function } \psi(r) = \frac{r + |r|}{1 + |r|} \quad (5.20)$$

Accuracy: 2nd order

2. SUPERBEE-[Roe, 1986]

$$\psi(r) = \max[0, \min(2r, 1), \min(r, 2)] \quad (5.21)$$

Accuracy: 2nd order

3. KOREN –[Koren, 1993]

$$\psi(r) = \max\left[0, \min\left(2r, \frac{(1+2r)}{3}, 2\right)\right] \quad (5.22)$$

Accuracy: Third order for sufficiently smooth data

4. UMIST –[Lien & Leschziner, 1982]

$$\psi(r) = \max\left[0, \min\left(2r, \frac{(1+3r)}{4}, \frac{(3+r)}{4}, 2\right)\right] \quad (5.23)$$

Accuracy: 2nd order

All of the above limiters are symmetric that it exhibits the property

$$\frac{\Psi(r)}{r} = \Psi\left(\frac{1}{r}\right) \quad (5.24)$$

This is a desirable property as it ensures limiting action for forward and backward gradients operate in the same way. Testing of the limiters is discussed in section 5.18

5.15 Solution Techniques for Systems of Linear Algebraic Equations

The system of linear algebraic equations created by the discretisation of equation 5.6 form the shape as

$$a_p \phi_p + \sum_1^n a_N \phi_N = S_p \quad (5.25)$$

The term S_p is called source term, a_p , and a_N are constants. The symbol n denotes number of faces in the control volume. Rather than using fully coupled approach as in the solution of compressible flow cases, the present study devices sequentially coupled continuity, momentum and turbulence equations. Iterative solvers are used to solve the equations. The LAPACK sparse matrix library was used in assembling equation and solving the same. It has several iterative solvers such as Jacobi, successive over relaxation (SOR), Chebyshev, and conjugate gradient methods (CG) which can handle non-symmetric sparse systems:

CGN, GMRES, BiCG, QMR, CGS, and BiCGStab .

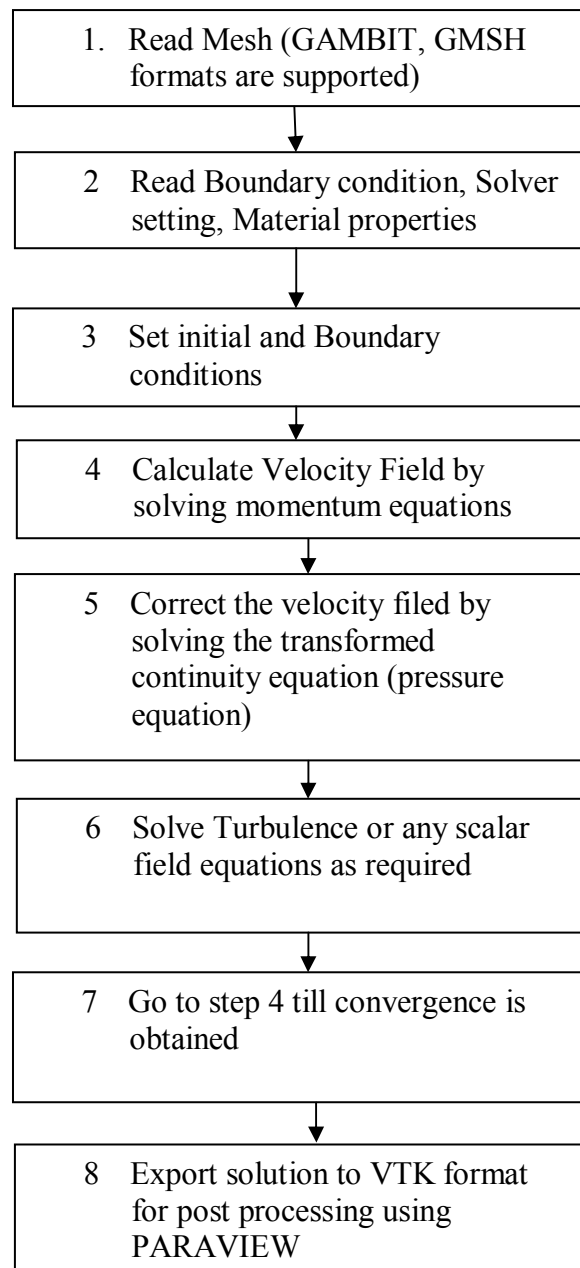


Figure 5.3a Numerical solution procedure

5.16 Test cases

The developed computer code in C-programming language has been tested with two cases for which results from literature are available [White, 2010]. For test no: 1, the flow past a solid cube was selected. The drag and lift parameters are estimated numerically by the equation.

$$\text{Drag} = \sum_{i=1}^{\text{nofowallfaces}} p_i n_i dA + \text{viscous Drag} \quad (5.26)$$

Where, p_i and n are the local wall face pressure and area direction cosines respectively. The viscous drag was obtained by multiplying shear stress term with local wall face area. For the second test, the flow past a cylinder was taken. The results are summarised as shown below. The solution was exported through the VTK format supported by open source visualiser PARAVIEW (shown in figure 5.4 and 5.5).

Table 5.1 Test Cases and results

Parameters	Test-1		Test-2
	Flow past a cube Size 1cm		Flow past a cylinder Diameter 1cm, length 1cm
Reynolds number	1e4		1e4
Free stream velocity	1m/s		1m/s
FLUENT Simulation	Drag	1.22N	0.94 N
	Lift	0.02N	0.01 N
Custom C code	Drag	1.20N	0.95 N
	Lift	0.02N	0.02 N
Experimental data From literature[White,2010]	Drag	1.07 N	0.90 N

Table 5.2 Solver setting

Type of solver	Serial
No of Cells	154656 (test1) 125348(test2)
Formulation	cell centred
Mesh Type	Tet, Unstructured
Convention interpolation scheme (vector)	2 nd order Upwind
Scalar flux estimation	NVA
Time advancement	Backward Euler
Turbulence scheme	SST-K- ω
Pressure velocity coupling	PISO
Solution procedure	Segregated
No of orthogonal correction	6 (minimum correction)
Iterative solver	BiCGStab
Preconditioner	ILU

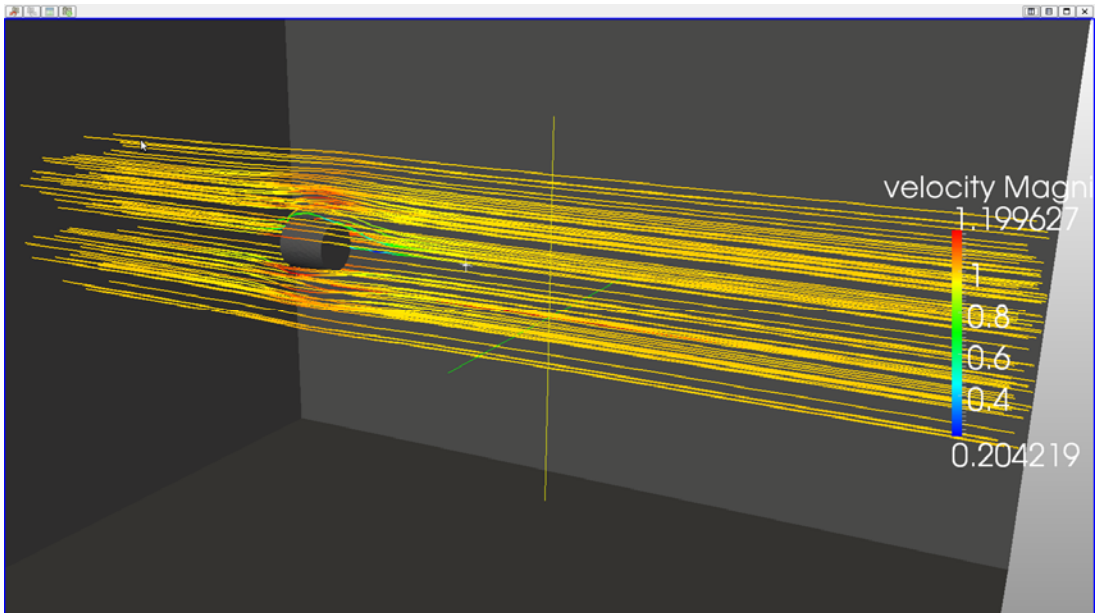


Figure 5.4. Plotted Stream lines using PARAVIEW (test case-1)

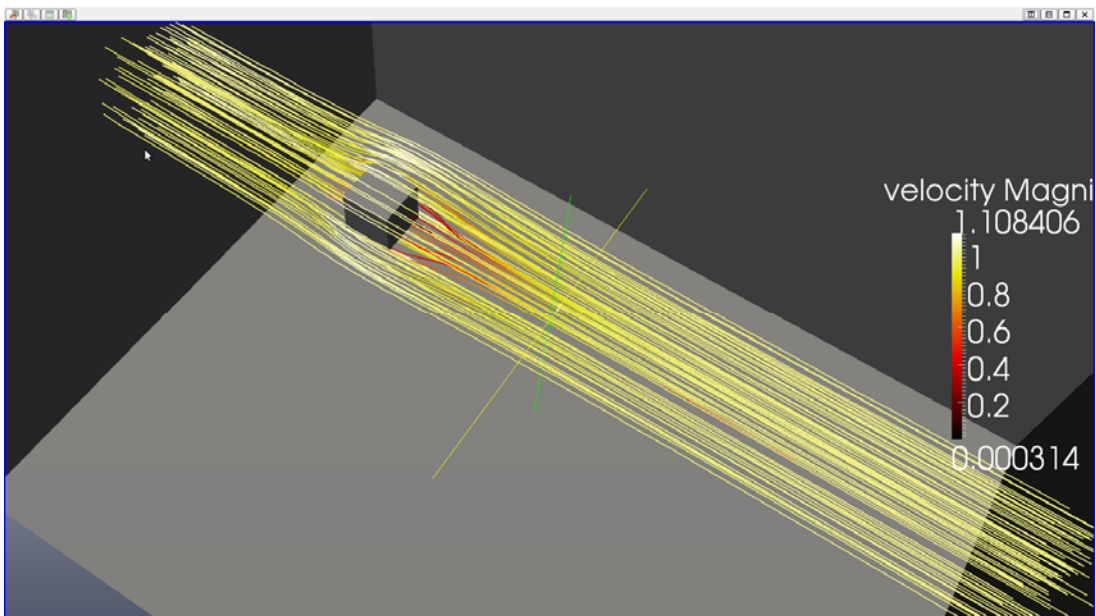


Figure 5.5. Plotted Stream lines using PARAVIEW (test case 2)

5.17 Gradient estimation

Estimation of gradient of flow parameters is routinely encountered in finite volume discretisation process. Precise estimation of the same is mandatory for obtaining good quality CFD solution. The gradient accuracy is highly governed by a combination of grid and solution. Generally, two gradients are important in FVM, they are C-Gradient (within cell gradient) and F-gradient (within face gradient). While, C gradients are used for inviscid flux reconstruction within control volume, F-gradient has been devised to estimate viscous fluxes. In this section the accuracy of different gradient estimation methodologies are evaluated by comparing the reconstructed C-gradient by Green-Gauss theorem and with exact analytical gradient. For a scalar Φ , the C-gradient as per Green-Gauss theorem is given by,

$$\nabla\phi = \frac{1}{V_p} \sum_{f=1}^n \phi_f A_f \quad (5.27)$$

The accuracy of C-gradient is measured as the relative gradient error. In the present study, the conventional L1 and L2 error definitions have been replaced by more robust volume weighed error measure developed by Sun and Takayama[Sun M & Takayama K,2003]. The error measure commonly used to evaluate the accuracy and convergence of solution is

$$\|\phi - \phi^{\text{ex}}\|_{L_k} = \left(\frac{\sum (\phi^i - \phi^{\text{ex}})^k}{N} \right)^{1/k} \quad (5.28)$$

Where Φ^i and Φ^{ex} are the numerical and exact value of Φ at cell i . N is the number of cells in the domain of interest. If $k=2$ the error of the solution is measured in the L2 sense. However Takayama has shown that this error measure is not appropriate for evaluating the numerical solutions for non-uniform grids. He suggested an improvised volume-weighted measure of error which was found more reasonable in evaluating the accuracy of quantities that involves volume and contour integral such as drag and lift coefficients. The form of volume weighed error measure is

$$\|\phi - \phi^{\text{ex}}\|_{L_k} = \left(\frac{\sum \Omega_i (\phi_i - \phi^{\text{ex}})^k}{\sum \Omega_i} \right)^{1/k} \quad (5.29)$$

Where, Ω_i is the volume of the cell i . This error measure has been devised throughout of this particular study and various gradient estimation methods are tested. The testing of accuracy of the gradient constructed through different methodologies was done by using three varieties of grids.

Type 1: Regular triangular grid (see figure 5.6a).

Type 2: Random triangular grid (see figure 5.6b).

Type 3: Perturbed triangular grid (see figure 5.6c).

The regular and random grids were created by MATLAB's PDE (Partial Differential Equation) toolbox. The perturbed grid was created by perturbation of the node points of the unstructured grid except boundary nodes. For the computational tests, the random node perturbation in each dimension was set as $\frac{1}{4} rh$. Where $r \in [-1,1]$ is a random number and h is the local mesh size along the given dimension.

Considering a square domain of size 6m as shown in figure 5.6a with assumed distribution of a scalar Φ (see figure 5.6d)

$$\Phi = a_0 + a_1x + a_2y. \quad (5.30)$$

Where, a_0, a_1 and a_2 are assumed to be constants. C-gradients of the scalar Φ were evaluated using Green-Gauss theorem with cell face values reconstructed using CDS, node based and blended methods. In the blended methodology, CDS and node based approaches are blended by using a suitable scalar blending factor. Assuming $a_0 = 3$, $a_1 = 6$ and $a_2 = 3$, and substituting in equation 5.30, the gradients along x and y directions such as $gr.x$ and $gr.y$ are evaluated. The exact $gr.x$ was plotted as shown in figure 5.6d. Subsequently $gr.x$ was estimated by Green-Gauss theorem (equation 5.27).

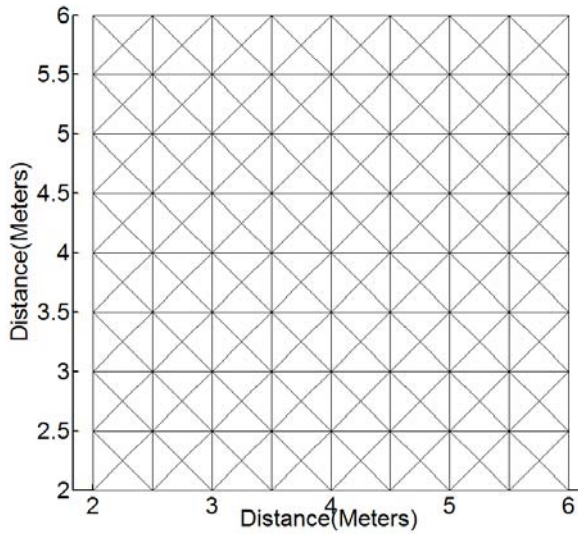


Figure 5.6a. Type 1 Mesh Regular - 256 cells

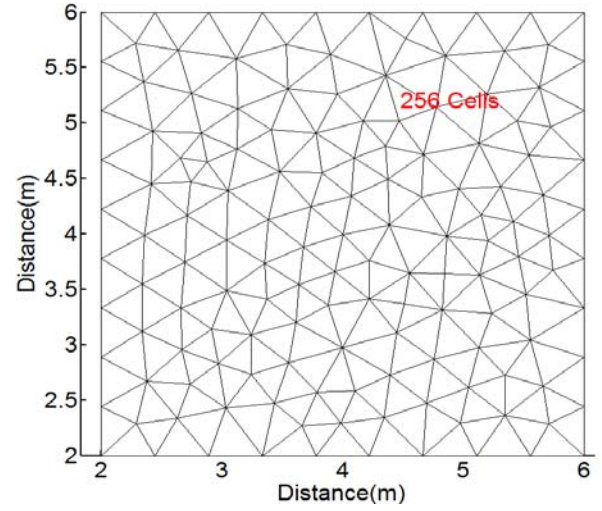


Figure 5.6b, Type 2 Mesh Random 256 cells

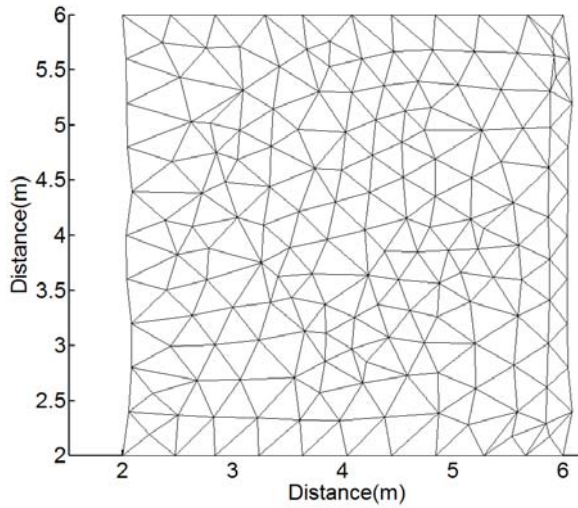


Figure 5.6c, Type 3 Mesh Perturbed, 256 cells

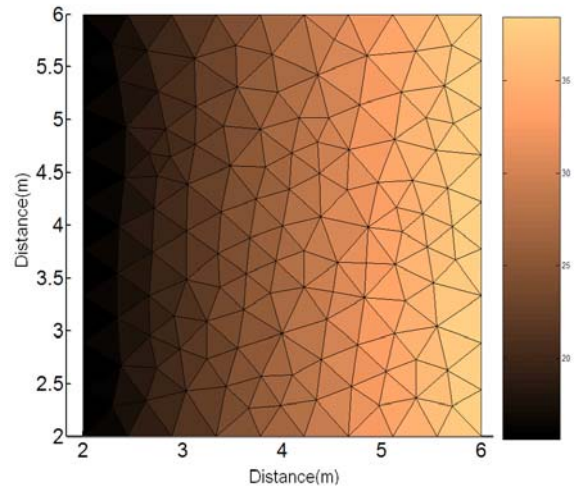
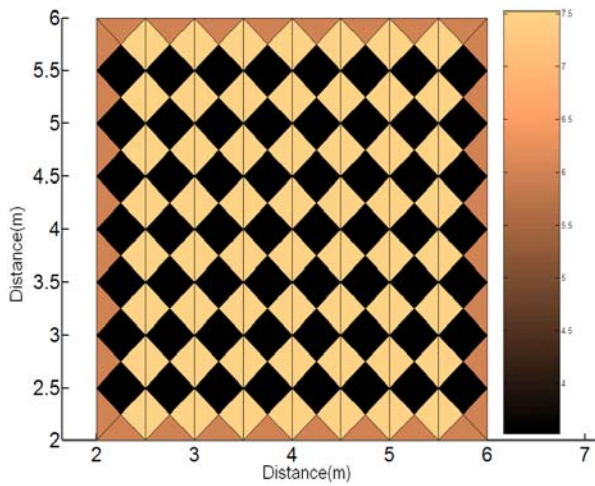
Figure 5.6d. Assumed distribution of scalar Φ 

Figure 5.7 Gradient CDS

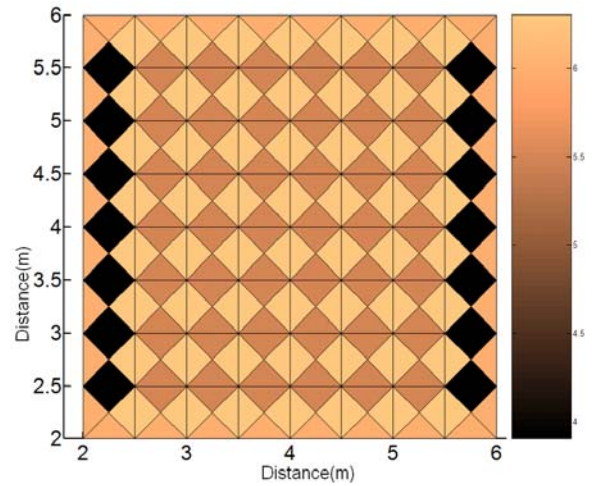


Figure 5.8 Gradient: Node based

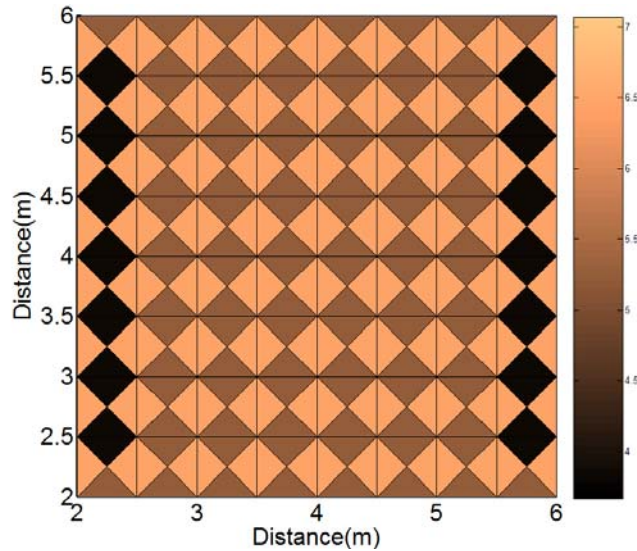


Figure 5.9. Gradient: blended scheme

Figure 5.7, 5.8, 5.9 shows the C-gradients (gr.x) evaluated for type 1 mesh (regular) through CDS, node based and blended flux methods. It was found that, a there exists a checker board type oscillations in the gradient field for CDS, node based and blended type formulations. For the last two cases, this tendency has been limited nearer to the boundary. Also highest gradient error (L2 norm) was observed for central difference scheme.

Figure 5.10, 5.11 and 5.12 shows the computed gradient in unstructured meshes (Type -II cells) through CDS, node based and blended schemes. Type-II cells shows entirely different pattern of L2 norm compared to type -1 cells, as shown in figure 5.12, here, CDS showed better gradient accuracy compared to pure node based formulation. The best L2 norm was obtained in a blended scheme wherein the formulation constitute 40% of node based and 60 % central difference flux (figure 5.14).

Further, for perturbed cell, obtained L2 norm is much higher than that of regular and random cells implying much lower accuracy in gradient estimation of these cells. Thus, skewness of a cell is significant factor which affects the accuracy of the Green-Gauss gradient. As the gradient estimation is a key activity in CFD simulations, highly skewed cells may produce reduced accuracy of the results. Also, it can be observed from the figure 5.10 is that sudden mesh grading is also a parameter that affects gradient accuracy.

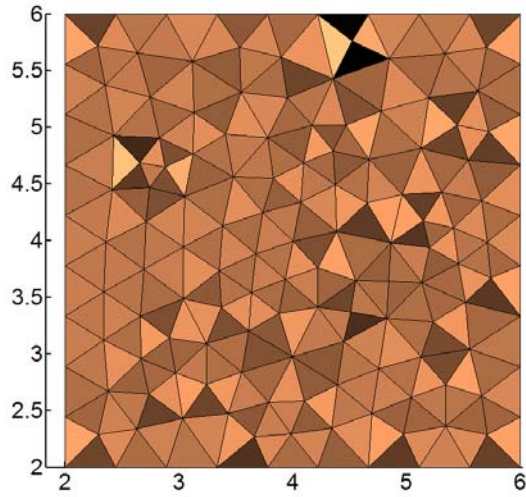


Figure 5.10 Gradient: CDS

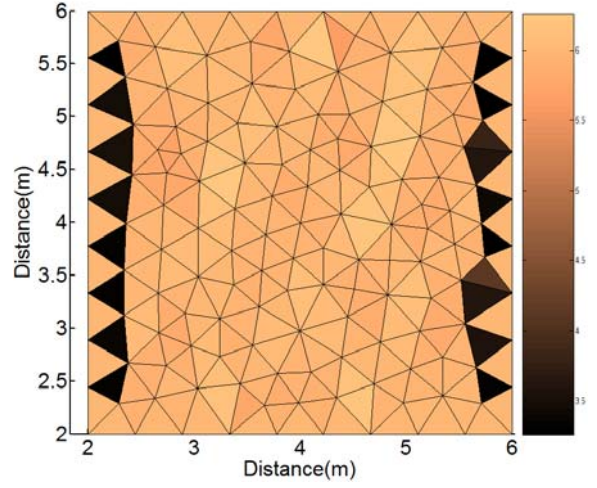


Figure 5.11 Gradient: Node based

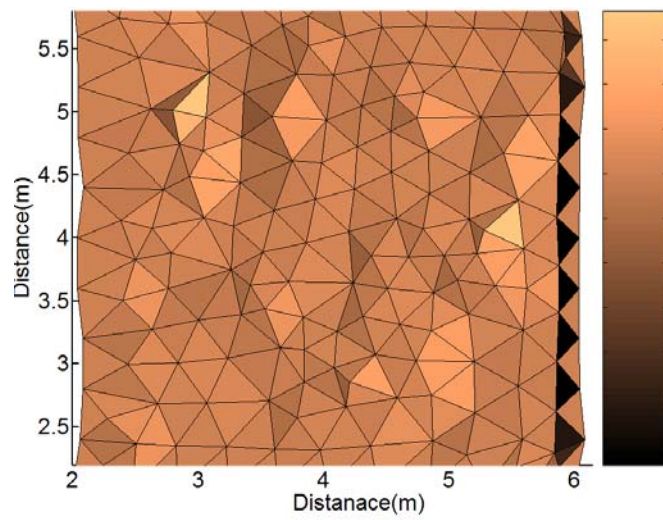


Figure 5.12 Gradient: blended scheme

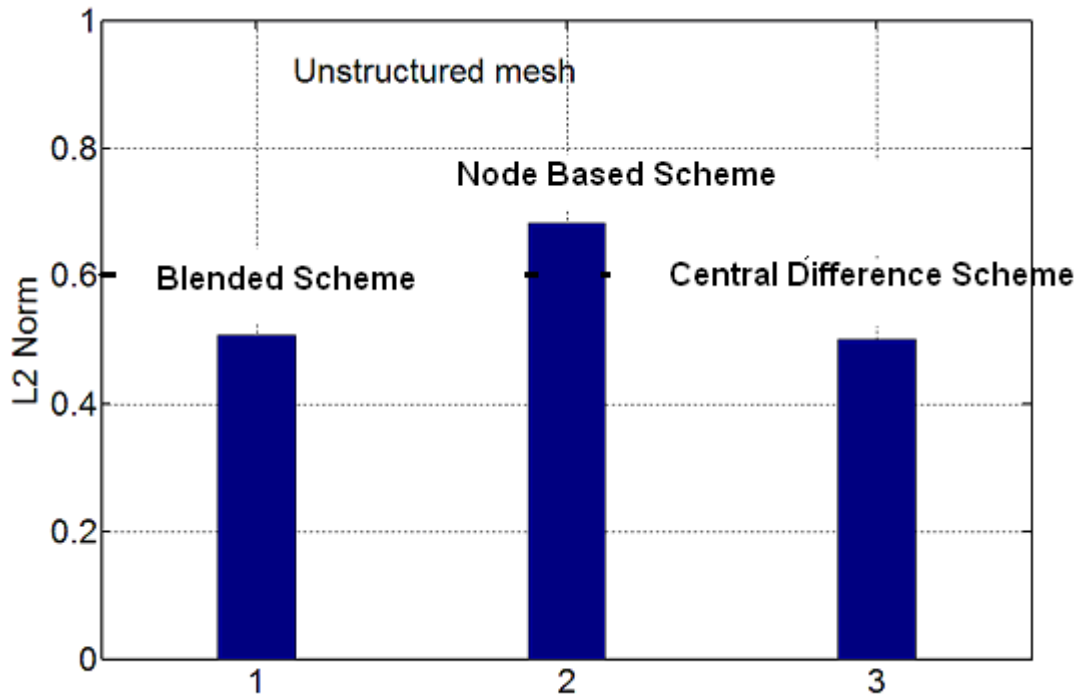


Figure 5.13 Comparison of L2 norms of various schemes.

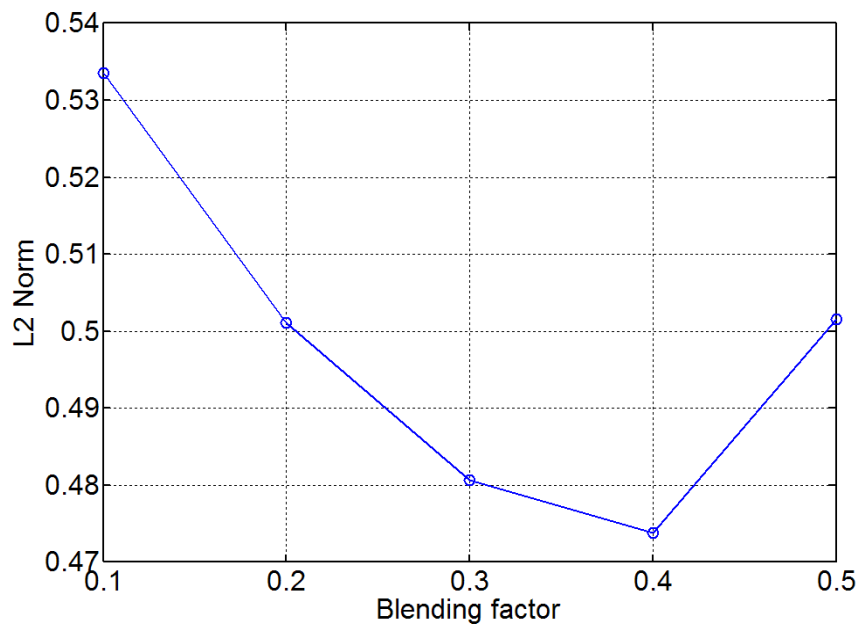


Figure 5.14 Variation of L2 Norm with blending factor

5.18 Blended Node and cell based Formulation for CFD simulations

Based on the numerical experiments done in the previous section it may be concluded that blended differencing produced maximum accuracy of gradient estimation through Green-Gauss method. Further testing was needed for getting better understanding of the efficient mixing of cell and node based formulation. For this, CFD simulation was done with test case as flow past a cube (test case 1, section 5.16). The selected side length of the cube is 0.005m instead of 0.01(as in test case 1). Subsequently drag values are evaluated for each case by CFD simulation

Following test case were investigated

- 1) Scalar blending factor with CDS flux reconstruction for Green-Gauss gradient.
- 2) Scalar blending factor with node based flux reconstruction for Green-Gauss gradient.
- 3) Use of Flux limited scheme as described in equation 5.19 and use of various limiters shown in section 5.14.

Table 5.3 Test case for Blended scheme

Test	Test case -1	
	Flow past a cube Size 5mm	
Reynolds number	0.5e4	
Free stream velocity	1m/s	
Experimental data From literature[White,2010]	C_d	1.10

For test case 1, the blended scheme means it is a mix of second order upwind and node based formulation. Numerical simulations were done with scalar blending factor ranges from 0.3 to 0.8. First order Euler time-integration procedure was used throughout the test cases with the objective of, getting a clear picture of convergence capability of the scheme and should be free from external numerical damping induced by the time integration scheme. It may be observed from the figures 5.15 a, b, c, d, e and f that a blending factor close to 0.7 gives maximum accuracy in drag estimation (simulated drag value 0.137 N while actual value 0.1375N [White,2010]) also the better convergence characteristics were observed at this value. A blending factor above 0.7 produced instability in the solution space with high frequency numerical oscillation (figure 5.15f).

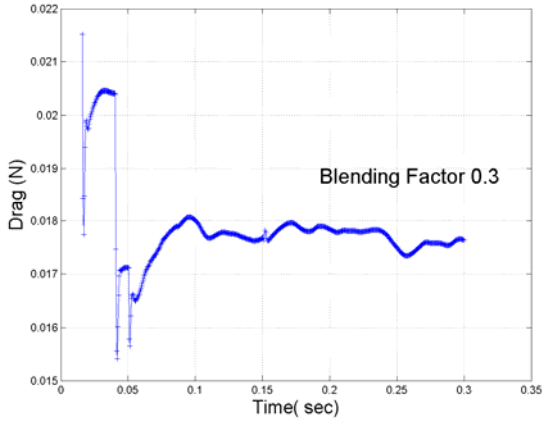


Figure 5.15 a

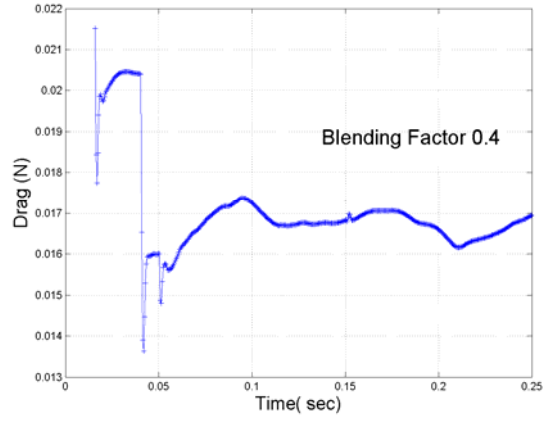


Figure 5.15 b

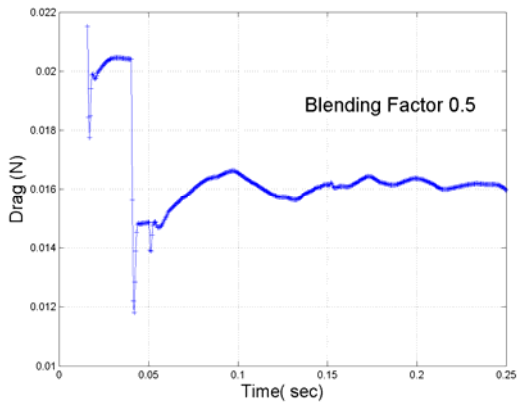


Figure 5.15 c

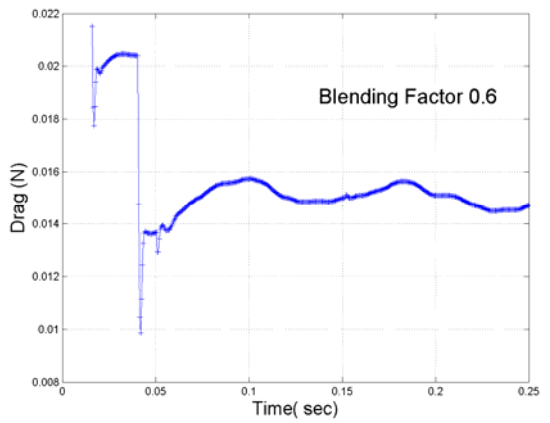


Figure 5.15 d

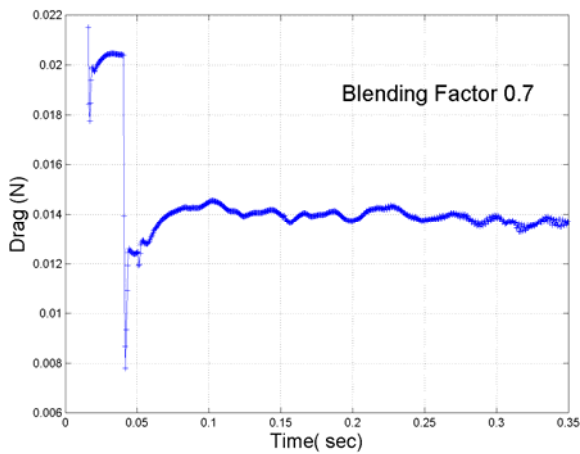


Figure 5.15 e

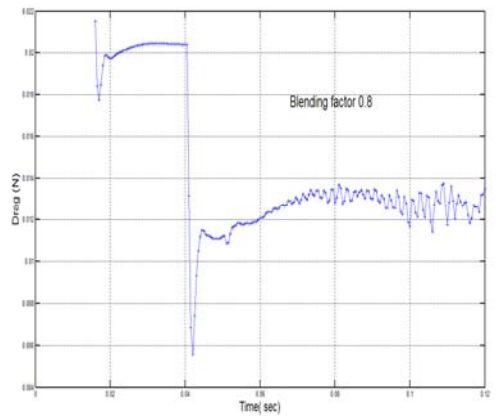


Figure 5.15 f

Figure 5.14 a,b,c,d,e and f: Test case 1, Effect of blending factor on stability and accuracy

In test case 2, two types of schemes were tested. In the first case, the blended scheme consists of first order upwind and node based formulation (BCUS1) while, second scheme was made of 2nd order upwind and node based formulation (BNCUS2). The Green-Gauss gradient was estimated based on node based flux formulation. The blending factor varied from 0.1 to 0.5 with three levels.

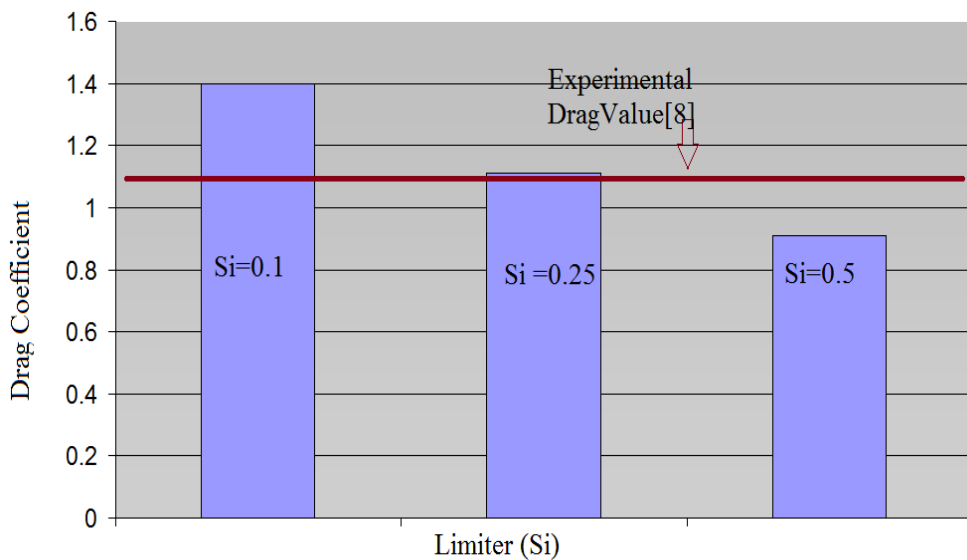


Figure 5.16 Performance of BNCUS2 at different blend factors

From the figure 5.16, it is evident that a limiter close to 0.25 produced results close to the experimental one obtained from the literature [White,2010]. Also, BNCUS2 produced better numerical values close to experimental one than the BNCUS1 (Figure 5.18).

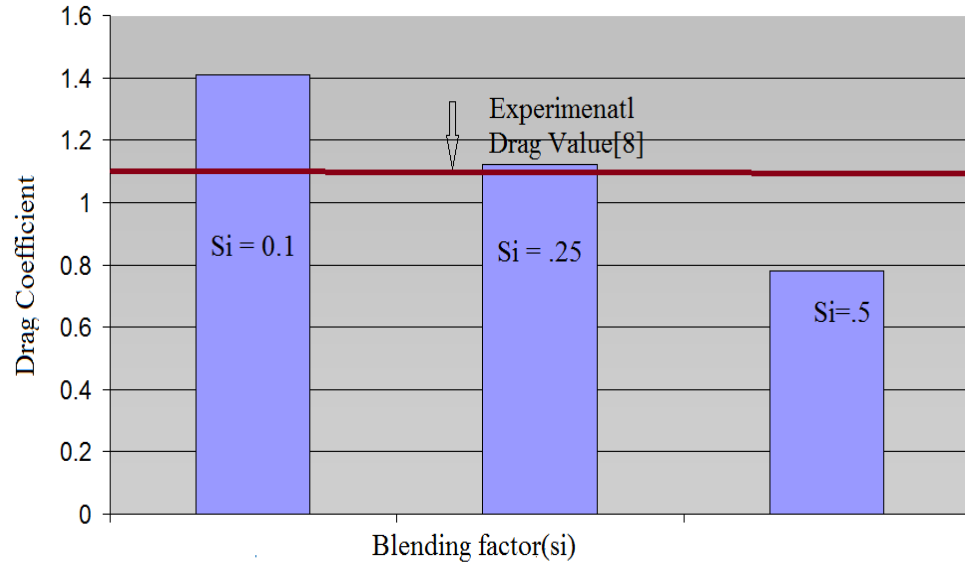


Figure 5.17 Performance of BNCUS1 at different blend factors

Comparing test case 1 and test case 2 in terms of scalar blending factor (test case 1 the optimum value for blending factor was 0.70 ,while test case 2 it was 0.25) It is evident that lower values of the same was sufficient to produce good results, when using node based gradient rather than that based on CDS.

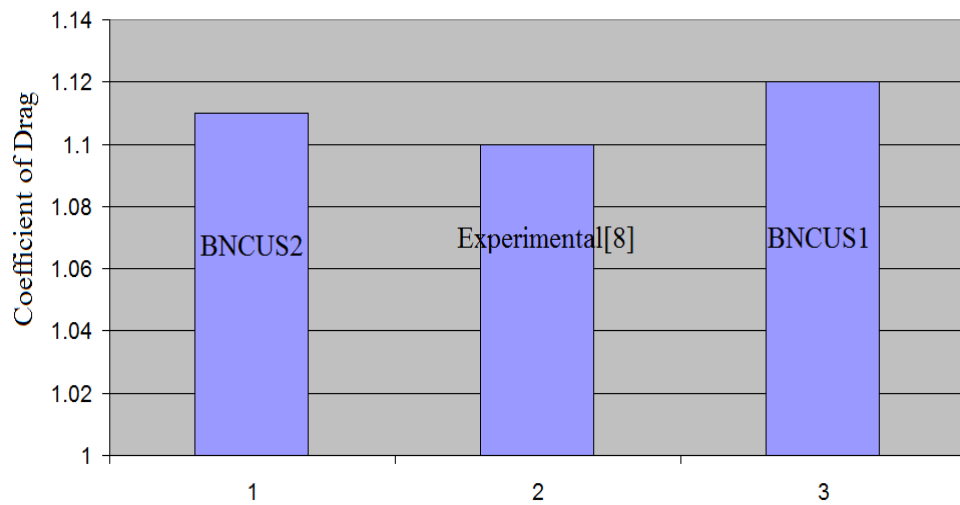


Figure 5.18 Performance comparison of BNCUS2 and BNCUS1.

Test case 3 involves a number of flux limited schemes in the CFD formulations. They are

- 1 VANLEER Limiter
- 2 SUPERBEE Limiter
- 3 KOREN Limiter
- 4 UMIST Limiter

In all these schemes blending factor is not a scalar value but depends upon the local slope of solution(r , refer equation 5.15) of the flow variables. The testing was done in stages. In the first stage the central difference scheme was chosen as the higher order scheme as described in equation 5.19 and in the second stage, node based formulation was put in place of higher order scheme. Time histories of the drag values are plotted as shown in figures 5.19a,b ,5.20a,b ,5.21a,b and 5.22 a,b.

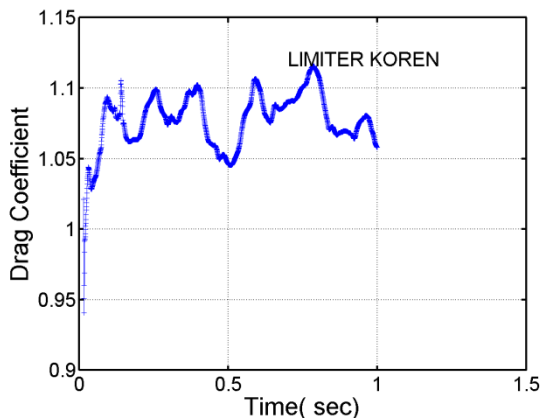


Figure 5.19a Node based higher order scheme

Limiter Koren

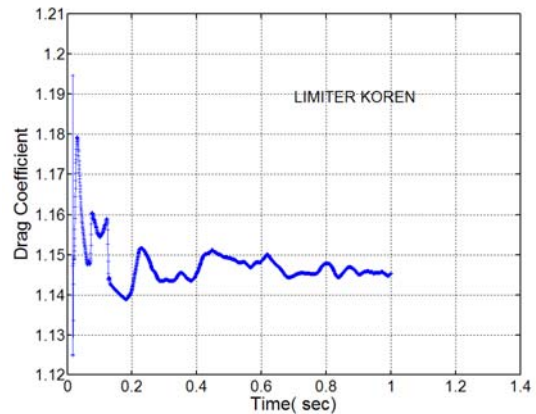


Figure 5.19b CDS as Higher order scheme

Limiter Koren

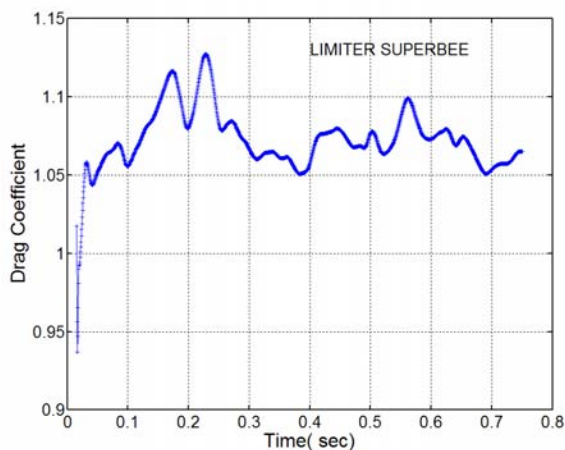


Figure 5.20a Node based higher order scheme

Limiter SUPERBEE

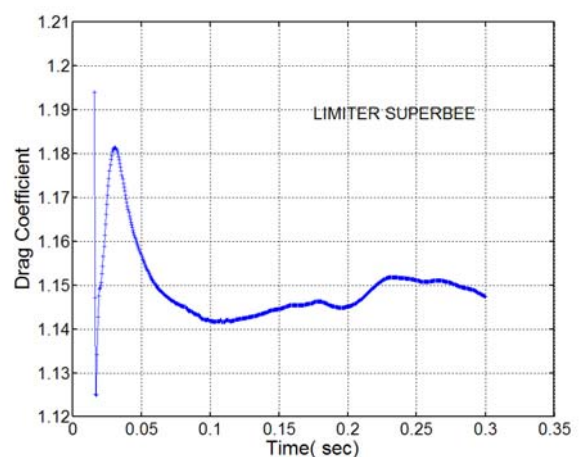


Figure 5.20b CDS as Higher order scheme

Limiter SUPERBEE

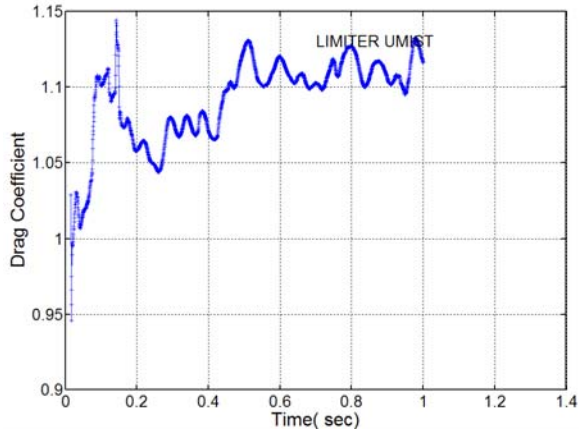


Figure 5.21a Node based higher order scheme
Limiter UMIST

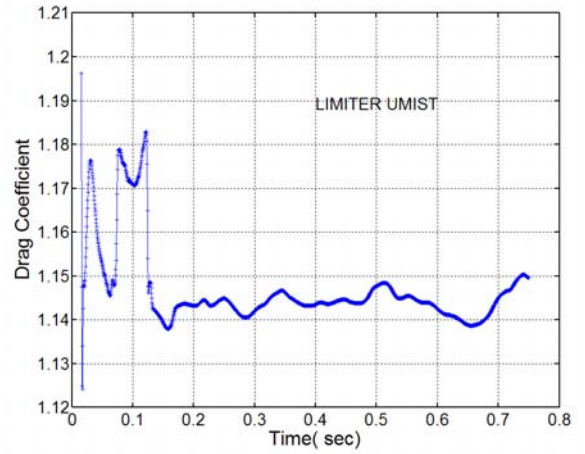


Figure 5.21b CDS as Higher order scheme
Limiter UMIST

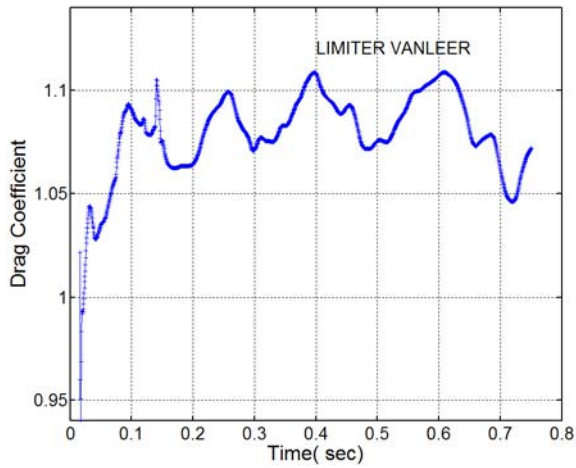


Figure 5.22a Node based higher order scheme
Limiter VANLEER

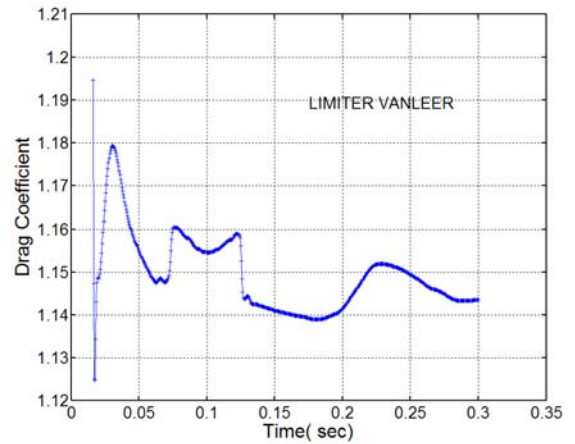


Figure 5.22b CDS as Higher order scheme
Limiter VANLEER

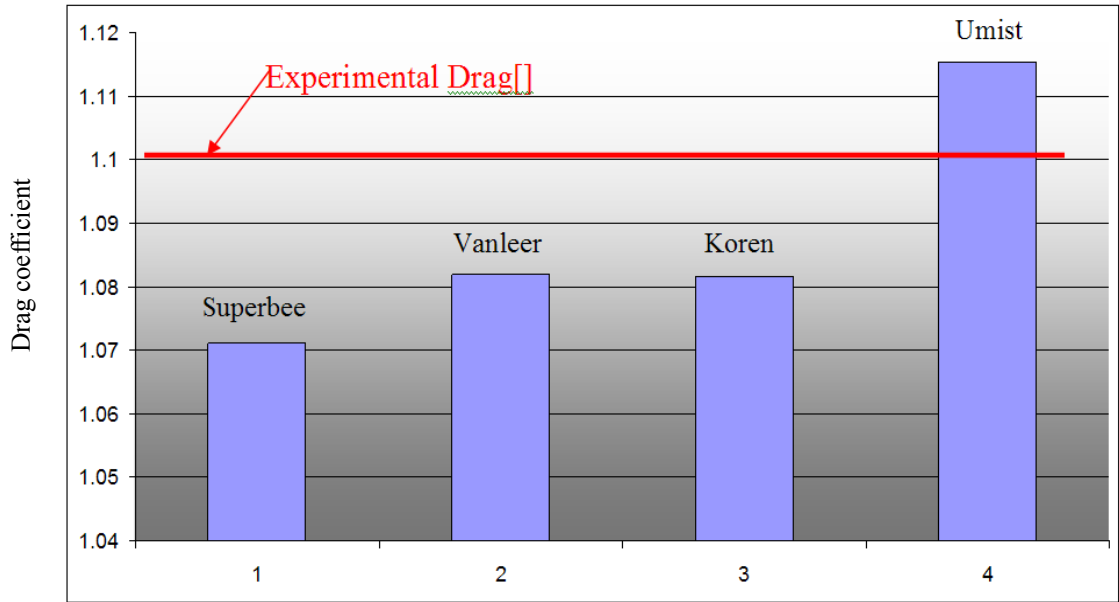


Figure 5.23 Relative performances of various limiters

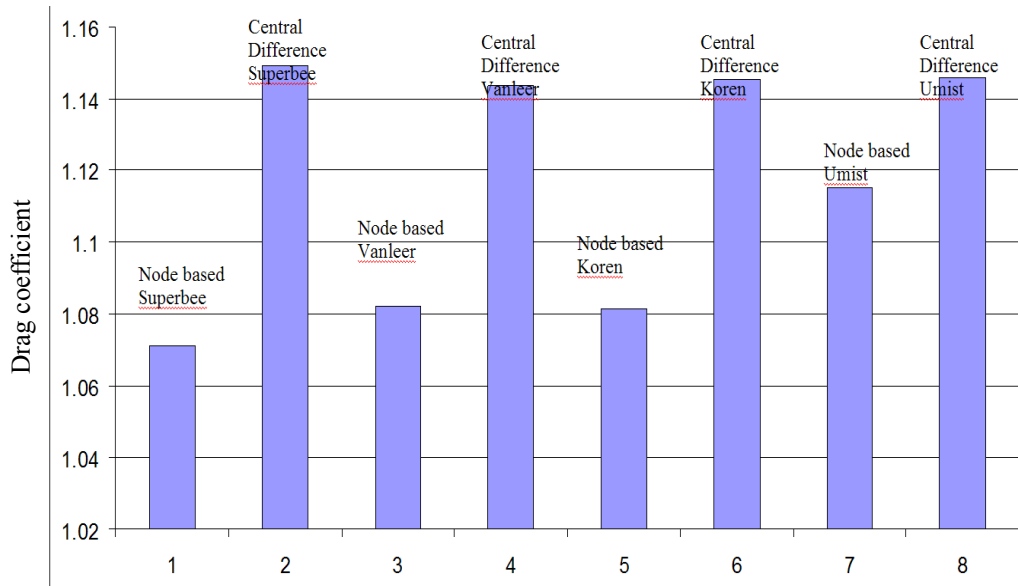


Figure 5.24 Comparison of CDS and Node based formulation with various limiters

It may be observed in the figure 5.23 that UMIST limiter produced maximum accuracy for this particular case and VANLEER also fetched results close to experimental values (Drag

coefficient equal to 1.1). Further, obtained results were more accurate when the node based scheme was selected as the higher order scheme compared to Central difference scheme (see Figure 5.24).

Form the numerical experiments it is clear that both BNCUS1 and BNCUS2 produced results with close agreement with the experimental values from the literature [White,2010]. Also, the blending factor Ψ is a critical factor which affects the overall accuracy of the scheme. A high value of Ψ introduces additional dissipation (for example across discontinuities and mesh is very course) and a reduction in accuracy. Therefore limiters are necessary one. Also, the higher accuracy of BNCUS2 over BNCUS1 may be attributed to the use of 2nd order upwind scheme as the lower order scheme.

5.19 Hydrodynamic Analysis of the tow-fish hull

The hydrodynamic forces and moments acting on the tow-fish hull were calculated by using developed CFD code. The program was executed in a serial way. The drag and lift forces are calculated at three different angle of attack (0,15,40°)and subsequently fitted a 2nd degree polynomial curve using GNU -OCTAVE polyfit function for the use of the dynamic solver (as shown in figure 5.25). The free stream velocity was assumed to be 1m/s. The simulated data were used for assembling the equation of motion in the subsequent dynamic analysis.

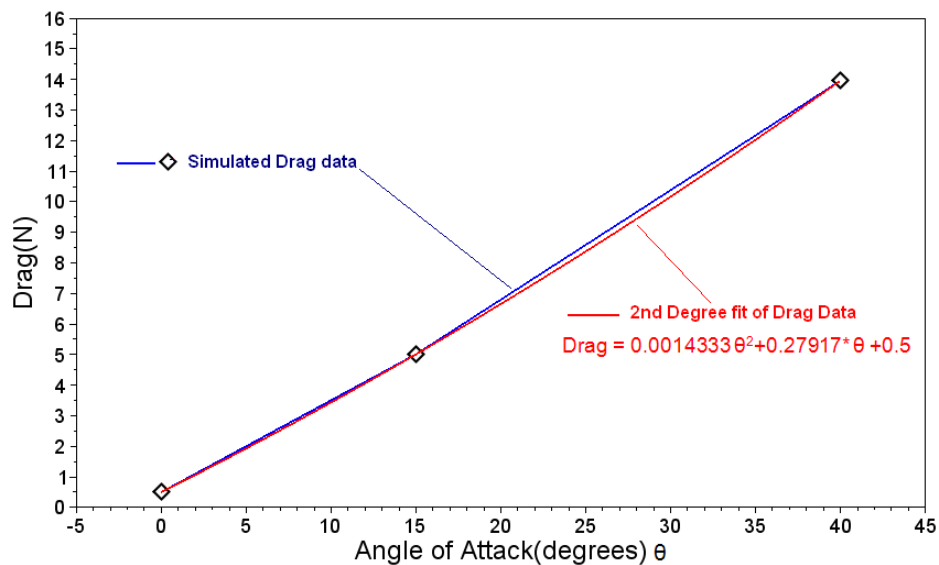


Figure 5.25 Drag v/s angle of attack of the towed body.

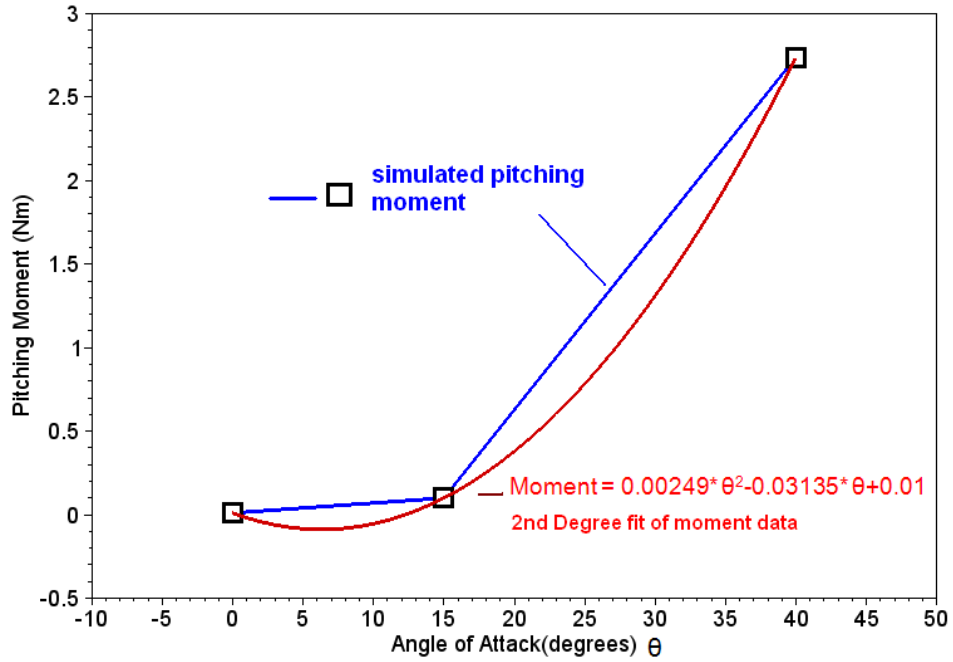


Figure 5.26 Pitching moment v/s angle of attack of the towed body.

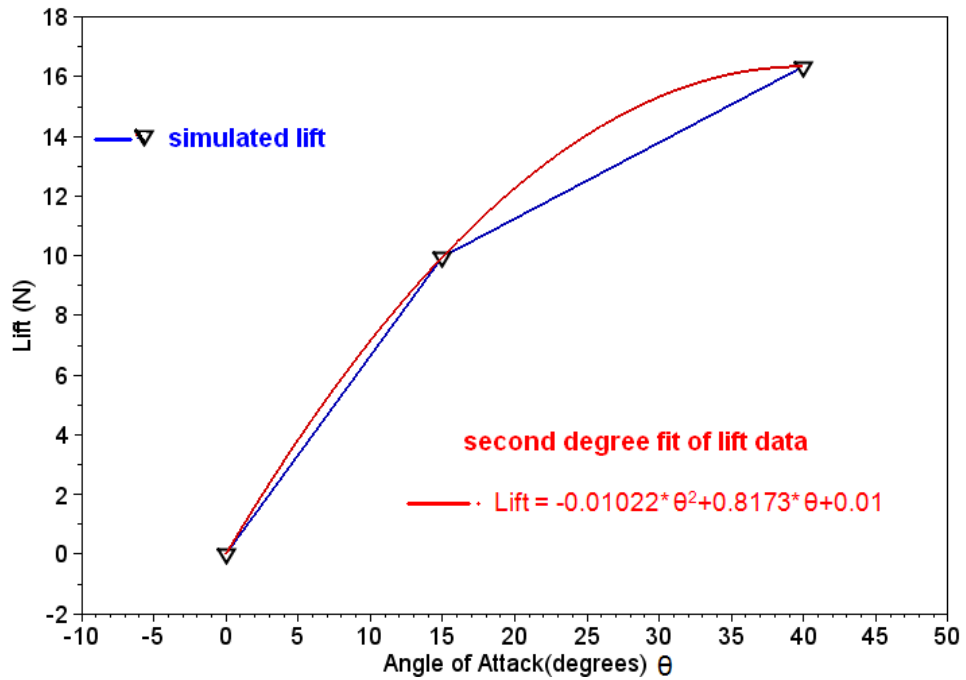


Figure 5.27 Lift v/s angle of attack of the towed body

5.20 Conclusion

The developed serial CFD code, which devises finite volume technique to solve convection-diffusion equations in fluid dynamics produced results in satisfactory agreement with the experimental values from the literature [White, 2010]. The discretisation of convection term and estimation of spatial gradient is major factor which affects the accuracy of simulation of convection dominated flows. It is a matter of fact that gradient values are significantly affected by the mesh grading and mesh quality parameters like skewness. Out of the various gradient estimation methodologies we tested, the blended scheme produced least L2 norm implying, superior accuracy of the scheme compared to other schemes tested. Also amount of blending (blending factor) has bearing on accuracy of the predicted Green-Gauss gradient.

To discretise the convection flow process, a new numerical scheme (BNCUS) was introduced and simulated results of the same are compared with experimental one. It has found that BNCUS2 produced better results (though marginal) than BNCUS1. It may be due to the application of second order upwind scheme (BNCUS2) for the place of lower order scheme. Here also the amount of blending have the influence on the numerical results obtained. Out of the flux limited schemes devised to blend the node and cell based formulation UMIST scheme produced best results for the numerical experiments done. It is also revealed that there is an upper bound to the value of scalar blending factor to be used and above and below this value performance of the numerical scheme may not be satisfactory.

Chapter 6

Numerical Experiments

Contents	6.1	<i>Overview</i>
	6.2	<i>Test case1: Two-Part Towing</i>
	6.2.1	<i>Results and Discussion</i>
	6.3	<i>Test Case 2 : Tow-Ship Manouvering Examples - Single Point Towing</i>
	6.4	<i>Testing of Time Integration Schemes</i>
	6.4.1	<i>Euler Scheme</i>
	6.4.2	<i>HHT-a</i>
	6.4.3	<i>Newmark's method</i>
	6.5	<i>Parallel Computations</i>
	6.5.1	<i>Shared-memory multiprocessors</i>
	6.5.2	<i>Distributed-memory multiprocessors</i>
	6.6	<i>Parallel Programming Paradigms</i>
	6.7	<i>Message Passing</i>
	6.8	<i>Parallisation of Simulation code for Shared Memory Architecture</i>
6.9	<i>Parallel Performance</i>	
6.10	<i>Parallisation of Simulation code for Distributed Memory Architecture</i>	
6.11	<i>Parallellisation of CFD code</i>	
6.12	<i>Domain Decomposition</i>	
6.13	<i>Parallel test case</i>	
6.14	<i>Conclusion</i>	

6.1 Overview

For the demonstration of the developed numerical model described in the previous chapters, numerical experiments were performed with test cases from single point and two-part towing process. At first, a numerical example of the towing ship traveling in a wave field is considered. In this, the effect of tow point disturbances on the motion stability of a two-part towing system was investigated. Only two-dimensional simulation is attempted. The towing ship travels sinusoidally on the horizontal plane with fixed horizontal velocity V_0 . Subsequently the simulated data are compared with the experimental values obtained from the literature [Wu, 2002]. Because of the limitation in the availability of the experimental data, only heaving is compared.

Further, the developed numerical model was tested with single point towing with classical test cases as examples. Two tow-ship manoeuvring cases are explored. In the first case, circular towing of the single-point tow system was considered while, in the second case, the tow-ship was given a sudden stoppage and resulting tow configuration was studied.

Finally, the effect of various time integration procedures on the stability of numerical scheme and accuracy of the solution was studied. The tested time integration procedures are Houbolt, Newmark, Euler and HHT- α scheme. The strength and weakness of each scheme are tested by incorporating them into LMSM cable formulation and subsequent simulations of two-part towing process.

6.2 Test case1: Two-Part Towing

Wu [Wu, 2001] conducted numerical experiments to study the performance of the two-part underwater towing system with sinusoidal input motion as the tow point disturbance. In this study, the performance parameters studied are heave and pitch response of the towed body. Further, the simulated data were compared with experiments one by conducting trials on a model ship towing tank. In his numerical model, the cable has been treated as continuous system and force and moment balance equations are discretised using finite difference method. For temporal discretisation, he devised the BOX scheme, which is centered on space and time. Rigid body mechanics was assumed for modeling of the towed body. In the experimental side, he devised a slider crank mechanism to provide the sinusoidal input

disturbances at the end of the primary cable. A pressure based depth sensor has been devised to measure the heave response of the towed body. Similarly the pitch was measured using accelerometer. The real time tension at the primary cable was also recorded. The experiments were conducted under the conditions of straight towing with constant towing speed in the horizontal direction. The input heave given at the tow point is given by

$$Z_p = -r \cos\left(\frac{2\pi}{T} t\right) + l \left[1 - \sqrt{\left(\frac{r}{l}\right)^2 \sin^2\left(\frac{2\pi}{T} t\right)} \right] \quad (6.1)$$

Where r and T are the length and rotation period of the crank and l is the length of the connecting link for the slider crank mechanism. The value for the above is discussed in table 6.1. Three $\phi 2\text{mm}$ steel wires were used as primary, secondary and tertiary cables. The depressor used in his experiment was a steel sphere of diameter 0.11m and 5.25 kg weight in water. The tow-fish was built by using circular nylon cylinder 0.11m in diameter and 2mm in thickness. The tow-fish is adjusted to be neutrally buoyant and the tow point is fixed at left end point of the tow-fish.

Table 6.1 Kinematic details of tow-point

V_0 (m/sec)	l (m)	T (sec)	r (m)
1.75	0.35	1.6	0.1

The particulars of composite cables, depressor and tow-fish are

Depressor:-Diameter = 0.11m Weight in air = 5.25kg. Weight in water = 4.58 kg.

Towed Tow-fish: Diameter = 0.11m . Length = 1.30m . Weight in air 12.50 kg . weight in water = 0 kg .

Primary cable:- length 2.84m . Weight in air = 0.181 kg/m . Weight in water = 0.104kg/m .

Depressor Cable:- Length = $.30\text{m}$ weight in air = $.063\text{ kg/m}$. Weight in water = 0.039kg/m

Secondary cable :-Length = 1.5m . Weight in air 0.124kg/m .Weight in water = 0.065 kg/m .

Cable material: MS steel wire. Young's modulus= 200 gPa .

The data from his experiments are taken to benchmark the developed computer code.

6.2.1 Results and Discussion

By taking input data from the experiment described in the literature [Wu, 2002], the dynamic simulation were performed using LMSM based cable formulation. Figure 6.1 shows the simulated spatial configuration of the two-part towing system. The main centenary is the primary cable and the tail section represents the secondary cable. Figure 6.2 shows the time based input motion given to the tow point. The simulated depth variation of the depressor and towed body is shown in figure 6.3. It can be seen that the heave response (amplitude of depth variation) of the towed body is considerably less than that of the depressor. Also the input disturbance from the ship is considerably reduced at the towed body end. The heave amplitude ratio (ratio of amplitude of the towed body to that of depressor) was found to be approximately 0.20. The same ratio obtained from the experimental values from literature [Wu, 2001] is found to be 0.23(as shown in figure 6.4).

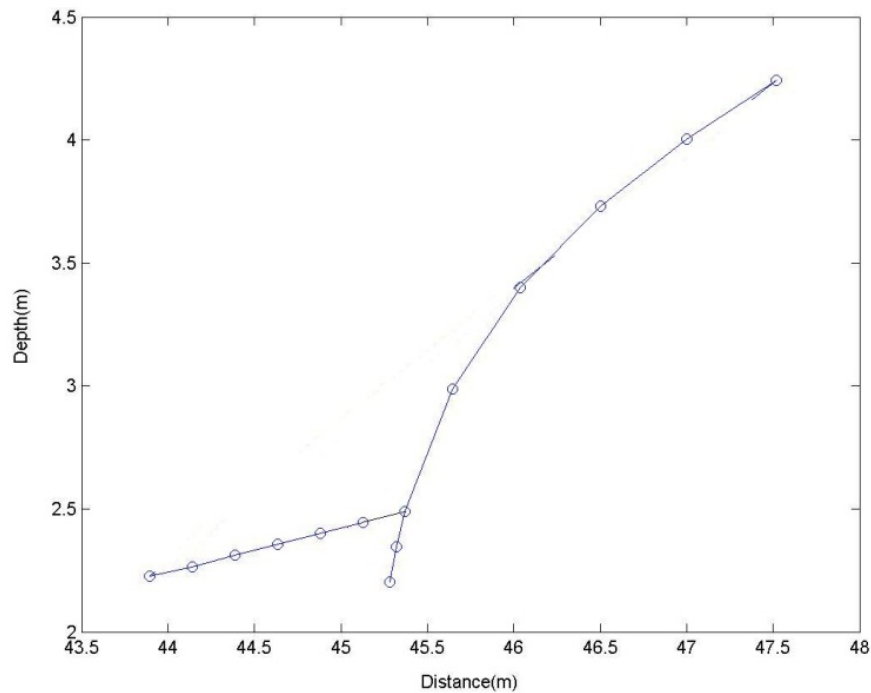


Fig 6.1 Simulated configuration of the two-part towing system

The theoretical results in the investigation indicate that the hydrodynamic response of a towed vehicle to the wave induced motion of a towing ship can be significantly reduced by applying a two-part towing method and also provides an evidence of the soundness of the mathematical model devised.

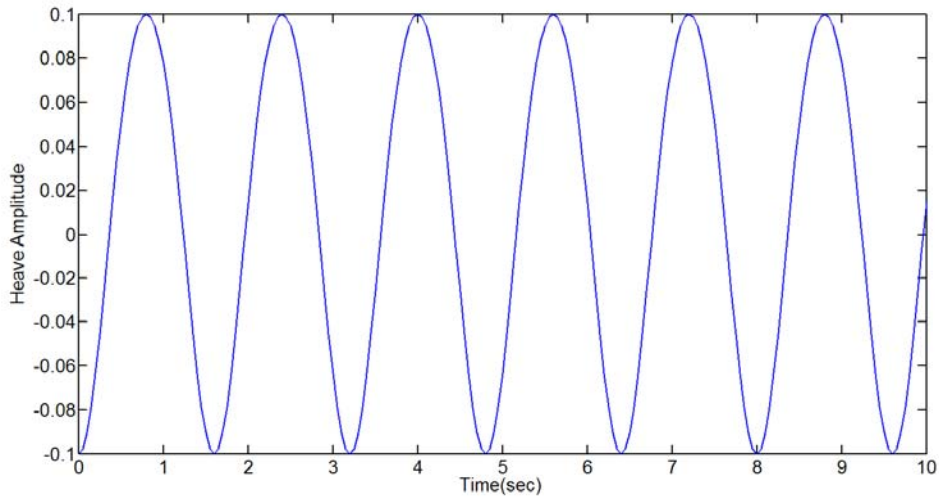


Figure 6.2. Sinusoidal input motion (heave) given to the tow-point

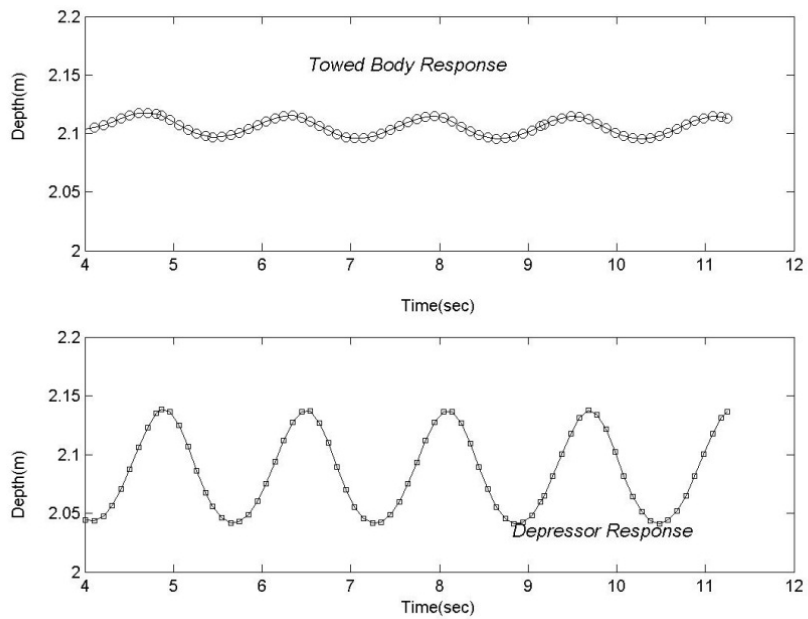


Figure 6.3 Towed body and depressor heave

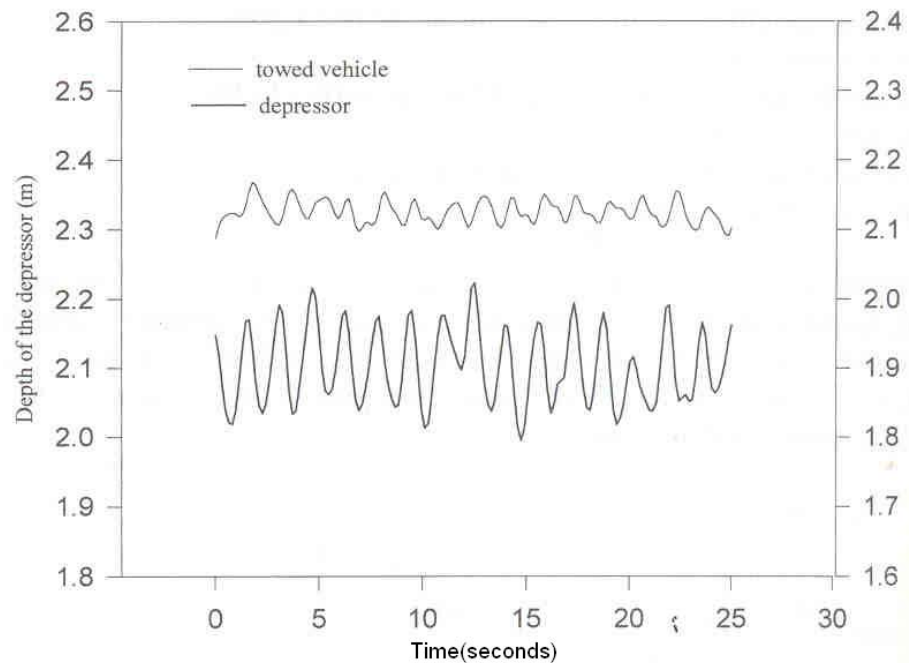


Figure 6.4. Experimental heave values from literature [Wu, 2001]

6.3 Test Case 2: Tow-Ship Manouvering Examples - Single Point Towing

As a further verification of the developed model, we performed dynamic simulations of a tow cable system (ship, tow cable, and towed vehicle) going from a straight-tow configuration to one in which the tow ship is making a constant radius turn (i.e. steady-state turning configuration). This example is documented in literature [Shan,1995]. The full three dimensional numerical simulation was performed in this study. The simulation was allowed to proceed until the towed system reached a steady state with the vehicle making its own constant radius turn and maintaining a constant depth.

In this case the tow-ship was undergone straight line run for nearly 700m and turns left and undergoes a circular manoeuvre with radius equal to 150m. After having a full circular path, the ship again runs straight. The simulation starts from rest and advances with a velocity of 2m/s. The positions of cable as well as sub-sea unit are continuously monitored.

Test Data

Cable radius = .047m, Cable Length = 300m. Young's Modulus = $9e9\text{N/m}^2$

Coefficient of Normal and Tangential drag C_n and $C_t = 1.2$ & $.01$

Mass of the sub-sea unit = 3000 kg. Drag coefficient of the sub-sea vehicle = 1.5

Figure 6.5 shows the plan view of path of the ship and towed body. It can be seen that trajectory of the towed body is well inside the path of tow point.

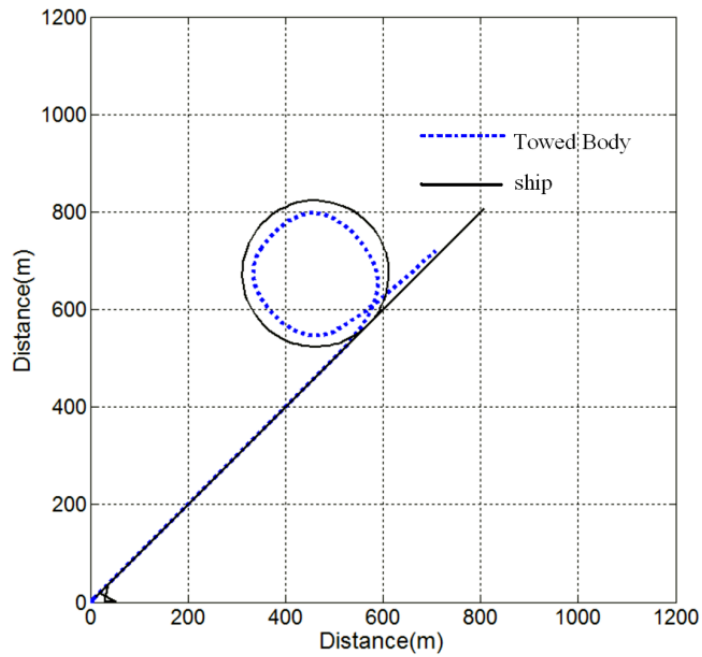


Figure 6.5. Simulated Plan View of the path of ship and towed body

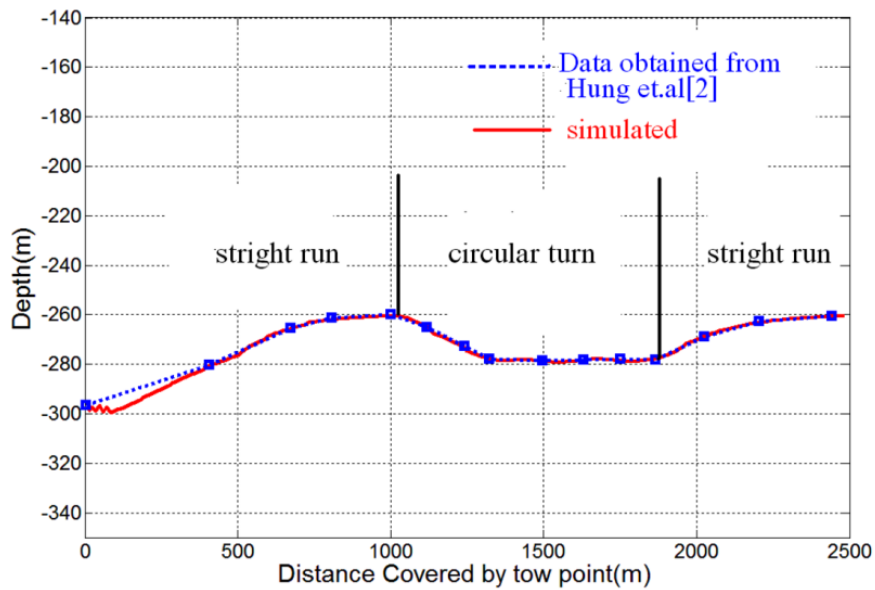


Figure 6.6 Simulated depth variations

Figure 6.6 shows the simulated depth variation of the towed body when the ship undergoes straight line and circular manoeuvre. The simulated depth data are compared with that obtained from Shan [Shan,1995] which employs classical LSM as the numerical model. It can be seen that in spite of the flexibility introduced in the equation motion as per the HHT- α method, the numerical scheme was capable of predicting the real-time depth of towed body to sufficient accuracy during the cable motion under circular manoeuvre of the ship.

In the third test, the numerical simulation of sudden stoppage of a steady moving tow-ship was attempted. The same tow configuration discussed in the test number 2 was selected. Dynamic simulation was continued until towed body velocity becomes zero. Figure 6.7 shows the real-time depth of the tow system when the ship was suddenly stopped as the tow point was moving at a speed of 2m/s. It can be seen that even after the ship was stopped, it takes considerable time in stoppage of the whole towing system. Further, it can be concluded that the developed model is physically capable of simulating this type of ship manoeuvres.

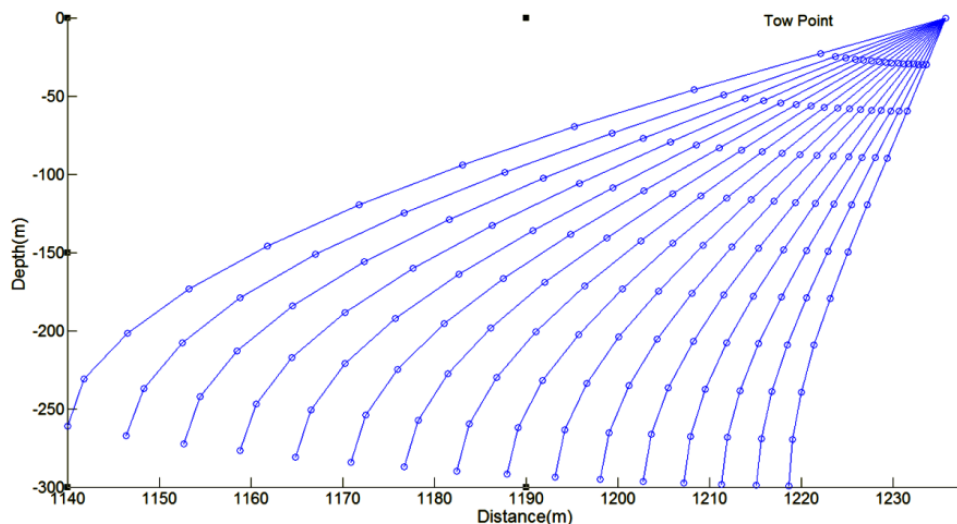


Figure 6.7 Depth variation of the towing system when the ship is suddenly stopped

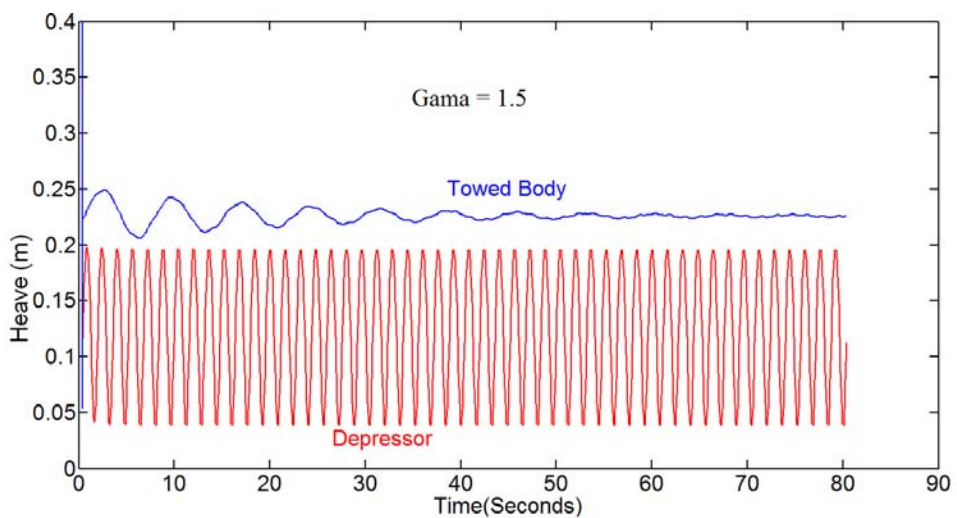
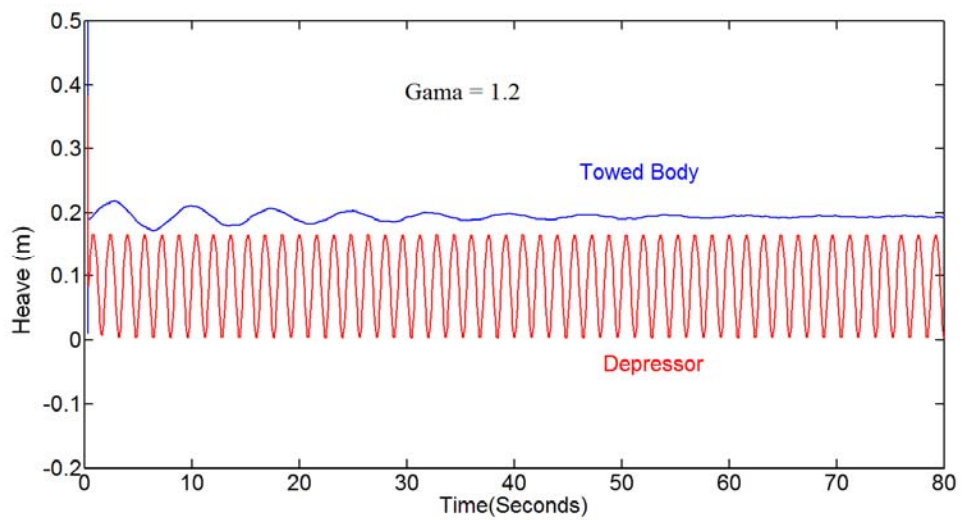
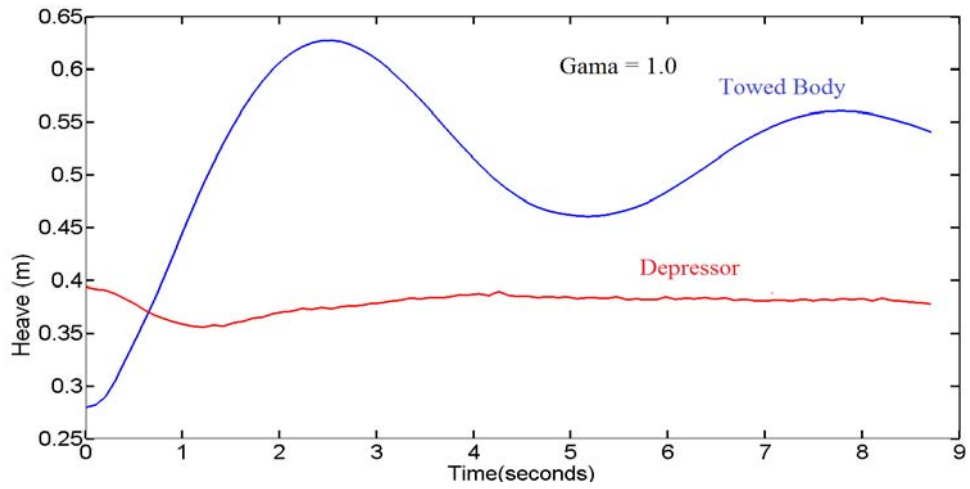
6.4 Testing of Time Integration Schemes

In this section the following time integration schemes (discussed in chapter 3) were tested. The test case 1, discussed in section 6.1 was selected as the benchmark problem.

Tested time integration procedures are

1. Houbolt scheme
2. Newmark Scheme
3. Euler scheme
4. HHT- α scheme

The obtained results are compared with experimental values from literature [Wu,2001]. Out of the various performance parameters that are to be measured for evaluation of a numerical scheme, the characteristic ‘accuracy’ was given maximum importance. Some of the other parameters investigated are convergence characteristics, degree of numerical damping, overshoot in displacement field etc. To study the performance of Houbolt scheme (single step Houbolt) discussed in literature [Hughes, 1987], a number of numerical simulations were carried out with controlling parameter γ varies from 0.5 to 1.5. Subsequently, the time based heave amplitude of the towed body as well as that of the depressor was plotted as shown in figure 6.8 a,b,c and d. It may observed that when the controlling parameter of the scheme, γ equal to 1.0, the obtained heave ratio (the ratio of heave of towed body to the depressor heave) of the towed body is much higher (heave ratio more than 5) while, the actual value is 0.24 (from literature [Wu,2001]). On the other hand when γ changes from 1.2 to 1.6 the simulated heave ratio falls to very low value (nearly 0.03) implying that Houbolt scheme is unsuccessful for simulating the motion dynamics of two-part towing at least within the tested range. The observed reduced accuracy may be attributed to the inherent damping characteristics of the scheme which damps out not only high frequency modes but also useful low frequency ones. Further, considerable overshoot in the displacement field is observed at all values of γ within the test range. Also, It was found that solution become unstable with γ values in the range [0.5, 1.0].



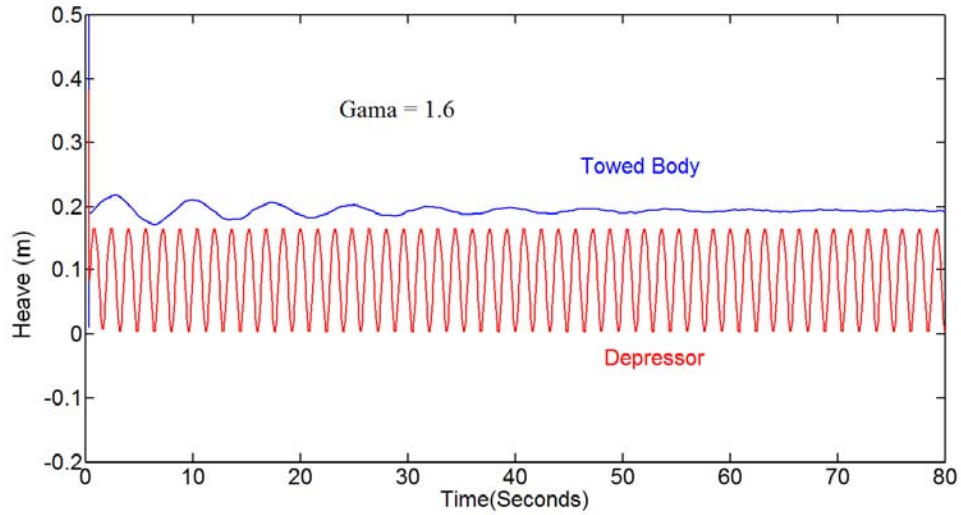


Figure 6.8d Heave response for Hoboult Schme $\gamma = 1.6$

6.4.1 Euler Scheme

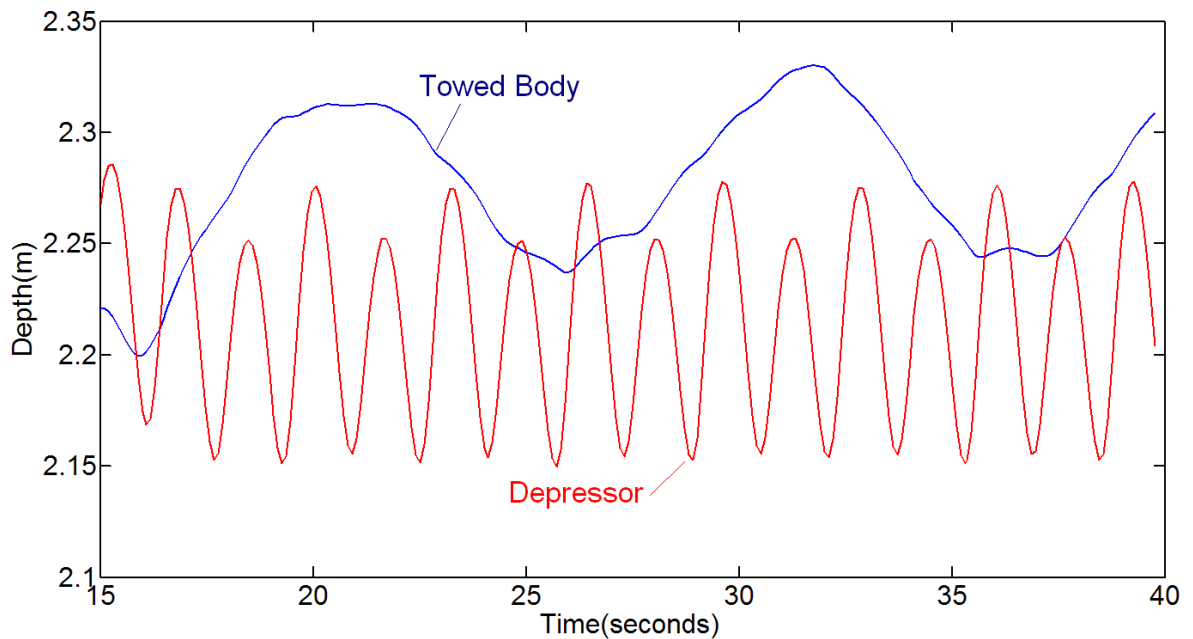


Figure 6.9 Heave response for Euler Scheme

In this study forward Euler scheme was used to discretize the time space and it can be seen from the figure 6.9 that, the solution becomes unstable after few time steps leading to a heave ratio of more than 1 (which is highly unrealistic). Therefore, the Euler scheme in its current form is not suitable for simulation of dynamics of two-part underwater towing system.

6.4.2 HHT- α

In this scheme the controlling parameter that decides the level of numerical diffusion and accuracy is α for which, the recommended value [Hughes, 1987] lie in the range $[-0.33, 0]$. Numerical simulation was done with varying in α and the heave responses for each case are plotted as shown in figures 6.10 to 6.16. The obtained heave ratio is equal to 0.201 in the case when α is equal to -0.33 (figure 6.16) while the correct value from the literature [Wu,2002] is 0.24 and in all other cases the simulated heave ratio was found less than 0.02. Therefore HHT- α method with $\alpha = 0.33$ is the only case for which the results obtained were satisfactory implying, the parameter α plays a significant role in providing accury and numerical damping of high frequency oscillation. Further, the displacement overshoot is also least when $\alpha = -0.33$.

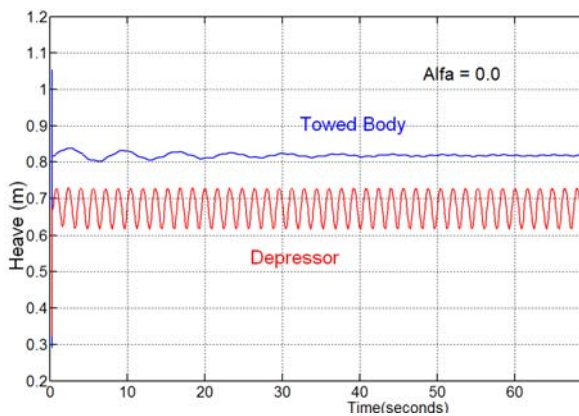


Figure 6.10 Heave response $\alpha=0.0$

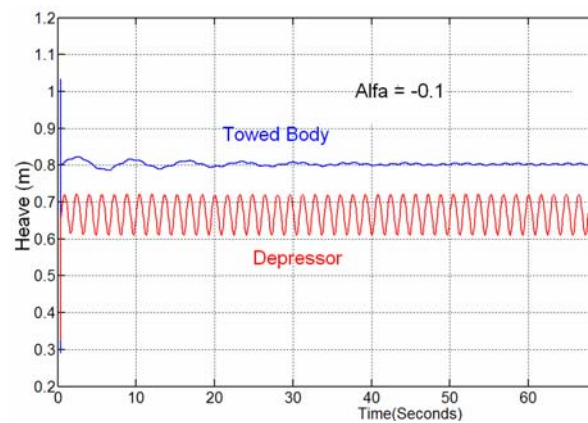


Figure 6.11 Heave response $\alpha=-0.1$

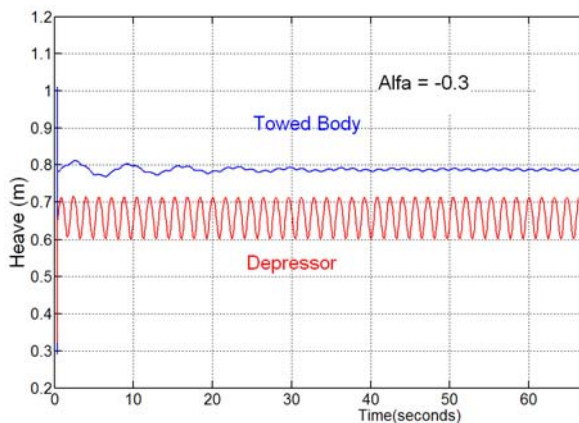


Figure 6.12 Heave response $\alpha=-0.3$

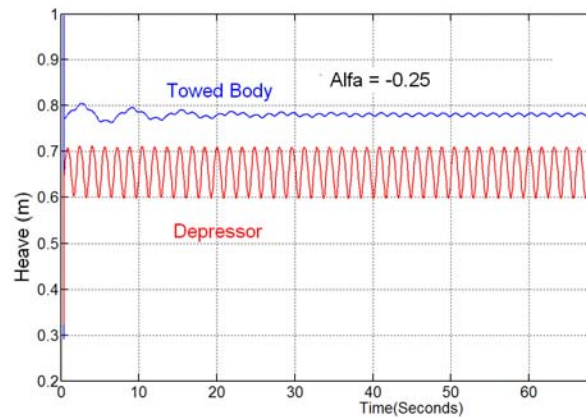
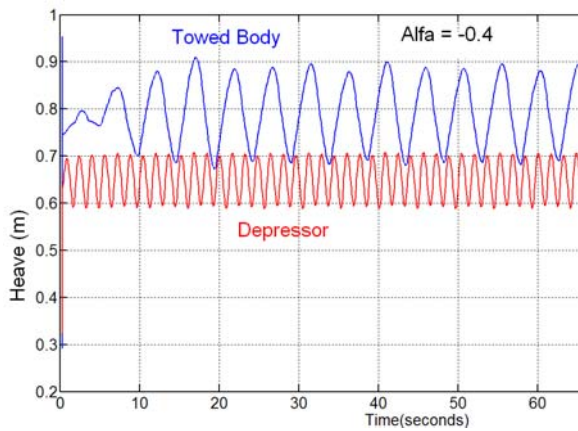
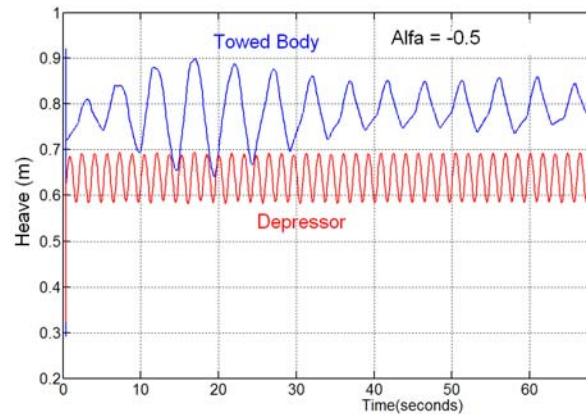
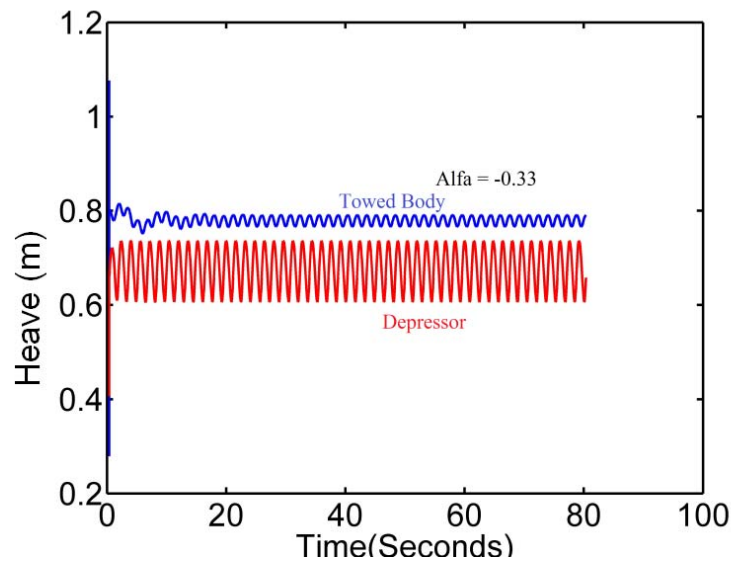


Figure 6.13 Heave response $\alpha=-0.25$

Figure 6.14 Heave response $\alpha=-0.4$ Figure 6.15 Heave response $\alpha=-0.5$ Figure 6.16 Heave response $\alpha=-0.33$

6.4.3 Newmark's method

In the Newmark's method, unconditional stability is guaranteed for $\beta=1/4$ and $\gamma = 1/2$ for linear system of equations. At this point the accuracy will be the maximum and it does not provide algorithmic dissipation [Hughes, 1987]. Therefore, only one test case has been done in the present numerical experiment using Newmark's time integration procedure with the controlling parameters $\beta=1/4$ and $\gamma = 1/2$. Figure 6.17 shows the simulated heave response of the towed body and the depressor. It may be observed from the figure that obtained heave ratio is well below the actual value, 0.24.

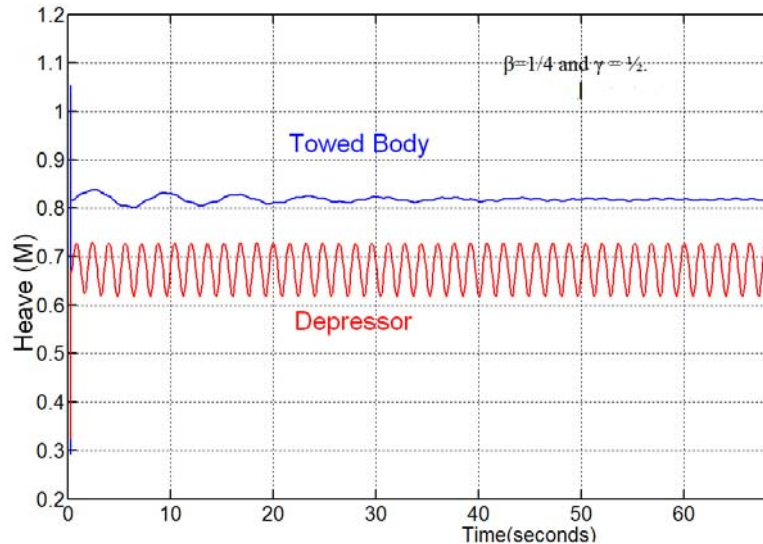


Figure 6.17. Heave response with Newmark method

6.5 Parallel Computations

It is a matter of fact that numerical algorithms for fluid and structural mechanics have been matured enough in its development, over the years though, proportional gain in the form of reduction of execution time in the computer based simulations is not comprehensive. Even today, simulation of an industrial flow situation requires considerable computer resources and execution time. So to reduce the later is of paramount importance for industries like automobile one where, fluid, structural analysis of the sub-systems consume considerable time during the development of newer products. The parallel computing is one of the answer to this situation which mainly focus on two aspects i.e hardware and software. The chapter mainly discuss about application of parallel computing technologies to speed up the numerical code developed for this project.

The common approaches for parallel computing falls into following categories.

- For shared memory systems
- Distributed memory systems

6.5.1 Shared-memory multiprocessors

Shared memory architecture is defined as a group of processors sharing a single memory in the sense that all processors are working within a single memory address space, whereas it is possible that the memory is physically distributed.

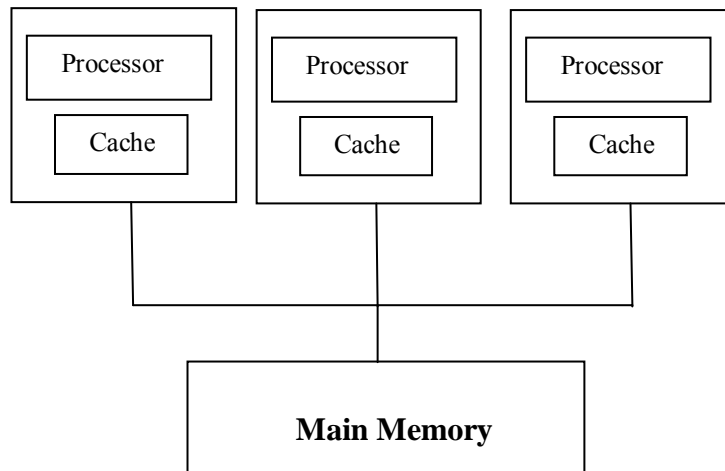


Figure 6.18 Shared memory system

It is important that every processor can access every memory location. Thus different processors can communicate via shared variables in memory.

Multiprocessors with a physically distributed memory and a shared memory address space are called distributed shared memory (DSM) architectures. Usually this architecture offers a non-uniform memory access (NUMA), because the access time depends to the data location in memory.

6.5.2 Distributed-memory multiprocessors

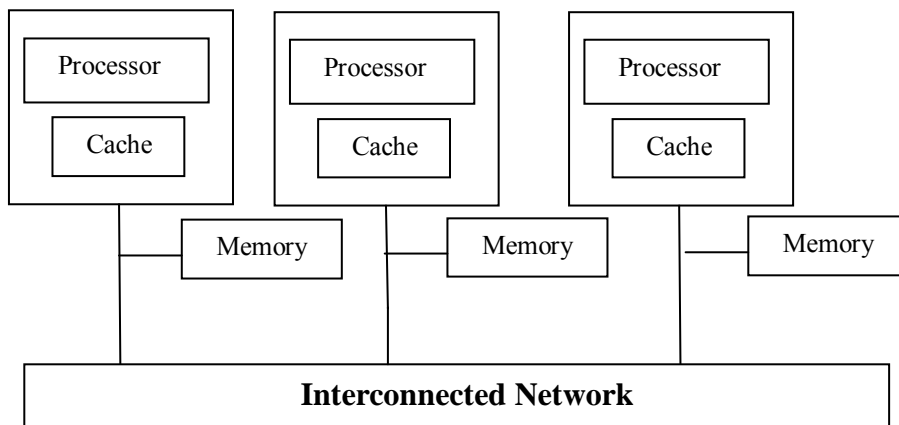


Figure 6.19 Distributed-memory multiprocessors

6.6 Parallel Programming Paradigms

Parallel programming approaches are also classified on the basis of the processor architectures available. Distinct programming tools or methodologies are available for shared memory and distributed memory systems. In this section, programming tools for shared memory processors are discussed. Most common approaches are OPENMP, Pthreads, POSIX libraries. Out of these OPENMP is the most important and has been implemented in the codes developed for this project.

OPENMP is a concurrency platform for multithreaded, shared memory parallel processing architecture for C, C ++, and FORTRAN. OPENMP is best suited when the code contains loops and the data dependency is low. Main advantage of OPENMP is that sequential codes can be very easily parallelized with little programming effort. The user does not need to create the threads nor worry about the tasks assigned to each thread. In that sense, OPENMP is a higher - level programming model compared with Pthreads in the POSIX library.

OPENMP uses three types of constructs to control the parallelization of a program:

- Compiler directives
- Runtime library routines
- Environment variables

Table 6.2 Some OPENMP Directives

OPENMP pragma directive	Description
#pragma omp atomic	Defines a memory location to be updated automatically
#pragma omp barrier	Synchronizes all threads in a parallel region
#pragma omp critical	Defines the code section that follows the directive to be executed by single thread at a time
#pragma omp for	Specifies that the for loop iterations should be run in parallel using multiple threads
#pragma omp parallel	Defines a parallel code region to be run by multiple threads : the original process will be master thread
#pragma omp parallel do	Splits up the loop iterations among threads
#pragma omp parallel for	Similar to parallel do pragma

6.7 Message Passing

The message-passing programming model is based on the abstraction of a parallel computer with a distributed address space, where, each processor has a local memory to which it has exclusive access. There is no global memory. Data exchange must be performed by message-passing: To transfer data from the local memory of one processor *A* to the local memory of another processor *B*, *A* must send a message containing the data to *B*, and *B* must receive the data in a buffer in its local memory.

A message-passing program is executed by a set of processes, where, each process has its own local data. Usually the program executed in a SPMD way. The processes executing a message-passing program can exchange local data by using communication operations. By far the most popular portable communication library is MPI (Message-Passing Interface) but PVM (Parallel Virtual Machine) is also often used,

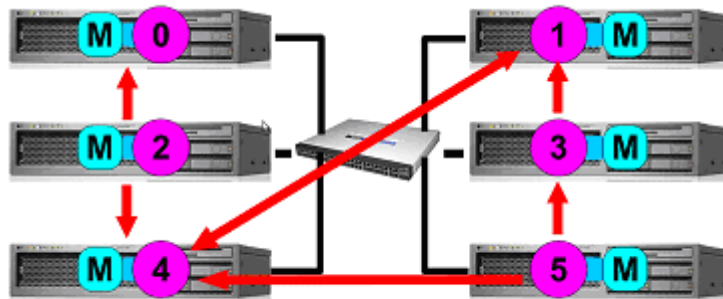


Figure 6.20 Cluster systems

There are two versions of the MPI standard: MPI-1 defines standard communication operations and is based on a static process model. MPI-2 extends MPI-1 and provides additional support for dynamic process management, one-sided communication, and parallel I/O. Commercial and free versions of MPI standard implementation are available. Freely available MPI libraries are MPICH, LAM/MPI and OPEMPI.

We can identify the following types of communication modes available in MPI standards:

1. One to one (unicast)
2. One to many (multicast)

3. One to all (broadcast)
4. Gather
5. Reduce

6.8 Code Parallelisation Simulation code for Shared Memory

Architecture

The primary requirement of code parallelization comes from the fact that, the original FORTRAN code developed for the simulation of two-part underwater towing system takes considerable execution time as the number of LMSM segments increases beyond say, two-hundred. This may be due to, the use of dense solver, which is based on Newton-Krylov method leading to the assembly large dense Jacobean with double precision attribute. Subsequently, the processor may take significant amount of computational time in evaluation of Jacobean, QR factorization etc. The reason for the selection of shared memory programming model for towing simulation is the lower order of the problem size compared to CFD simulation, where millions of flow equations need to be solved simultaneously, necessitating a dedicated distributed computing setup.

Table 6.3 MINPACK functions

MINPACK Function	Purpose
ENORM	Computes the Euclidean norm of the vector x
FDJACI:	Computes the forward difference approximation to the jacobian
QFORM	Accumulate orthogonal matrix from QR factrisation
QRFAC	Compute QR factrorisation of rectangular matices
QRSOLV	Complete the solution of least square problem
RIUPDT	Upadate QR fatorisation after rank-1 addition
DOGLEG	Finds the combination of Gauss-Newton and gradient step which minimises the least square error.

It was also found that do loop parallism offered by OPENMP is a good choice because of multiple reasons such as, it is simplest OPENMP directive available and the original FORTRAN code for towing simulation consists of a number of loop iterations. Further, the

code involves two parts which are: modules for the assembly of dynamic equations and the solver, MINPACK . Out of these two, solver part takes considerable computational overhead in terms of time, necessitating parallelization of that part. Thus the functions listed in table 6.3 from the original MINPACK serial code was paralledised using OPENMP directives.

6.9 Parallel Performance

To evaluate the performance metrics of the developed code in FORTRAN, the same has been run in different computing platforms. The input parameters considered in test are total number of degrees of freedom to be solved and number shared memory CPUs. The output parameter is the computational time. The program has been tested in Intel Quad core CPU ,AMD phenom Quad and AMD Dual core machines with Linux kernel 2.6. The number of CPU used also varied from 1 to 4 by using the global environment variable OMP_SET_NO_THREADS. The opensource GOMP libraries are used for OPENMP and the threads were executed without any sort of inbuilt compiler optimisation.

Table 6.4 Platforms tested

SI No	System	OS
1	Intel QUAD core Q8200 1.33 GHz 4 GB RAM	Linux Kernel 2.6.38
2	AMD PHENOM QUAD 2.33 GHz 2GB RAM	Linux Kernel 2.6.38
3	AMD Dual core E-350 RAM 2GB	Linux Kernel 2.6.38

To monitor the CPU usage, network traffic etc, during the computation process, opensource GKRELLE utility which is supposed to have advanced capabilities compared to conventional GNOME monitor. Figures 6.21 ,6.22 and 6.23 show the computational time for the solution of towing problems with 26 , 120 and 170 degrees of freedom. Unlike,

linear simultaneous equations, the solution of nonlinear ones, takes considerable computational time, even for small number of equations, especially when dense solvers are used. The use of dense solver leads to the assembly large dense Jacobean with double precision attribute. Subsequently, the processor may take significant amount of computational time in evaluation of Jacobean, QR factorization etc. This was the reason for taking small number of degrees of freedoms (maximum 170) for benchmarking the parallel solver. While, the red line shows the ideal scaling of the computational time when number of processor changes from 1 to 4, blue lines shows the actual one. Figure 6.21 shows the computational time in seconds in which, the number of variables to be solved are limited to 26. It can be seen that, as the number of CPUs increases from 1 to 4 the corresponding computational time shows an increasing tendency, rather than decreasing. Therefore, it may be concluded that for the case of only a few variables are to be solved as in the test case no:1, the thread level parallelism offered by OPENMP has little effect on total computational time. While, in test case 2 the number of variables to be solved was increased to 120, resulting in a marginal gain in the computational time as the number of processors increased to 4. The observed computational efficiency is nearly 132% and in the ideal case, the same should have been 400%. When, the number of degrees of freedom increased to 170, the actual computational efficiency rose to 156% implying that, a further increase in degrees of freedom to be solved, will have more computational advantage by code parallelism through OPENMP directives.

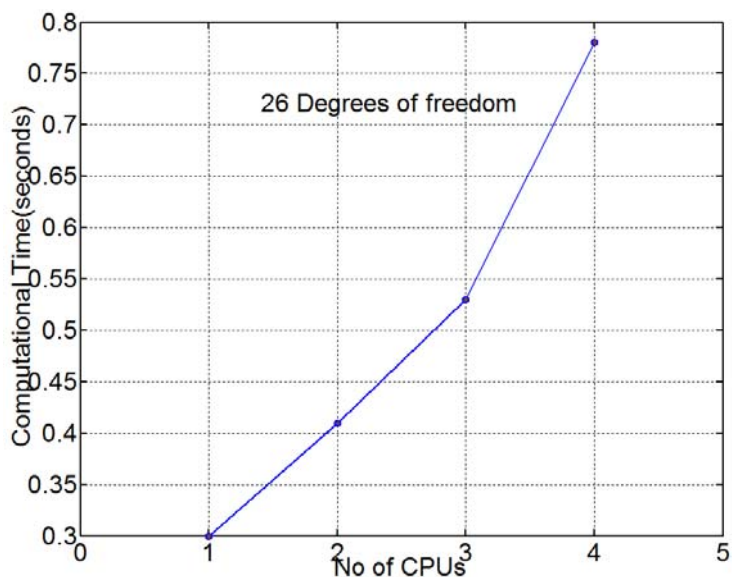


Figure 6.21 Computational time for 26 degrees of freedoms

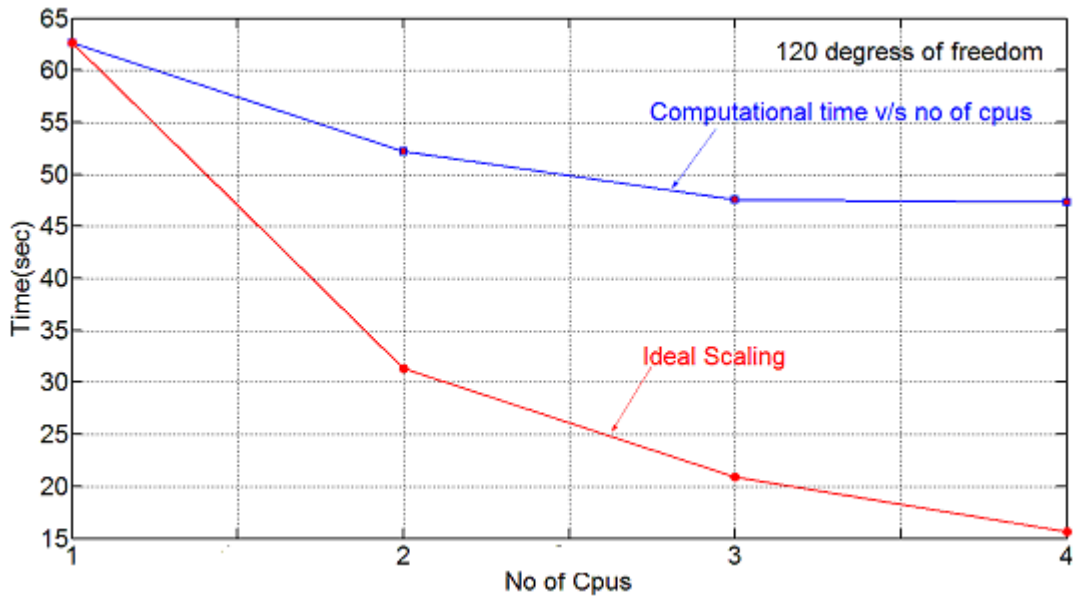


Figure 6.22 Computaional time for 120 degrees of freedoms

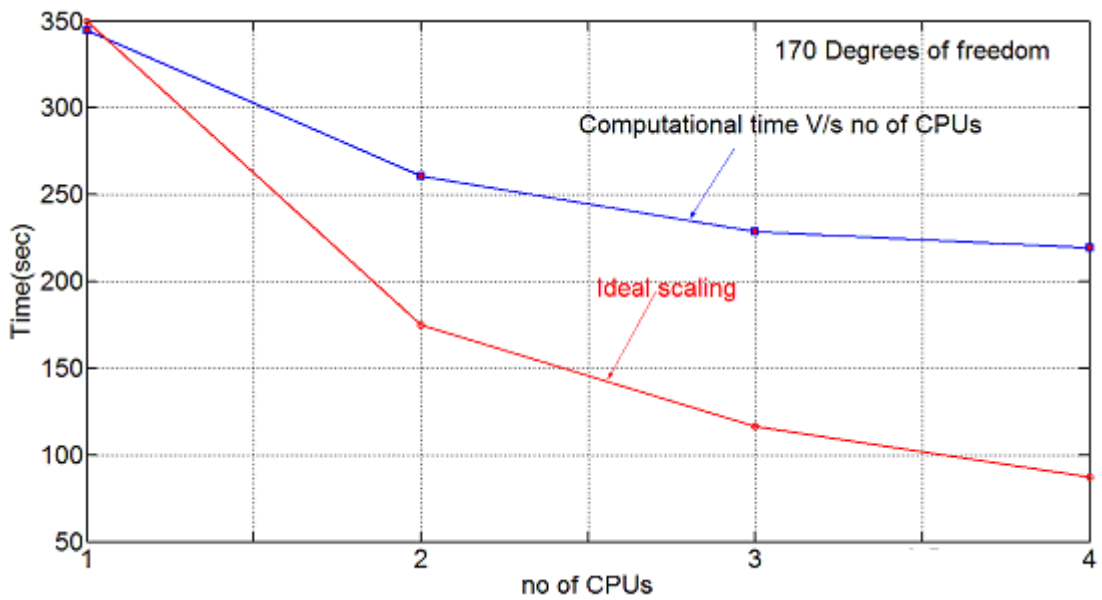


Figure 6.23 Computaional time for 170 degrees of freedoms

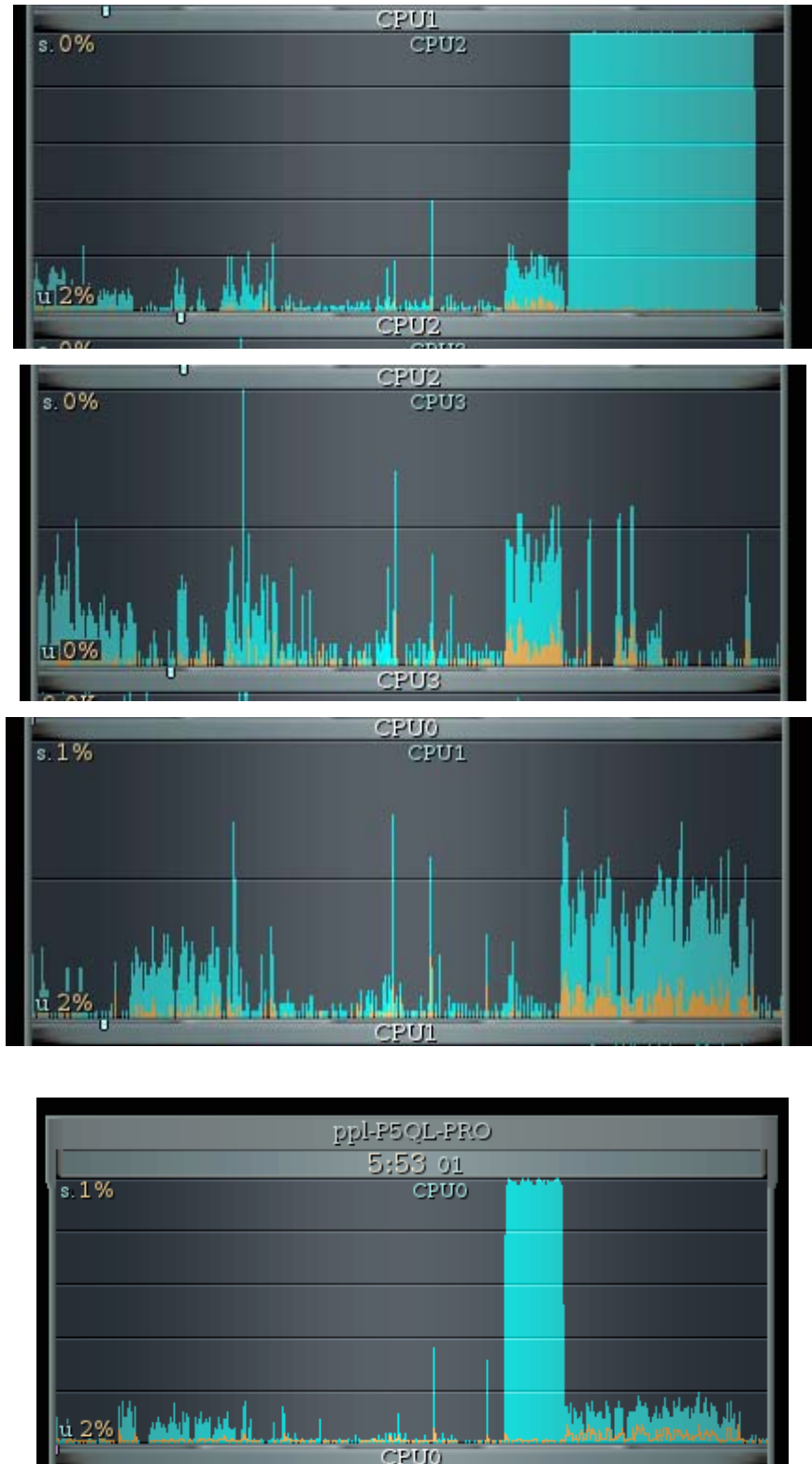


Figure 6.24 CPU utilization of the serial code (without OPENMP)

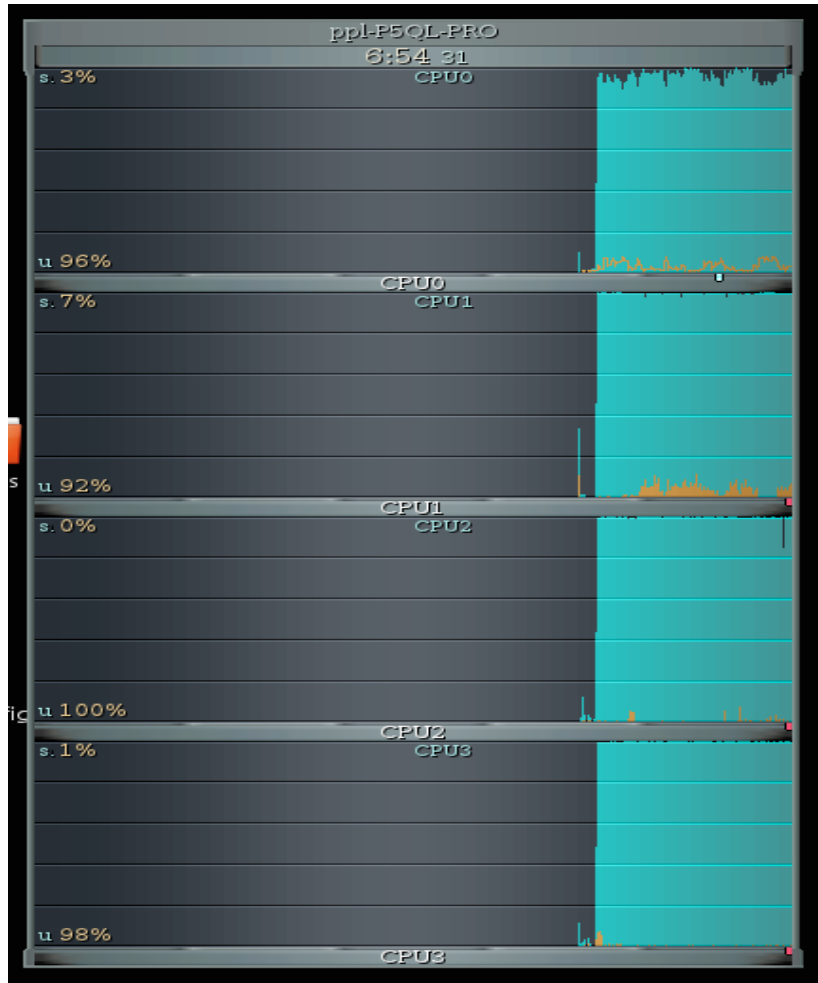


Figure 6.25 CPU utilization of the Parallel code (with OPENMP no of CPU =4)

Figure 6.24 shows the output from GKRELLE CPU monitor, when the simulation was done in a serial way (single CPU) using shared memory QUAD core CPU (Platform no 1). It is evident from the figure is that overall CPU utilization is very low nearly (25%) without any OPEENMP directive. Figure 6.25 shows the CPU utilization, when all of the available cores take part in the computation. Much better overall CPU utilization was observed in this case (nearly 100%) leading to reduced computational time.

6.10 Code Parallelisation for Distributed Memory Architecture

Unlike shared memory systems, distributed memory ones have multiple CPUs, with each having its own memory space that is not shared. Distributed memory systems are mainly used in tasks, which are computationally intensive, such as CFD simulations where shared memory programming models are less successful due to the requirement of large number of equation (millions) to be solved simultaneously. Out of the MPI and PVM based programming models available for distributed memory architecture, the present study devises former approach as the latter one is less popular.

6.11 Parallelisation of CFD code

Parallelization of the code is done using the PETSc framework. PETSc is a suite of data structures and routines suitable for the development of large-scale scientific applications on parallel and serial computers. The inbuilt sparse storage systems, their matrix algebra and linear solvers inside PETSc, were utilized to form and solve fluid dynamic equations. The C-code developed for this project makes use of Single Program Multiple Data (SPMD) message passing model, i.e. each process runs the same program and performs computations on its own subset of data. MPI-2 compatible OPENMPI was used as message passing interface. Dependent variables are stored in global vectors with ghost cell padding. Communication is performed when necessary to update information of the ghost cells.

Table 6.5 Cluster Details

CPU Specifications	AMD PHENOM QUAD 2.33 GHz
Memory (RAM)	2GB /node
Disk Memory	4 Terra byte
Total number of CPUs	32
Interconnect	Gigabit ETHERNET
Message Passing Interface	OPENMPI
Operating System	Linux Kernal 2.6.38



Figure 6.26 Parallel computing setup

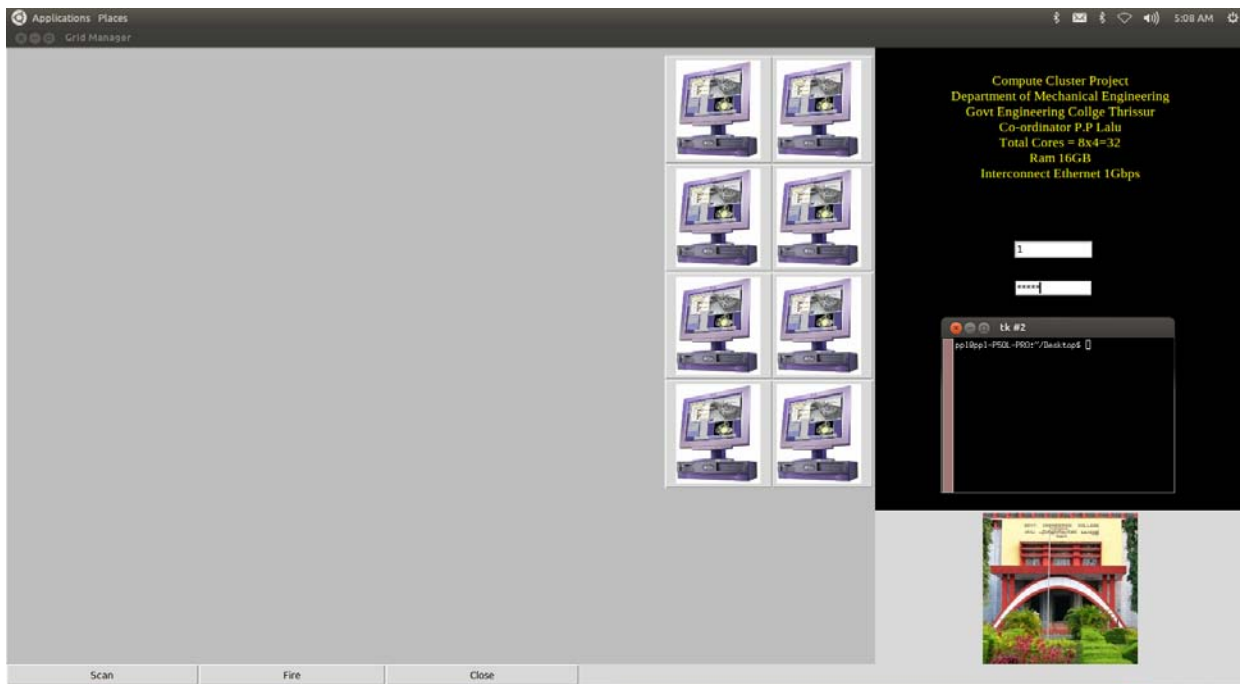


Figure 6.27 Software Front End for logging into the network and application deployment

Figure 6.26 shows the front end of the Cluster computing software, which is mainly used for user-login into the master node and subsequent deployment of applications. Apart from regular computational loads, master node (node0) has the additional work of scheduling jobs, user prompting, coordination of threads etc. The user interface (UI) was developed in PYTHON programming language with Tk/Tcl libraries. There is a scan utility in the UI, which automatically search over the network and detect the available nodes. Subsequently we can select the individual nodes from a list and form a cluster for further computation. The remote execution of system commands of the individual nodes were done by using SSH (Secure socket shell). There a NFS share for each node in the master computer, where we can put applications for parallel execution. The first step in the computation process is the dividing of the whole domain into multiple pieces which will serve as the local domain for individual processors. This process is called domain decomposition.

6.12 Domain Decomposition

The computational domain (mesh) can be divided into several regions for parallel processing. The domain decomposition is obtained using open source package METIS . Two partitioning schemes are implemented in METIS: the recursive bisection scheme and the k-way scheme. The former scheme is used when the number of regions is less or equal to 8, while the second is used for all other cases. After the domain was divided, cells are renumbered and stored in separate mesh files. Each processor computes one region of the domain. Therefore, the number of processes should be equal to the number of regions. Each process uses local indices to minimize memory storage. Relationship between global and local indices is guaranteed by PETSc data structures.

A mesh visualizer has been specially made using MATLAB software, for visualizing the partitioned mesh (figure 6.28).

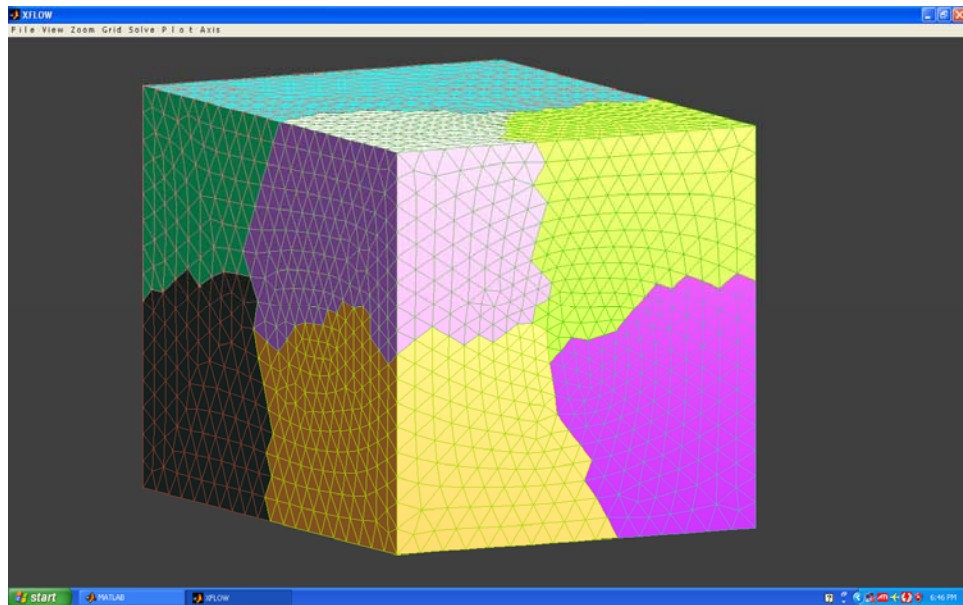


Figure 6.28 Mesh visualiser for partitioned mesh

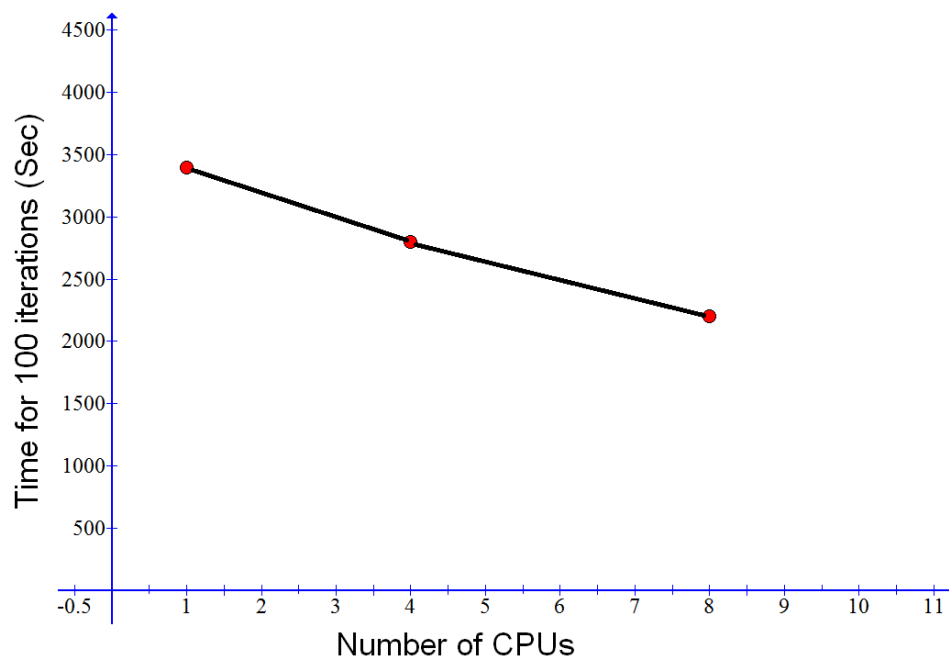


Figure 6.29 Computational time v/s no of CPUs for test case -1

6.13 Parallel test case

For estimating the parallel performance of the newly developed cluster (sponsored by CERD, Govt of Kerala) test case-1 discussed in section 5.16 was selected as the benchmark problem. All nodes are interconnected by 1Gbps Ethernet LAN with Message Passing Interface as OPENMPI. The domain is decomposed into 8 computational regions using METIS graph partitioning algorithm and the assembled flow as well as turbulence equations are solved using PETSC framework. While a total of 32 CPUs are available in the cluster, only 8 CPUs (maximum) are taken part in the simulation. Figure 6.28 shows the corresponding speedup obtained.

6.14 Conclusion

The numerical study indicates that the hydrodynamic response of a towed vehicle to the wave induced motion of a towing ship can be significantly reduced by applying a two-part towing method. The modified LMSM discussed in the previous chapters was successful in simulating the dynamics of two-part underwater towing system.

Further, traditional lumped mass spring system which uses Euler time stepping is vulnerable to numerical oscillation when towing with multiple cables and complicated tow configurations. Also in spite of the flexibility introduced in the equation of motion as per HHT- α time integration procedure, to provide sufficient numerical damping, the model is still capable of simulating different ship maneuvering situations in the real time. This has been verified by comparing the depth data from the simulation of Huang et.al [Shan, 1994] where it uses traditional backward Euler time integration method.

When comparing the numerical performance of time integration procedures like Houbolt, Newmark, Euler, HHT- α schemes in simulating the heave response of the towed body and the depressor of a two-part underwater towing system, HHT- α is the only scheme which produced comparable results with experimental values.

Further the controlling parameter α in HHT- α scheme plays a significant role in producing good results and when α values nearly equal to -0.33 the results obtained were satisfactory.

Parallel computations is an emerging area, where intense research is going on with the sole purpose of reducing the time involved in computer based simulations. Out of various programming paradigms available, shared and distributed memory systems are widely used in engineering simulations. The former approach based on OPENMP offers relatively simple procedures to parallelize the serial code.

Based on the speedup test done with FORTRAN code developed in-house for structural dynamic simulation of two-part towing system, and parallelized through one of the leading shared memory programming model like OPENMNP, it was found that, the code has got reduced execution time compared to serial one.

Unlike shared memory programming model, the distributed memory systems using MPI can handle large scale computation process and is widely used in CFD simulation. From the speed up test done using the C-code developed for CFD simulation and parallelised through MPI, it is observed that there is only a marginal improvement of speed up by using multiple CPUs. This may be attributed to poor performance of the Ethernet based interconnect.

Design Optimizations of the Two-part towing system

Contents	<i>7.1 Parametric Study</i>
	<i>7.2 Conclusion</i>

The focus of the present chapter is to study the effect of geometrical as well as a number of other parameters on the stability of the towed body. The proper selection of length of primary, secondary and depressor cable is important for better hydrodynamic stability of the towed body. Similar to that, the weight and shape of the depressor, frequency of the external disturbance have bearing on the same. The present investigation sets out to address this aspect, there by aiming to study the effect of above said parameters on the heave response of the towed body. To achieve this numerical simulations are done with varying towing configurations and effect of individual parameters is plotted. Based on that final optimisation of the tow system was made.

7.1 Parametric Study

The effect of following parameters on the heave stability was investigated

- Length of depressor cable.
- Length of Primary cable.
- Length of secondary cable.
- Weight in water of the depressor.
- Frequency of input disturbance.

- Effect of bending rigidity of the tow cable

To study the effect of these parameters, numerical problem discussed in section 6.2 was taken as the test case. The fixed horizontal velocity was assumed to be 1.75m/sec and sinusoidal vertical heave was taken as in the given equation 6.1. The time period of crank rotation was taken as 1.6sec and crank radius is equal to 0.1m. The length of the connecting rod was set to 0.35m. Further numerical experiments are done at various levels of these parameters.

The particulars of composite cables, depressor and towed tow-fish system are

Depressor:-Diameter = 0.11m Weight in air = 5.25kg. Weight in water = 4.58 kg.

Towed Tow-fish: - Diameter = 0.11m. . Weight in air 12.50. weight in water = 0 kg.

Primary cable:- Weight in air = 0.181 kg/m. Weight in water = 0.104kg/m.

Depressor Cable:- weight in air = .063 kg/m. Weight in water = 0.039kg/m

Secondary cable :- Weight in air 0.124kg/m.Weight in water = 0.065 kg/m

Figure 7.1 shows the variation of heave ratio (which is the ratio of the heave response of towed vehicle and that of the depressor) with respect to the length of the depressor cable. It can be seen that the heave amplitude decreases monotonically as the length of depressor cable decreases. Thus theoretically a near-zero-length depressor cable is ideally suited to enhance the stability of the towed vehicle in a two-part towing system. This may be attributed to the lower oscillating cable-tension nearer to the depressor due to fluid damping.

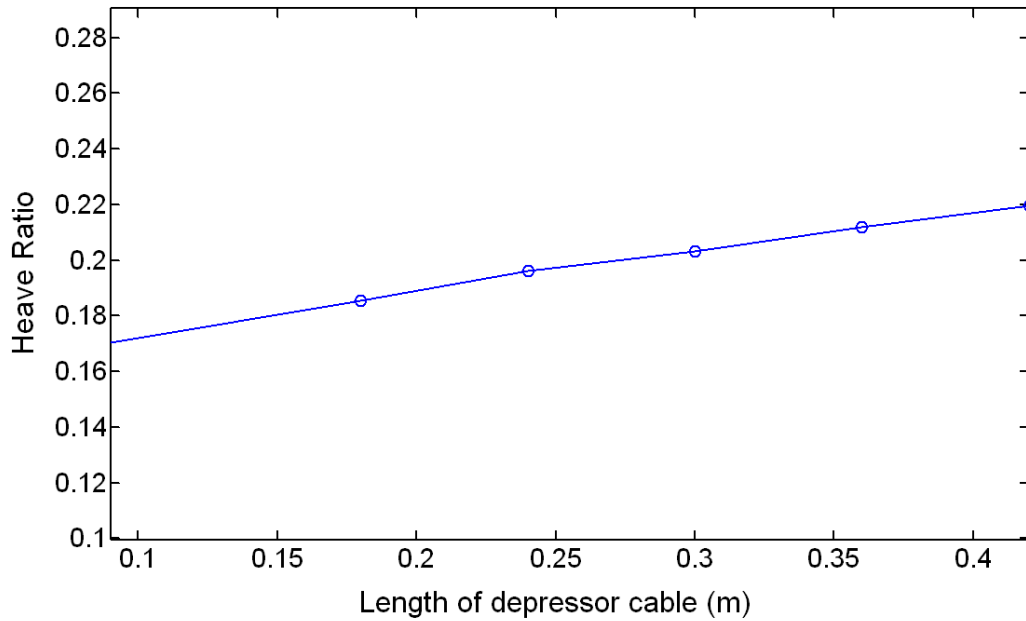


Figure7.1. Variation of heave ratio with length of depressor cable

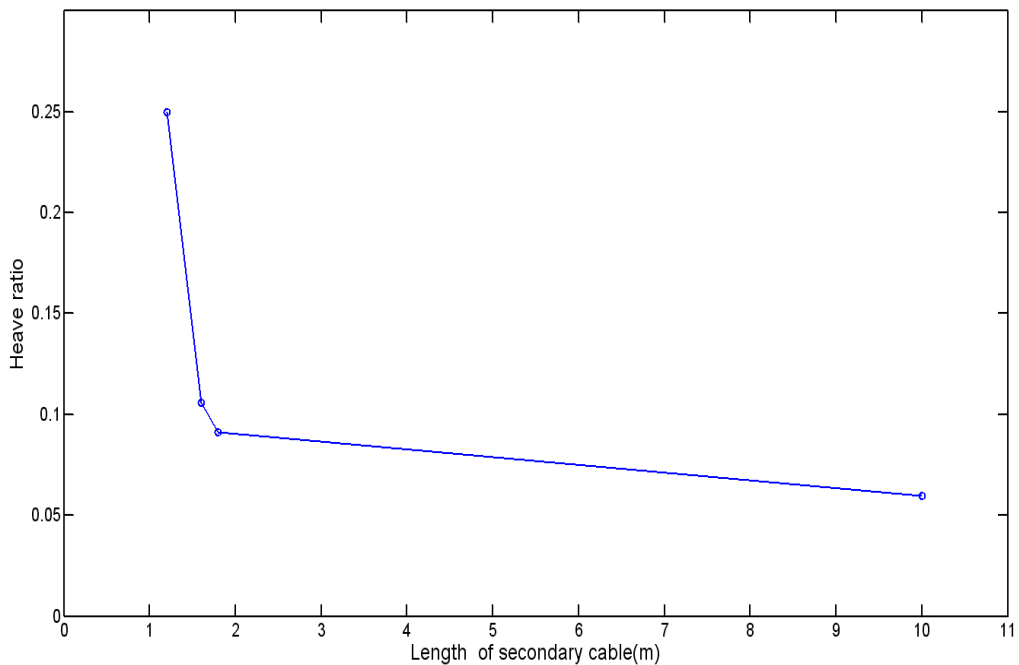


Figure 7.2. Variation of heave ratio with length of secondary cable

Figure 7.2 shows the variation of heave ratio of the towed body with respect to the length of the secondary cable. Higher heave amplitudes are observed at the lower lengths of

secondary cable. This may be due to heavy fluid damping of transverse mode of transfer of disturbance along the secondary cable. Chapman [Chapman,1984] had observed that transverse oscillations are heavily damped while longitudinal oscillations prevail in marine cable system. The dominant mode of transmission of disturbance in the primary cable is attributed to longitudinal one since they are having high geometrical slop due to high cable tension prevailing there. On the other hand cable tension observed in secondary cable is near zero because of the near neutrally buoyant towed body. Further the a long secondary cable makes long-distance-travel for the transverse oscillations , leading to gradual die-out of disturbances , Hence a long secondary cable may be desired for better stability of the towed body.

Figure 7.3 shows the variation of the heave amplitude of the towed body with respect to the length of the primary cable. It can be seen that as the length increases the heave amplitude decreases. This may be attributed to lower tension in the cable as the length of primary cable increases. Hence it may be conclude that long primary cable is preferred for better stability of towed body but this is often limited by the design depth

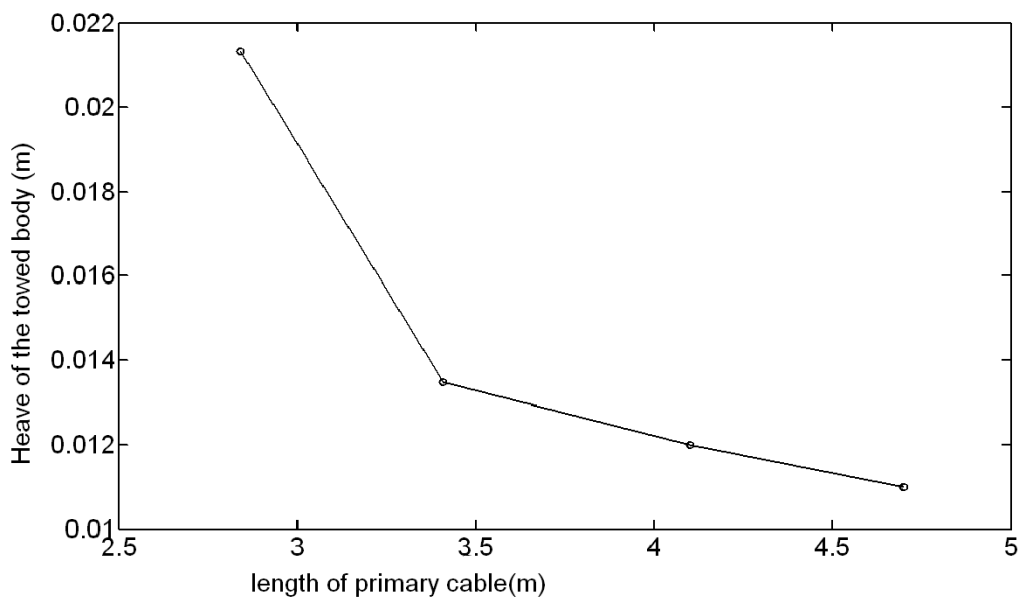


Figure 7.3. Variation of heave ratio with the length of the primary cable

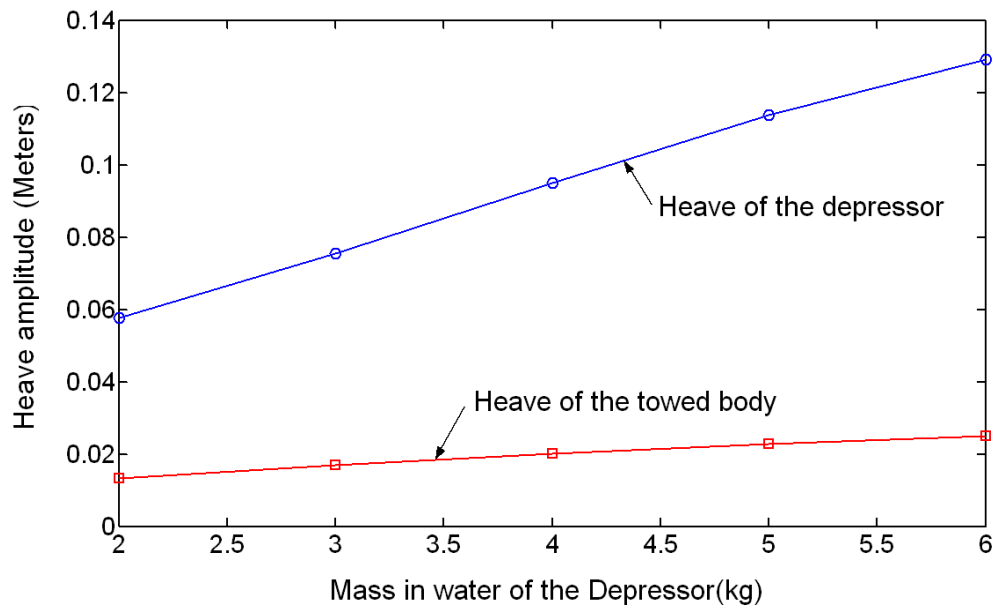


Figure 7.4. Effect of Depressor mass on the heave response of the towed body and depressor

Figure 7.4 shows the variation of the heave response of the towed body and depressor with respect to the mass in water of the depressor. As the mass of the depressor increases heave amplitude also increases monotonically leading to more instability. Chapman [Chapman,1984] has shown that the amplitude of heave motion of the towed body is proportional to the sine of the angle made by the top of the cable with the horizontal for single point towing system. The same reason is applicable to two-part towing system. As the depressor becomes heavy, this angle tends to increase, results in more instability.

Further, to study the effect of frequency of input wave motion at the tow-point on the heave stability of towed body, numerical simulations were done with frequency ranges from 0.1 to 2 hz.

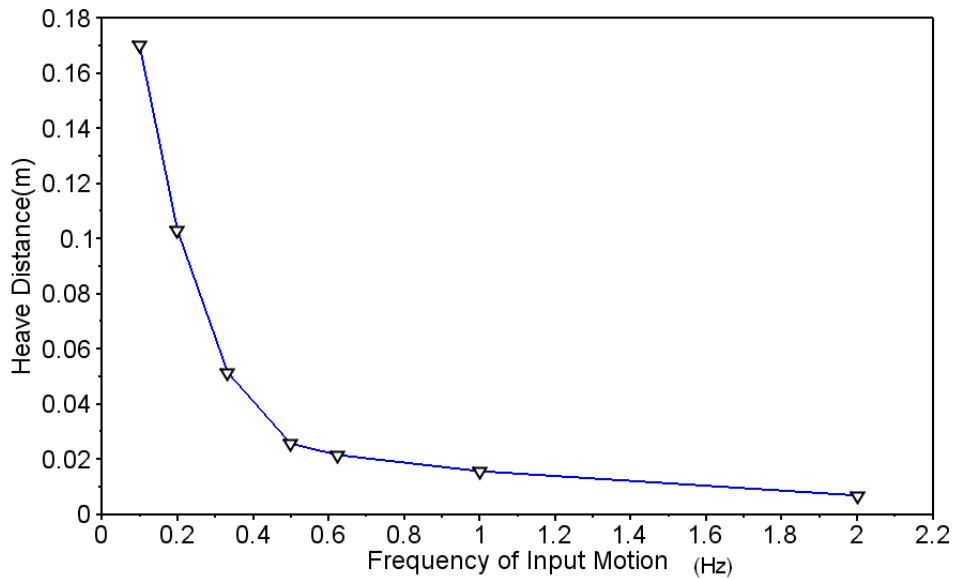


Figure 7.5 Effect of frequency of sinusoidal wave disturbances given on the tow-point on the heave response of the towed body

Figure 7.5 shows the variation of heave amplitude of the towed body with the frequency of the input wave motion given at the tow-point. The selected range of frequency is comparable with the normal ocean wave frequency [Sanil Kumar V, 2011]. It may be observed that characteristic peaks corresponds to natural frequency of the tow-system are absent in the frequency plot, implying that natural frequencies lie outside the test range of 0-2Hz. It can be seen that at high frequencies of the input disturbances, the heave amplitude of the towed body is considerably reduced while at low frequencies heave of the towed-body is considerably large. Thus two-part towing did improve the performance at high frequencies of excitation but at lower frequencies this effect was reduced at least within the test range. This may due to longer time periods at lower excitation frequencies thus allowing the tow-fish significant time to follow the motion of the junction of the three cables due to net force in that direction by the secondary cable.

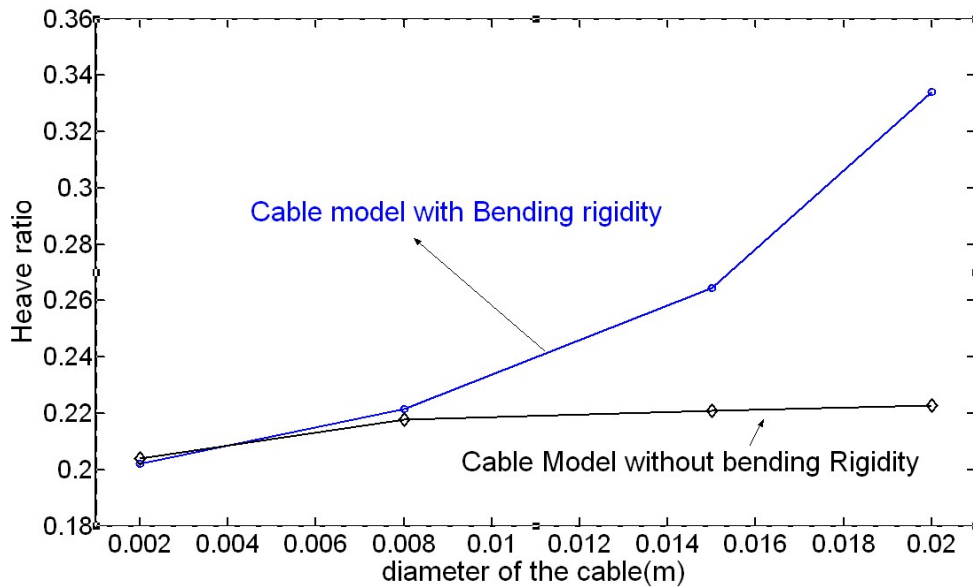


Figure 7.6 Effect bending rigidity of the cable on the heave ratio

Finally the effect of flexural rigidity of the marine cable on the hydrodynamic stability of the tow system was investigated. For this, simulations are done with diameter of the cable ranging from 2mm to 20 mm and keeping the rest of test conditions remains as that of problem discussed in section 5.1. The drag forces in all test cases are made constant to nullify the effect of 2nd order fluid damping on the heave response. Figure 7.6 shows the effect of bending rigidity of the cable on the stability of two-part towing system. In the first case the cable has been modeled using LMSM without bending rigidity and in the second case LMSM with bending formulation was considered by keeping other forces in the system like gravitational, buoyancy and the drag forces remains the same. It can be seen that when the diameter of the cable is low (up to 8mm), the predicted heave ratio by the two models are equivalent. But as the diameter increases further, this value differs considerably for the two models. This may be due to the enhanced bending rigidity (EI) at higher diameter of the cable. Thus it may be concluded that the bending rigidity of the cables plays a significant role in the motion stability of two-part towing system. As the cables diameter increases, it becomes stiffer results in the increase of the heave amplitude. So a highly flexible cable is suggested for the underwater towing process for the better stability of the towed vehicles.

7.2 Conclusion

The length of the primary secondary and depressor cable are important parameter which affects the stability of the towed body. The numerical analysis revealed that length of the depressor cable should be as small as possible for the better stability of the towed body. Similarly as the length of the primary cable increases, the body becomes more stable. But this is often limited by design depth. Same is the case of secondary cable. A long secondary cable is desirable for better heave stability. The study has revealed that a heavy depressor has the advantage of higher depths but often results in more instability. It has shown that two-part towing is very effective in isolating at high frequency tow-point disturbances as input motion but performance was found to be inferior at lower frequencies of the same. Finally the bending rigidity of the cables plays a significant role in the motion stability of two-part towing system. As the cables diameter increases, it becomes stiffer results in the increase of the heave amplitude. So a highly flexible cable is suggested for the underwater towing process for the better stability of the towed vehicles.

Experimentation

Contents	8.1	<i>Towed body Fabrication</i>
	8.2	<i>Electronic Suite</i>
	8.3	<i>Trimming of the Tow-fish</i>
	8.4	<i>Sinusoidal Input Motion Mechanism</i>
	8.5	<i>Estimation of Mass Moment of Inertia of Tow-fish</i>
	8.6	<i>Towing Tank trails</i>
	8.7	<i>Results and discussion</i>
	8.8	<i>Conclusion</i>

The present chapter discusses about an experimental investigation on a two-part underwater towing system, which was conducted in a model ship towing tank and the developed numerical model was evaluated based on this. The towing tank facility of offshore laboratory, NIT Calicut was utilised for performing experimentation. A dedicated experimental set-up has been fabricated which includes the towed body and associated electronics, sinusoidal input motion generation mechanism, sensors for real time measurement of pitch and heave etc. These are discussed in the subsequent sections.

The thrust of the current research has been put on the development of numerical scheme for the simulation of two-part towing system. Only limited experimentation could be performed for verifying the developed numerical scheme. Since, a comprehensive experimental study on the heave stability two-part system is much involved, which may include detailed study on a number of parameters, such as geometrical configuration of the tow-system (cable, towed body and depressor), hydrodynamic forces, frequency of input disturbances etc. Only,

an elaborate investigation with properly scaled model and with associated similitude can only reveal the exact heaving characteristics of the prototype. Such investigations are included in the future scope of the research. So only a qualitative sort of information of heave response of the towed body is expected from the experimentation.

8.1 Towed body Fabrication

The hull of the tow-fish was constructed by developing a shape that was reasonably hydrodynamic and was large enough to hold all the components needed for the tow-fish. The axi-symmetric hull form was adopted with overall length of 1.3m and hull diameter as 0.11m leading to a fines ratio of 11.81 for the towed body. The body was made of PVC and cast aluminium was used to fabricate nose-cone and tail section. To make the model to be simple, plane sections were used for aft fins rather than the NACA profiles. Two vertical and same number of horizontal fins were fixed at the tail end. Further, to resist hydrostatic pressure, the hull was reinforced with circular stainless steel frame and flanges. A stainless steel eye-bolt was fixed near to the nose cone which secures the tether to the tow-fish. The body was maintained near neutral buoyancy for better stability. This has been achieved by using ring shaped stainless steel ballast weights.

The electronic components are housed in two water tight pressure chambers. Further, to reduce the size of ballast weight and to make the body near neutrally buoyant, a flooded type hull was selected rather than water tight hull form.

8.2 Electronic Suite

The Motorola-MPX2050 series silicon-piezoresistive pressure sensors were used which can measure a maximum pressure 50KPa. The corresponding maximum depth that can be measured by this sensor is 5m with accuracy of 2.5%. The sensor is of diaphragm type and temperature and salinity compensated. Two pressure sensors are mounted, one inside the towed body and other inside the depressor to estimate the real-time heave response of both.



Figure 8.1 Towed body



Figure 8.2 Towed body structure



Figure 8.3 Pressure sensor



Figure 8.4 Tri-axis Accelerometer

The ST-Microelectronic's LIS3L06AL accelerometer was used to measure real-time pitch data. It is a MEMS type tri-axis accelerometer with a capacitive type sensing element and antilog output. The accelerometer has been reconfigured to work as a real-time inclinometer. The sensor was set a maximum inclination reading of ± 45 degree. Analog Device's 24 bit ADC was used to convert sensor data. The individual sensor output was further amplified by low noise Bur-Brown instrumentation amplifier. A 12 V DC power supply was devised to power the whole system. Figure shows the 4 channel data acquisition system

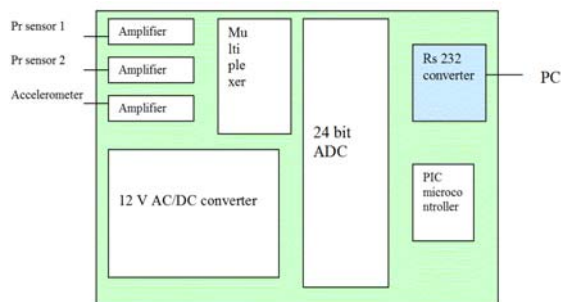


Figure 8.5 Electronic Diagram



Figure 8.6. 6 channel Data Acquisition System

The error/uncertainty analysis of the instrumentation to measure the heave responses was discussed in appendix-III.

8.3 Trimming of the Tow-fish

The tow fish consists of both flooded and pressure chambers and was designed to be 2% buoyant to account for the weight of the tow cables etc. The accelerometer and electronic boards are kept in a water tight capsule made of polystyrene. This electronic capsule was

positioned nearly the geometric centre of the body. Similarly the two pressure sensors are also housed in separate chambers. To nullify unwanted moments ballast weights are used. Two buoyancy modules are provided at the front and back side of the pressure chamber. Also 1st pressure sensor was housed in between buoyancy chamber and electronic capsule. The assembled tow fish as well as the electronic capsule is shown in figure 8.10 and 8.9



Figure 8.7 Depressor



Figure 8.8 Sinusoidal wave motion mechanism

Depressor was fabricated in a spherical shape and is made of concrete impregnated with steel shots to maintain sufficient negative buoyancy. The outer diameter of the depressor was set to 11cm and has weight-in-water of 5.5 kg. Provisions were made for housing a pressure sensor to its body for the purpose of estimating the real-time heave of the same. A vertical fin was added to this to get directional stability.

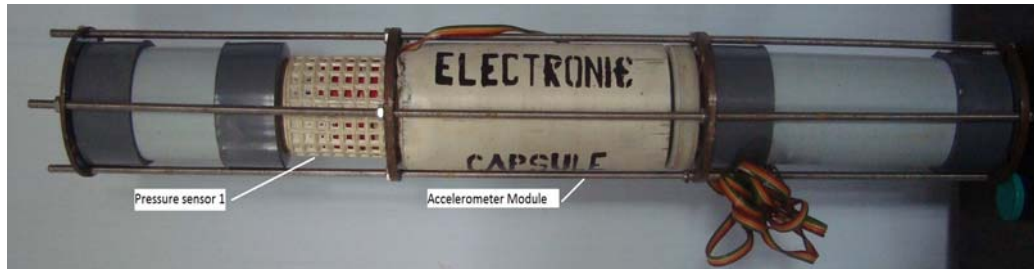


Figure 8.9 Assembled sensor array



Figure 8.10 Finished assembly of the towed body

8.4 Sinusoidal Input Motion Mechanism

To study the disturbances from the ship to the tow-body a sinusoidal input motion generation mechanism was fabricated. A rotating crank mechanism was used in this purpose and it was powered by 12V DC series motor. Maximum heave amplitude was constrained by the radius of the crank ie 6 cm. A voltage based RPM controller was used to set the motor to the fixed rpm of 30 thus providing a fixed wave frequency 0.5 Hz.

The instantaneous vertical heave is given by

$$Y = r_o \sin \omega t \quad \text{Where the } r_o \text{ is the crank radius and } \omega \text{ –angular frequency}$$



Figure 8.11 Carriage speed control

8.5 Estimation of Mass Moment of Inertia of Tow-fish

The method of bifilar suspension (Blagoveshchenky, 1962 and Battacharaya, 1978) is one of the empirical approaches used to determine the mass moment of inertia of a ship model in sea keeping experiments. The same method was adopted to estimate I_{zz} of the model. The model was suspended horizontally in air by two strings of equal length. It was ensured that centre of gravity of the model lies halfway between the strings. The length of the string was maintained a minimum of three times the distance between the strings. This would take care of the assumption of small angle oscillation in bifilar suspension method. The average period of the full oscillation of the same was measured with a stop watch. The radius of gyration k about the axis and mass moment of inertia I_{zz} about this axis is given by

$$k_z = \frac{\sqrt{gl}T_z}{4\pi\sqrt{L}} \quad (8.1)$$

$$I_z = Mk_z^2 \quad (8.2)$$

Where L is the length of the suspension string and l , the distance between the strings. The obtained values are shown in table 8.1.

Table 8.1 Weight and Mass Moment of Inertia of the Towed Body

Item	Weight(kg)		Mass Moment of Inertia (kgm ²)
	Air	wet	
Tow-fish(assembled)	5.2 (dry)	-	0.38
	6.4(water filled)	0.0	0.41
Depressor	6.2	5.1	

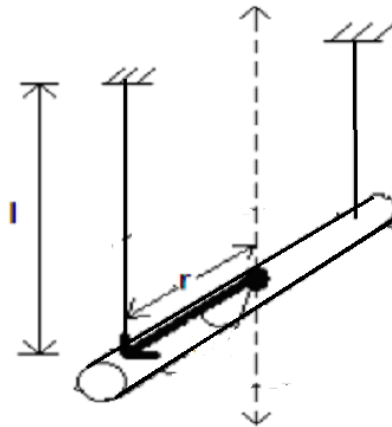


Figure 8.12 Mass Moment of Inertia Estimation

A cylindrical steel bar of uniform density was tested to verify the equation worked and the test setup could predict theoretical inertia within 10% uncertainty. The metal bar weighed 4 kg, was 1m long and had a 2.5 cm diameter. The theoretical inertia was calculated with the slender rod equation $I = mr^2/4 + mL^2/12$, where m was mass in kg and L was length in m, which was found to be 0.32515 kgm². The experimental inertia, turned out to be 0.3088 kgm² with an uncertainty of 0.016 kgm². The difference may have been due to secondary oscillation. The experimental measurement showed a difference of 5% from the theoretical measurement and the test was found to be adequate for the purpose of this research.

8.6 Towing Tank trails

The experiments were conducted in a model ship towing tank. The tank dimensions are 40m x 2m x 2.2m. It is equipped with a two-track, power driven towing carriage 2m x 2m area. The maximum speed of the same was limited to 5m/s. The carriage was controlled by digital control circuit with optical encoder. To generate sinusoidal wave motion a crank mechanism was used and the same was attached to primary cable end. Three, Φ 3mm steel wire ropes were used as the primary, secondary and depressor cables. The sensor cables are wound around these and are taped together to form a composite cable.

The experiments are conducted under the condition of constant towing speed and an excitation at the top end of the primary cable which is impelled by crank mechanism. The instantaneous vertical heave is given by

$$Y = r_0 \sin \omega t \quad \text{Where the } r_0 \text{ is the crank radius and } \omega \text{ –angular frequency of crank.}$$

In the experiments the carriage speed was kept at 1m/s, crank length r was 6cm and rotational speed 30 rpm. The error/uncertainty analysis of the measurements are discussed in appendix-III.

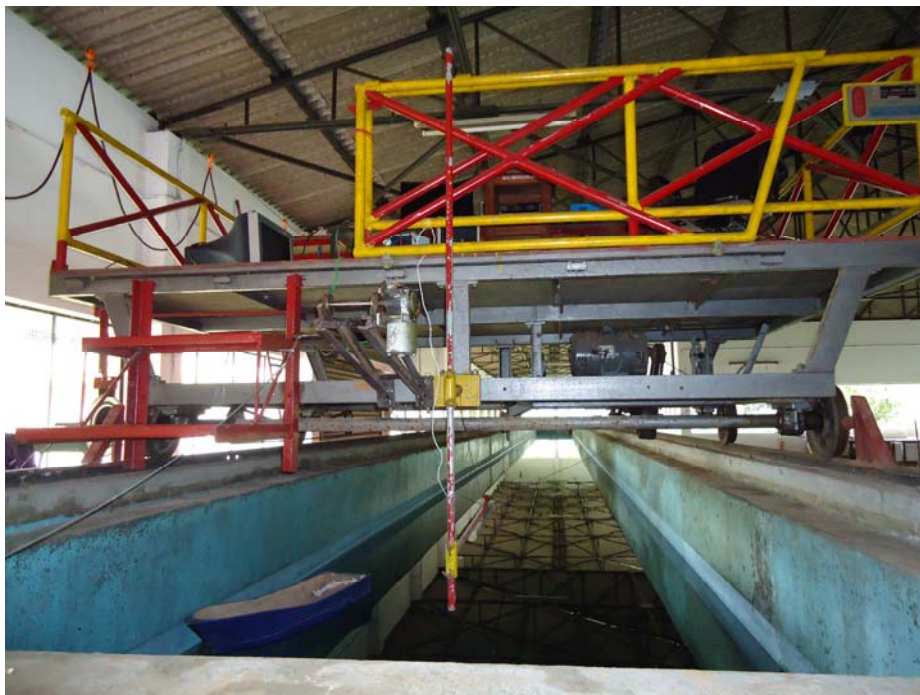


Figure 8.13 Towing tank

The real time pitch and heave data are acquired for 40 seconds. The transient effects are removed by trimming 10% of the initial and last data. Thus heave data and pitch data for 25 seconds are available for further analysis. Subsequently the experimental data are compared with the simulated one with the same test conditions.

The particulars of cables, depressor and tow-fish system are

Depressor: Diameter = 0.11m Weight in air = 5.25kg. Weight in water = 4.58 kg.

Tow-fish: Diameter = 0.11m. Length = 1.30m. Weight in air 5.50kg. Weight in water = 0 kg.

Primary cable: Weight in air = 0.241 kg/m. Weight in water = 0.154kg/m.

Depressor cable: Weight in air = .083 kg/m. Weight in water = 0.059kg/m

Secondary cable: Weight in air 0.144kg/m. Weight in water = 0.075 kg/m

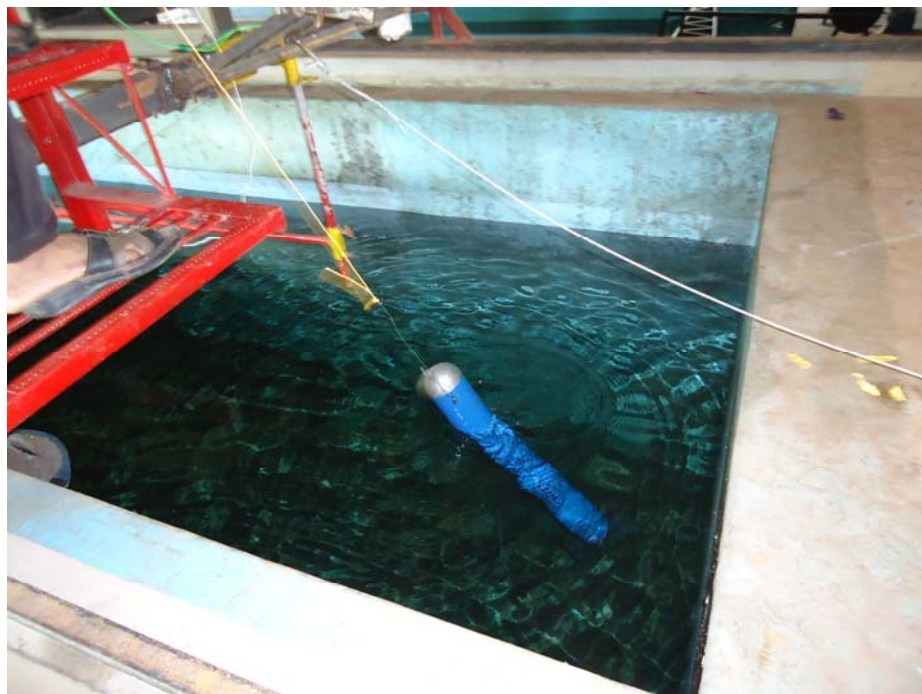


Figure 8.14 deployment of towed body

8.7 Results and discussion

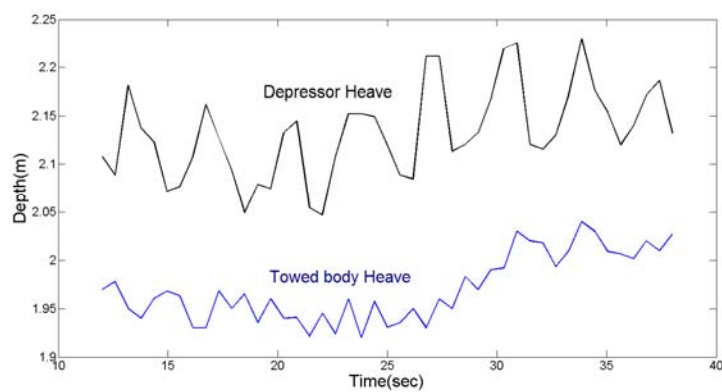


Figure 8.15 Measured time based heave data

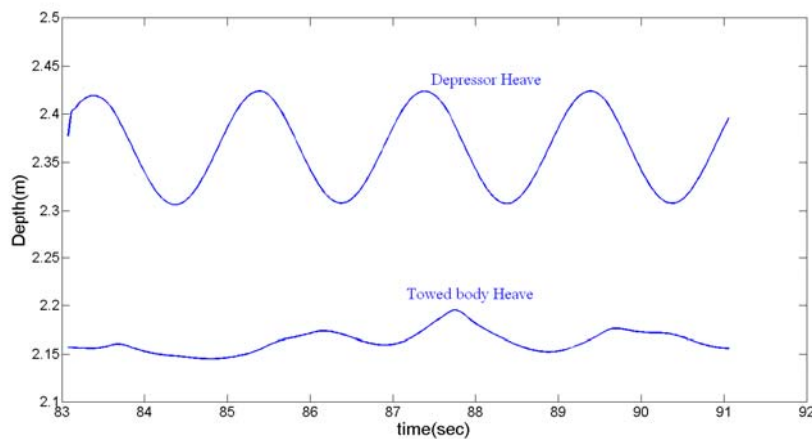


Figure 8.16 Simulated Heave data

Figure 8.15 and 8.16 show the experimental and simulated value of the heave of the towed body. It can be seen that the heave response of the towed body is less than that of the depressor. Also the input disturbance from the ship is considerably scaled at the towed body end. The simulated heave amplitude ratio of the towed body (have of towed body/heave of depressor) was found to be approximately 0.18. The same ratio obtained from the experiment was found to be 0.22.

8.8 Conclusion

Two-part towing system was found efficient in reducing the heave response of the towed body. Based on the real-time experiment performed in the model ship towing tank, it may be concluded that good agreement exists between numerically computed and actual experimental values within the test range.

Summary and Conclusions

The main focus of this study is the motion instability of a towed underwater vehicle (TUV), due to ship induced disturbances transmitted from the tow-point. A Two-Part towing system can effectively isolate a TUV, from these disturbances induced by the towing vessel's motion in waves. To arrive at this conclusion, numerical and experimental studies were performed in this area. In fact, the most tangible contributions of this work are the development of a number of numerical tools that can be used in the analysis and design of this type of systems.

Numerical Study

The numerical study carried out in this regard, mainly consists of physical system modeling of the two-part towing process and the subsequent dynamic analysis. The physical system modeling was a two-step procedure; mathematical modeling of tow-cable and tow-fish. Out of the various methodologies available for modeling of the marine cables, LMSM offers simplicity in implementation compared to conventional segmental or Finite Element model and the same has been selected for cable modeling. Traditional LMSM, when tried to apply for the simulation of two-part towing, failed to produce reasonable results, because of the stability issues involved in the numerical scheme. Therefore, two improvements in the modeling process are suggested and implemented. Firstly, an improved time integration procedure was implemented in the LMSM formulation. Second improvement is the inclusion of bending rigidity in the cable formulation.

A number of time integration procedures, such as Euler, Newmark, Houbolt and HHT- α , were implemented in the LMSM formulation and subsequently tested for stability of the numerical

scheme and accuracy in predicting the heave response of the towed body of a two-part system. It was found that HHT- α is the only scheme, which produced comparable results with experimental values. Further, the controlling parameter α in HHT- α scheme plays a significant role in producing good results and when α value nearly equal to -0.33 the results obtained were satisfactory.

The cable model, which uses traditional LMSM does not have bending rigidity in the formulation, hence that is suitable for long tow-cables having small diameter (negligible bending rigidity). But in the case of two-part towing, bending rigidity cannot be ignored as secondary and depressor cables are considered to be very short compared to primary cable. Hence, the present study implemented modifications in the LMSM, to include the bending rigidity in the cable formulation. A mathematical model, which uses only translational degrees of freedoms for solving beam equation, has been used in this particular study. This would avoid the assemblage of rotational degrees of freedom for the solution of equation of motion. It was also found by the numerical simulation that, bending rigidity of the marine cables has significant role in making the towed body more stable.

Numerical Experiments

To validate the developed model, numerical experiments are done first. For this, a test case from the literature was selected and the model was validated based on this. It was found that two-part system enhance the heave motion stability of the towed-body and the improved LMSM is capable of modeling two part towing system with ship induced disturbances as input.

Further, the developed numerical model was applied to simulate single point towing cases, with ship manoeuvres like circular towing and the situation of sudden stoppage of the ship. These maneuvering situations can create low tension regions which may affect the stability of the numerical scheme. It was found that improved LMSM was able to model this maneuver effectively.

Hydrodynamic Simulation

In most of the previous studies, hydrodynamic parameters such as drag and lift of the towed body was approximated as analytical expression, restricting the numerical model for the towing process to use simple cylindrical shaped towed bodies. To overcome this, a RANS based CFD code has been developed to estimate the drag and lift characteristics of the towed body. The developed serial CFD code produced results in good agreement with the experimental values from the literature [White 2010].

The discretisation of convection term and estimation of spatial gradient is major factor which affects the accuracy of simulation of convection dominated flows. It is a matter of fact that gradient values are significantly affected by the mesh grading and mesh quality parameters like skewness. Out of the various gradient estimation methodologies we tested, the blended scheme produced least L2 norm implying, superior accuracy of the scheme compared to other schemes tested. Also, amount of blending (blending factor) has bearing on accuracy of the predicted gradient.

Further, to discretise the convection flow process, a new numerical scheme (BNCUS) was proposed and used in the study. The simulated results obtained using the modified CFD model was compared with experimental values form literature. It has found that BNCUS2 produced better results (though marginal) compared to BNCUS1. It may be due to the application of second order upwind scheme in the place of lower order scheme during the blending process. Also, the amount of blending have the influence on the numerical results obtained. Out of the various flux limited schemes devised to blend the node and cell based formulation, UMIST scheme produced best results for the numerical experiments done

Parallel Computations

To reduce the execution time involved in the computation process, parallel computing methodologies are implemented in the present study. Out of various programming paradigms available, shared and distributed memory systems are widely used in engineering simulations. The former approach based on OPENMP offers relatively simple procedures to parallelize the serial code.

Based on the speedup test done with FORTRAN code developed in-house for structural dynamic simulation of two-part towing system, and parallelized through OPENMNP, it was found that, the code has got reduced execution time compared to serial one.

Unlike shared memory programming model, the distributed memory systems using MPI can handle large scale computation process and is widely used in CFD simulation. From the speed up test done using the C-code developed for CFD simulation and parallelised through MPI, it is observed that there is only a marginal improvement of speed up by using multiple distributed CPUs. This may be attributed to poor performance of the Ethernet based interconnect.

Design Optimisation of Two-Part Towing System

The proper selection of length of primary, secondary and depressor cable is important for better motion stability (heave) of the towed body. Similar to that, the weight of the depressor, and frequency of the external disturbance have influence on the same.

Towing Tank Trials

Finally the full numerical model has been validated experimentally through towing tank trials. For this purpose, a detailed experimental set-up has been made including the towed body and associated electronics, sinusoidal input motion generation mechanism, sensors for real time

measurement of pitch and heave etc. Only heave performance of the towed body could be compared and bench marked with simulated values, for which the results obtained were satisfactory.

Scope for Future Work

In the present work, hydro-structural analysis of the two-part towing process is conducted to study the stability of underwater towed bodies due to ship induced disturbances. Study is limited to sequential coupling of fluid and structural physics. A fully coupled analysis can have more insight into the towing problems.

Further, the distributed memory approach devised for parallel computing of fluid flow physics, there was only a marginal improvement in terms of reduction in computational time observed. This may be due to poor performance of ETHERNET interface. Future work can incorporate the use of bonded ETHERNET network to reduce computational time.

Finally, the experimentation performed in this study was slightly limited in the sense that an elaborate experimental study with a number of input parameters, such as geometrical configuration of the tow-system (cable, towed body and depressor), hydrodynamic forces, frequency of input disturbances etc, with properly scaled model and with associated similitude can only reveal the exact heaving characteristics of the prototype.

Appendix-I

Estimation of Drag on the cable segment.

The average drag acting on node i is given by (refer figure 3.1)

$$F_D^i = 1/2 (F_D^{i+1} + F_D^{i-1})$$

Where F_D^{i+1} and F_D^{i-1} are the drag forces acting on cable segments which lie on either side of the node i.

$$F_D^{i+1} = \left[-\frac{1}{2} \rho C_n^{i+1} l_{i+1} d_{i+1} |V_{cn}| V_{cn}, \frac{\pi}{2} \rho C_t^{i+1} l_{i+1} d_{i+1} |V_{ct}| V_{ct} \right] \quad (A1-1)$$

$$F_D^{i-1} = \left[-\frac{1}{2} \rho C_n^{i-1} l_{i-1} d_{i-1} |V_{cn}| V_{cn}, \frac{\pi}{2} \rho C_t^{i-1} l_{i-1} d_{i-1} |V_{ct}| V_{ct} \right] \quad (A1-2)$$

$$\begin{bmatrix} V_{ct} \\ V_{cn} \end{bmatrix} = \begin{bmatrix} V_y - U_y \\ V_z - U_z \end{bmatrix} * D \quad (A1-3)$$

Th symbols C_n and C_t are the tangential and normal drag coefficients for the cable and d is the diameter of the cable. Also, U_y , U_z denote the components of underwater current, which vary in both space and time dimension. The symbol D is explained in equation 3.8.

Estimation of tension in the cable segment

The tension in the cable segment was determined from the elastic properties of the cable and deformation. Assuming the cable to be linearly elastic and by utilizing the hooks law, the cable tensions at either side of the node i namely T_{i+1} and T_{i-1} are given by

$$T_{i+1} = \sigma_{i+1} E \left(\frac{\sqrt{(y_{i+1} - y_i)^2 + (z_{i+1} - z_i)^2}}{l_{i+1}} - 1 \right) \quad (A1-4)$$

$$T_{i-1} = \sigma_{i-1} E \left(\frac{\sqrt{(y_i - y_{i-1})^2 + (z_i - z_{i-1})^2}}{l_{i-1}} - 1 \right) \quad (A1-5)$$

Where, E is the Young's modulus of the cable material.

- l - Length of the cable segment,
- σ cross-sectional area of the cable

Towed-body Dynamics

The mass matrix M and moment of inertia matrix J discussed in section 3.8.1 is explained here. The contribution of added mass is also included in the rigid body mass. Hence the mass matrix becomes

$$M = \begin{bmatrix} m(1 + k_1) & 0 & 0 \\ 0 & m(1 + k_2) + Y_{vf} & 0 \\ 0 & 0 & m(1 + k_2) + Z_{wf} \end{bmatrix} \quad (A1-6)$$

Where k_1 , k_2 and k_3 are the coefficient of added mass in the three direction x , y and z . The symbols Y_{vf} and Z_{wf} are the added mass contribution of the fin towards y and z directions. The rigid body moment of inertia and added inertia matrix for the towed body is

$$J = \begin{bmatrix} I_x + K_{pf} & -I_{xy} & -I_{xz} \\ -I_{xy} & I_y(1 + k_3) + M_{qf} & -I_{yz} \\ -I_{xz} & -I_{yz} & I_z(1 + k_3) + N_{rf} \end{bmatrix} \quad (A1-7)$$

The M_{qf} and N_{rf} are the added mass contribution due to fins.

F_{ext} and M_{ext} are the external force and moment vectors defined as

$$F_{external} = \begin{bmatrix} F_{axial} \\ F_{lateral} \\ F_{normal} \end{bmatrix} = [F_{body} + F_{tail} + F_{tow} + F_{weight} + F_{buoyancy}] \quad (A1-8)$$

$$M_{external} = \begin{bmatrix} M_{roll} \\ M_{pitch} \\ M_{Yaw} \end{bmatrix} = [M_{body} + M_{tail} + M_{tow} + M_{damping} + M_{weight}] \quad (A1-9)$$

Appendix-II

Houbolt Scheme

The method is summarized below. By assuming viscous damping not present the general equation of motion becomes

$$M\mathbf{a}_{n+1} - \frac{1}{2}M\mathbf{a}_n + \alpha K\mathbf{d}_{n+1} = \alpha F_{n+1} \quad (\text{A2.1})$$

$$\mathbf{d}_{n+1} = \mathbf{d}_n + \Delta t \mathbf{v}_n + \left(\frac{1}{2} - \beta_1\right) \Delta t^2 \mathbf{a}_n + \beta_1 \Delta t^2 \mathbf{a}_{n+1} \quad (\text{A2.2})$$

$$\mathbf{v}_{n+1} = \mathbf{v}_n + \frac{1}{2} \left(\frac{1}{2} - \gamma_1\right) \Delta t \mathbf{a}_n + \gamma_1 \Delta t \mathbf{a}_{n+1} \quad (\text{A2.3})$$

$$\beta_1 = \frac{1}{2} \left(\frac{1}{2} + \gamma_1\right) \quad (\text{A2.4})$$

$$\alpha = \frac{1}{2\beta_1} \quad (\text{A2.5})$$

Where \mathbf{d}_n , \mathbf{V}_n , and \mathbf{a}_n are approximations to the position, velocity, and acceleration vectors at time step. M and K denote mass and stiffness matrix respectively. F is the external force vector.

NewMark's method

$$\left[M + \beta h^2 K \right] \mathbf{a}_{n+1} = F_{n+1} - K \left[\mathbf{q}_n + \Delta t \mathbf{v}_n + \left(\frac{1}{2} - \beta\right) \Delta t^2 \mathbf{a}_n \right] \quad (\text{A2.6})$$

$$\mathbf{d}^{n+1} = \mathbf{d}^n + \Delta t \mathbf{v}_n + \frac{\Delta t^2}{2} \left[(1 - 2\beta) \mathbf{a}_n + 2\beta \mathbf{a}_{n+1} \right] \quad (\text{A2.7})$$

$$\mathbf{V}^{n+1} = \mathbf{V}^n + \Delta t \left[(1 - \gamma) \mathbf{a}_n + \gamma \mathbf{a}_{n+1} \right] \quad (\text{A2.8})$$

HHT- α method

$$M\mathbf{a}^{n+1} + (1 + \alpha)C\mathbf{v}^{n+1} - \alpha C\mathbf{v}^n + (1 + \alpha)K\mathbf{d}^{n+1} - \alpha K\mathbf{d}^n = F(t_{n+\alpha}) \quad (\text{A2.9})$$

$$\text{Here } F(t_{n+\alpha}) = (1 + \alpha)t^{n+1} - \alpha t^n \quad (\text{A2.10})$$

$$\mathbf{d}^{n+1} = \mathbf{d}^n + \Delta t \mathbf{v}_n + \frac{\Delta t^n}{2} [(1 - 2\beta)\mathbf{a}_n + 2\beta\mathbf{a}_{n+1}] \quad (\text{A2.11})$$

$$\mathbf{V}^{n+1} = \mathbf{V}^n + \Delta t [(1 - \gamma)\mathbf{a}_n + \gamma\mathbf{a}_{n+1}] \quad (\text{A2.12})$$

If $\alpha=0$ the equations reduces to that of Newmark's method. It has been found that if the parameters are selected such that $\alpha = [-1/3, 0]$ and $\gamma = (1 - 2\alpha)/2$ and $\beta = (1 - \alpha^2)/4$ an unconditional stable, second order accurate scheme results. Decreasing α may result in the increase of the numerical dissipation.

Appendix-III

Uncertainty/ Error Analysis of real-time depth measurement.

To measure the real-time heave data two identical pressure sensors were devised. The Motorola-MPX2050 series silicon-piezoresistive pressure sensors were used which can measure a maximum pressure 50KPa. Sensor consists of a single monolithic silicon diaphragm with a strain gage and film resistor network on each chip. The chip is laser trimmed to give a precise span, offset and temperature calibration.

The transducer output is fed to a computer controlled data acquisition system and the depth is displayed on the screen. Before each test, the transducer is zeroed by a command to the data acquisition system. Hence, the specified offset errors are of no real practical importance. The key issue is the specified errors in the full-scale span.

The data sheet of the sensor is shown below.

Operating temperature	: 0 – 85 °C
Differential pressure range	: 0 – 50 kPa
Full scale span	: 80 ± 1.0 mV
Zero pressure offset	: 0.5 mV-minimum, 1 mV maximum
Linearity	: % 0.25

Temperature effect on full scale span, 1mV maximum

Temperature effect on offset, 1mV Maximum

Maximum measurable depth = 5.09m (corresponds to 50kPa)

Since the maximum operating depth in the current project is equal to 2.2m the corresponding estimate of depth error was found by

Full scale error (corresponds to 50kPa) = 1mV equivalent to $1/80 \text{ mV} * 50 \text{ kPa}$

Part scale error (correspond to 2.2 m or 21.560kPa) = $1/80 * 21.560/50 = 0.431 \text{ mV}$, which is equivalent to 0.2694kPa.

Since the pressure (P) = $h\rho g$ or $h = P/(\rho g)$ the corresponding error is found to be 2.74cm for a maximum depth of 2.2m or the percentage error is 1.24% .

Where, h is the vertical depth, ρ is density of water and is assumed to be 1000 kg/m^3

References

1. Ablow and S. Schechter. "Numerical simulation of undersea cable dynamics". *Ocean Engineering*, 10:443–457, 1983.
2. Argyris J.R, Papadrakakis M, Apostolopoulou C, "The TRIC shell element: theoretical and numerical investigation", *Computer. Methods Appl. Mech. Engineering*. 182, 217–245,2000.
3. Aris, R, "Vectors, tensors and the basic equations of fluid mechanics": Dover Publications, USA, 1989.
4. Bardina J E , "Turbulence Modeling Verification , Testing and Development", Prentice Hall,USA,1997
5. Bathe K.J ,Finite element procedures, prentice Hall,USA,2000
6. Bettles, R.W., Chapman, D.A., "The experimental verification of a towed body and cable dynamic response theory". *Ocean Engineering* 12 (5), 453–469, 1985.
7. Boris D,James L. Thomas Eric J , "Comparison of node-centered and cell-centred unstructured finite-volume discretizations. Part I: viscous fluxes" 47th AIAA Aerospace Sciences Meeting Including The New Horizons Forum and Aerospace Exposition 5 - 8 January 2009, Orlando, Florida,AIAA 2009-597
8. Buckham, B., Nahon, M., Seto, M., In: *Proceedings of OMAE '99*, "Three-dimensional dynamics simulation of a towed underwater vehicle". 1999
9. Buckham, B., Nahon, M., Seto, M., Zhao, X., Lambert, C. "Dynamics and control of a towed underwater vehicle system", Part I: Model development. *Ocean Engineering*, this volume., 2002.
10. Burgess J J. "Bending stiffness in a simulation of undersea cable deployment". *International Journal of Offshore and Polar Engineering*, 3:197–204, 1993.
11. Campa G, Wilkie J and Innocenti M, "Robust control and analysis of a towed underwater vehicle," *Int. J. Adapt. Control Signal Process.* 12, pp. 689-716, 1998.
12. Chakravarthy, S.R. and Osher, S.: "High resolution application of the OSHER upwind scheme for the Euler equation": *AIAA Paper 83-1943*, 1983.
13. Chapman D A "Towed Cable Behavior During Ship Truing Manoeuvres" , *Ocean Engineering*, Vol. 1, No.4, pp.327-361, 1984.
14. Chiou, K. C ,Leonard, J., "Slack Elasto-Plastic Dynamics of Cable Systems," *ASCE Journal of the Engineering Mechanics Division*, Vol. 105, No. 2, pp. 207-222, 1979,
15. Chung and G.M. Hulbert. "A time integration algorithm for structural dynamics with improved numerical dissipation". *Journal of Applied Mechanics*, 60:371–375, 1993.
16. Darwish M., Moukalled F."Convective Schemes For Capturing Interfaces of Free-Surface Flows on Unstructured Grids", *Num. Heat Trans. part B: Fundamentals*, vol. 49, no 1, pp.19-42 2005.
17. De E .,S G Maciel ,*Jnl of Brazilian Society of Mechanical Engineering*, July 2005,pp223-235

18. Delmer, T. M., Stephens, T. C., and Coe, J. M., "Numerical Simulation of Towed Cables," *Ocean Engineering*, Vol. 10, No. 2, pp. 119-132,1983.
19. Driscoll, R., Nahon, M. "Mathematical Modelling and Simulation of a Moored Buoy System". Proceedings of the MTS/IEEE OCEANS '96, Fort Lauderdale, FL. 1, 517-523,1996.
20. Eric Le Guerch, "The deep towing of underwater fish behaviour patterns during half-turn manoeuvres", *Ocean Engineering* Volume 14, Issue 2, Pages 145–162,1987.
21. Eric M Schuch , "Tow fish Design and Control", PhD thesis Virginia Polytechnic Institute. 2004.
22. Feng Z, Allen R, "Evaluation of the effects of the communication cable on the dynamics of an underwater flight vehicle *Ocean Engineering*", 31 1019–1035,2004.
23. Ferziger, J.H. and Perić, M.: *Computational methods for fluid dynamics*: Springer Verlag, Berlin-New York, 1995.
24. Gobat, Jason I and Grosenbaugh, Mark A. WHOI Cable v2.0: "Time Domain Numerical Simulation of Moored", Woods Hole Oceanographic Institution, 2000.
25. Gobat, Jason I. "The dynamics of geometrically compliant mooring systems". Woods Hole, MA : PhD thesis, Massachusetts Institute of Technology and Woods Hole Oceanographic Institution Joint Program, 2000.
26. Harten, A. "On a class of high resolution total variation stable Finite Difference schemes", *SIAM J. Numer. Analysis*, 31:1 23, 1984.
27. Hoff and P.J. Pahl. "Development of an implicit method with numerical dissipation from a generalized single-step algorithm for structural dynamics". *Computer Methods in Applied Mechanics and Engineering*, 67:367–385, 1988.
28. Hover F S and D. R. Yoerger, "Identification of low-order dynamic models for deeply-towed underwater vehicle systems," *Proc. First Int. Offshore Polar Eng. Conf.*, pp. 97–105, 1991.
29. Howell, C. T., "Numerical Analysis of 2-D Non-linear Cable Equations with Applications to Low-tension Problems," *International Journal of Offshore and Polar Engineering*, Vol. 2, No. 2, 1992, pp. 110-113.181
30. Hrvoje Jasak Error Analysis and Estimation for the Finite Volume Method with Applications to Fluid Flows, University of London,1996.
31. Hughes. T.J.R "The Finite Element Method: Linear Static and Dynamic Finite Element Analysis". Prentice-Hall, Englewood Cliffs, NJ, 1987.
32. Huston, R.L., Kamman, J.W. "Validation of finite segment cable models". *Computers and Structures* 15 (6), 653–660,1982.
33. Irvine, H. M. *Cable Structures*. Cambridge: MIT Press, 1981.
34. Jones, W.P. and Launder, B.E. The prediction of laminarization with a two-equation model of turbulence. *International Journal of Heat and Mass Transfer*, 15, 1972.
35. Kamman, J. W. and Huston, R. L., "Modeling of Variable Length Towed and Tethered Cable

- Systems,” *Journal of Guidance, Control, and Dynamics*, Vol. 22, No. 4, pp. 602-608,1999.
36. Kane, Thomas R. and Levinson, David A. *Dynamics, Theory and Applications*. McGraw-Hill, 1985.
 37. Kato N, “Guidance and control of underwater towed vehicle maneuverable in both vertical and horizontal axis,” *Proc. Second horizontal axis (Part1: Principal configuration and attitude control)*,”*Journal of the Society of Naval Architects of Japan*, no. 169, pp. 111-122, 1991.
 38. Koh, Y. Zhang, and S.T. Quek. *Low-tension cable dynamics: numerical and experimental studies*. *Journal of Engineering Mechanics*, 125:347–354, 1999.
 39. Lambert. C, M. Nahon c,B. Buckham a, M. Seto b, *Ocean Engineering* 30 471–485 “Dynamics and control of towed underwater vehicle system, part II: model validation and turn manoeuvre optimization”, 1979,
 40. Large angular motions of tethered surface buoys. Leonard, J. W., Idris, K. and Yim, S. C. S. 12, s.l. : *Ocean Engineering*, 2000, Vol. 27.
 41. Le Guerch, E., 1987. “The deep towing of underwater fish behaviour patterns during half-turn manoeuvres”.
 42. Leonard B.P, ”Simple high accuracy resolution program for convective modeling of discontinuities”. *Intl. Jnl. Num. Meth. in Fluids*,8:1291-1318,1988
 43. Leonard, B.P. “The ULTIMATE conservative difference scheme applied to unsteady one-dimensional advection”, *Comp. Meth. Appl. Mech. Engineering*, 88:17 -74, 1991.
 44. Leontiev, “Extension of LMS formulations for L-stable optimal integration methods with U0–V0 overshoot properties in structural dynamics: The level-symmetric (LS) integration methods”, *International Journal For Numerical Methods In Engineering Int. J. Numer. Meth. Engng* 2007; 71:1598–1632, 2007
 45. Lo, A., Leonard, J.W., 1982. “Dynamic analysis of underwater cables”. *Proceedings of the American Society of Civil Engineers* 108 (EM4), 605–621.
 46. Masciola, M., Nahon, M., and Driscoll, F. (2012). ”Static Analysis of the Lumped Mass Cable Model Using a Shooting Algorithm.” *J. Waterway, Port, Coastal, Ocean Eng.*, 138(2), 164–171.
 47. Menter F R, M. Kuntz1 and R. Langtry, “Ten Years of Industrial Experience with the SST Turbulence Model”, *Turbulence, Heat and Mass Transfer* ,Begell House, Inc. 2003
 48. Menter, F.R. “Influence of free stream values on k-omega-turbulence model predictions”. *AIAA Journal*, Vol. 30, No. 6.1992.
 49. Milinazzo, M. Wilkie, and S.A. Latchman. “An efficient algorithm for simulating the dynamics of towed cable systems”. *Ocean Engineering*, 14:513–526, 1987.
 50. Nakamura, W. Koterayama, and Y. Kyojuka. “Slow drift damping due to drag forces acting on mooring lines”. *Ocean Engineering*, 18:283–296, 1991.
 51. Naomi E Leonard. “Stability of a Bottom-Heavy Underwater Vehicle”. *Automatica*, March 1997.*Ocean Engineering* 14 (2), 145–162.

-
52. Ohkusu, M., Kashiwagi, M., Koterayama, W., 1987. "Hydrodynamics of a depth controlled towed vehicle". *Journal of the Society of Naval Architect of Japan* 162, 99–109.
 53. Palo, P.A., Meggitt, D.J., Nordell, W.J., 1983. "Dynamic cable analysis models". *Proceedings of the Offshore Technology Conference* 1, 487–491.
 54. Patankar, S.V.: *Numerical heat transfer and fluid flow*: Hemisphere Publishing Corporation, 1981.
 55. Paul, B., Soler, A.I., 1972. "Cable dynamics and optimum towing strategies for submersibles". *MTS Journal* 6 (2), 34–42.
 56. Peric, M.: "A fourth-order Finite Volume method with collocated variable arrangement", *Computers and Fluids*, 24(3):239–252, 1995.
 57. Press, W.H., Teukolsky, S.A., Vetterling, W.T., Flannery, B.P., 1992. *Numerical Recipes in C*. Cambridge University Press, UK.
 58. Ranmuthugala, S.A Gottschalk, "Investigation into two-part underwater tow", proceedings of first international conference on underwater tow, Wuxi, China, pp 663-670, 1994.
 59. Reklaitis, G.V., Ravidran, A., Ragsdell, K.M., 1983. *Engineering Optimization—Methods and Application*. John Wiley and Sons.
 60. Rhie, C.M. and Chow, W.L.: A numerical study of the turbulent flow past an isolated airfoil with trailing edge separation": AIAA-82-0998, AIAA/ASME 3rd Joint Thermo physics, Fluids, Plasma and Heat Transfer Conference, St.Louis, Missouri, 1982
 61. Robert E. Cornwell and David S. Malkus. "Improved numerical dissipation for time integration algorithms in conduction heat transfer". *Computer Methods in Applied Mechanics and Engineering*, 97:149–156, 1992.
 62. Roe, P.L."Large scale computations in fluid mechanics, Part 2", In *Lectures in Applied Mathematics*, volume 22, pages 163 193. Springer Verlag, 1985.
 63. Samuel M.Welch, Marshall P.Tulin, "An Experimental Investigation of the Mean And Dynamic Tensions In Towed Strumming Cables Ocean Engineering Laboratory, *International Journal of Offshore and Polar Engineering* Volume3, Number 3 1993, pp -102-111
 64. Sanders V. A three-dimensional dynamic analysis of a towed system. *Ocean Engineering*, 9:483–499, 1982.
 65. Seto, M. L., Watt, G. D., and Hopkin, D., "A Fully Interactive Dynamic Simulation of a Semi-Submersible Towing a Large Towfish," *Proceedings of MTS/IEEE OCEANS '99*, 1999, pp. 1194-1204.
 66. Shan Huang. Dynamic analysis of three-dimensional marine cables. *Ocean Engineering*, 21:587–605, 1994.
 67. Spalding, D.B, "A novel Finite-Difference formulation for differential expression involving both first and second derivatives", *Int. J. Comp. Meth. Engineering*, 4:551, 1972
 68. Sun M Takayama K "Error Localisation in solution adaptive grid", *Jonl. Of Computational*

- Physics, V190, pp346-350, 2003
69. Sun, Y. and Leonard, J. W., "Dynamics of Ocean Cables with Local Low-tension Regions," *Ocean Engineering*, Vol. 25, No. 6, 1998, pp. 443-463.
 70. Sweby, P.K., "High resolution schemes using flux limiters for hyperbolic conservation laws", *SIAM J. Numer. Analysis*, 21:995-1011, 1984.
 71. Sanil Kumar V, Jai Singh, P. Pednekar and R. Gowthaman, Waves in the nearshore waters of northern Arabian Sea during the summer monsoon, : *Ocean Eng.*, vol.38(2-3); 2011; 382-388
 72. Ted Belytschko, T J R Hughes, *Computational Methods for transient analysis*, North-Holland, 1983
 73. Thomas, D. O. and Hearn, G. E., "Deepwater Mooring Line Dynamics with Emphasis on Seabed Interference Effects," *Proceedings of the 23rd Offshore Technology Conference*, 1994, pp. 203-214.
 74. Thor I Fossen, "Guidance and Control of Ocean vehicles" John Wiley and Sons, 1994.
 75. Tjavaras ,The Mechanics of Highly-Extensible Cables., A. A., et al., et al. 4, s.l. : *Journal of Sound and Vibration*, 1998, Vol. 213.
 76. Van Leer, B.: "Towards the ultimate conservative differencing scheme", *Proceedings of the Third International Conference on Numerical Methods in Fluid Mechanics*, volume 1, pages 163-168. Springer, 1973
 77. Vanka, S.P.: "Block-implicit multigrid solution of Navier-Stokes equations in primitive variables", *J. Comp. Physics*, 65:138-158, 1986.
 78. Vaz, M.A., Patel, M.H., 1995. "Transient Behaviour of Towed Marine Cables in Two Dimensions". *Applied Ocean Research* 17, 143-153.
 79. Vidwans, A. and Kallinderis, Y.: "A 3-D Finite-Volume scheme for the Euler equations on adaptive tetrahedral grids", *J. Comp. Physics*, 113(2):249-267, 1994.
 80. Vilsmeier, R. and Hanel, D.: "Adaptive methods on unstructured grids for Euler and Navier-Stokes equations", *Computers and Fluids*, 22(4-5):485-499, 1993.
 81. W. Raman-Nair, R. E. Baddour "Three-dimensional coupled dynamics of a buoy and multiple mooring lines: formulation and algorithm" . : Oxford University Press, 2002.
 82. Walton, T. S. and Polacheck, H., "Calculation of Transient Motion of Submerged Cables," *Mathematics of Computation*, Vol. 14, No. 69, pp. 27-46, 1960.
 83. WASFY , "A Torsional Spring-Like Beam Element For The Dynamic Analysis Of Flexible Multibody Systems", *International Journal For Numerical Methods In Engineering*, Vol. 39, 1079-1096, 2000
 84. White F.M , "Fluid Mechanics", Tata Mc Graw Hill , 2010.
 85. William C. Webster. "Mooring induced damping". *Ocean Engineering*, 22:57-591, 1995.
 86. Wu J, A.T Chwang, "A Hydrodynamic Mode Of A Two-Part Underwater Towing System", *Ocean Engineering*, Vol. 27, pp.455-472, 2000,
 87. Wu J, A.T Chwang," Experimental Investigation of a two-part underwater towed system".

- Ocean Engineering, Vol. 28, pp.735-750, 2001.
88. Yamamoto, C., Inoue, M., Nagatomi, O., Koterayama, W., and Nakamura, M., “Study on Dynamics of Submarine Cable during Laying and Recovery”. Proceedings of the 1997 16th International Conference on Offshore Mechanics and Arctic Engineering. Part 1-B, 183-189,1997.
 89. Yang Sun and John W. Leonard. “Dynamics of ocean cables with local low-tension regions”, Ocean Engineering, 25:443–463, 1998.
 90. Zhou‡ and K. K. Tamma, Design, analysis, and synthesis of generalized single step single solve and optimal algorithms for structural dynamics International Journal For Numerical Methods In Engineering, pp- 59:597–668,2004
 91. Zienkiewicz, O. C. and Taylor, R. L.:The Finite Element method, vol 1: Basic formulation and linear problems: McGraw-Hill, 4th edition, 1989.

Publications

1. Lalu P.P , Numerical Simulation of Two-Part Underwater Towing System - A Lumped Mass- Spring System Approach, Paper No: OMAE 2007-29166, 26th International Conference on Offshore Mechanics and Arctic Engineering, San Diego, California, USA,2007.
2. P.P lalu , K.P Narayanan, CFD Analysis Of A Towed Underwater Body: A Parallel Computing Approach, Proceedings of the ASME 2012 31st International Conference on Ocean, Offshore and Arctic Engineering OMAE2012, ASME, June 10-15, 2012, Rio de Janeiro, Brazil
3. P.P. Lalu K.P. Narayanan, Parallel Computing Issues in the Development of Underwater Towing Simulation Code, proceedings of the international conference on advanced computing and communication technologies for high performance applications,(volume-ii) ,pp24-26 September. 2008,FISAT, Kerala
4. P.P Lalu, K.P Narayanan “Effect of Bending Rigidity of marine Cables on the Dynamic Stability of Two-part Underwater Towing System”,July,2011, International Journal of Engineering Science and Technology,ISSN:0975-5462, pp 5599-5608

Bio-data

Name : Lalu P.P.
 E-mail : lalujesus@yahoo.co.in
 Contact Tel. No : 9447921327 or 0480-2746082
 Date of Birth : 1st December 1971.
 Age : 41 years.
 Gender : Male.
 Marital Status : Married.
 Religion : Roman Catholic.
 Permanent Address : Pullockaran(H), Near St. George School
 Pariyaram P.O , Chalakudy (via)
 Thrissur Dt Kerala,
 Total Work Experience : 12years till date(Total).

Academic qualifications

Duration	University	Subjects
Feb 2000 M-Tech	Calicut University,	Production Engineering
Oct 1996 B-Tech –Bachelor degree in Mechanical Engineering	Calicut University	Mechanical Engineering

Work Experiences

Institution	Post	Duration
Goovt Engg College Thrissur	Asst Professor	2008 to till today
SCMS college of Engineering Karukutty	‘ ’	2007-2008
Jyothi Engineering College	Lecturer	2006-2007
DRDO, NPOL	Sr Research Fellow	2004-2006
Amal Jyothi engineering College Kanjirapilly	Lecturer	2001-2004

Courses / Training Programs Attended

1. Attended 6 day STTP on Scripting for Engineering and Scientific Applications, Govt. Engineering College, Sreekrishnapuram, (January 2012)
2. Attended 13 day STTP on “Application of Tensors, Fractals and. Integral Transforms” at the Department of Mathematics,. Govt. Engineering College Thrissur.
3. Attended 3 days training on “Taguchi methods on innovation and optimisation using TRIZ and Taguchi techniques” April 2001 at IIT Mumbai.
4. Attended 6 day software training on I-Deas software at SDRC Pune sponsored by IIT Mumbai.

Research Grant

CERD, Govt of Kerala funding on research project entitled” Development of a parallel CFD code for the simulation of two-part underwater towing system.

Total Budget : 2 lakh Rupees

Duration 3years 2010-2013